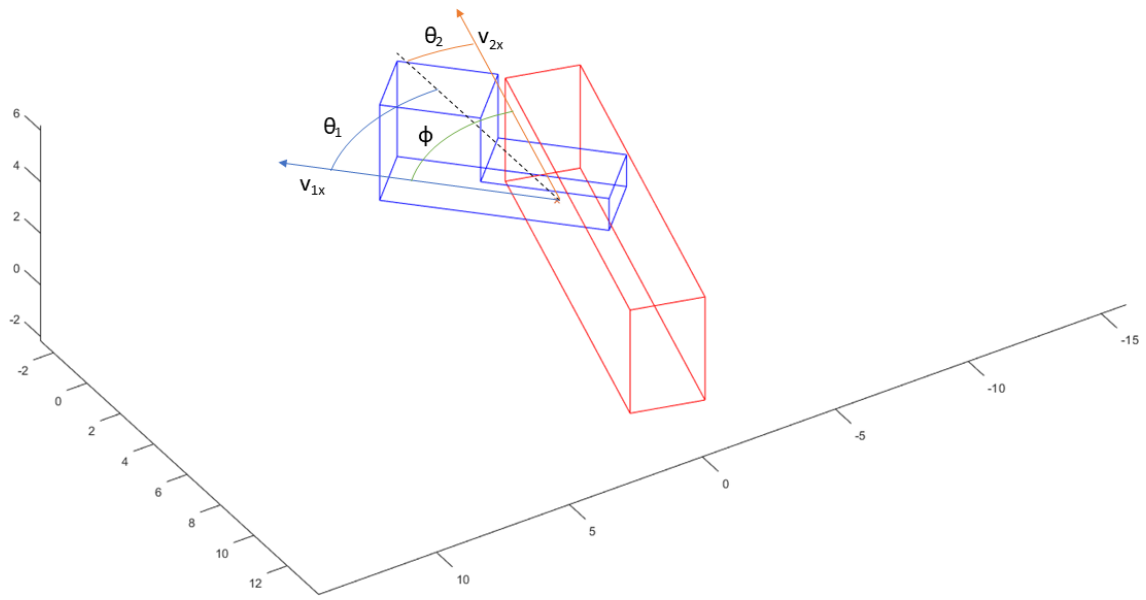

Truck and Semitrailer Articulation Angle Estimation

Master's thesis in Systems, Control and Mechatronics

AXEL CEDER
JONATHAN OLSSON

Department of Mechanics and Maritime Science

CHALMERS UNIVERSITY OF TECHNOLOGY
Gothenburg, Sweden 2020
www.chalmers.se

Master's thesis 2020

Truck and Semitrailer Articulation Angle Estimation

Axel Ceder
Jonathan Olsson

Department of Mechanics and Maritime Sciencee
Division of Vehicle Engineering and Autonomous Systems
Vehicle Dynamics Group
Chalmers University of Technology
Gothenburg, Sweden 2020

Truck and Semitrailer Articulation Angle Estimation
Axel Ceder
Jonathan Olsson

Supervisors: Mats Jonasson, Chalmers University of Technology
Thorsten Helfrich, Volvo Trucks
José Vilca, Volvo Trucks
Leon Henderson, Volvo Trucks

Examiner: Bengt Jacobson, Chalmers University of Technology

Master's Thesis 2020:43
Department of Mechanics and Maritime Science
Chalmers University of Technology
SE-412 96 Gothenburg
Telephone +46 31 772 1000

Cover: Truck backing with visualized angle between tractor and trailer.

Typeset in LaTeX
Printed by Chalmers Reproservice
Gothenburg, Sweden 2020

Trailer Motion Estimation
Axel Ceder, Jonathan Olsson
Department of Mechanics and Maritime Science
Chalmers University of Technology

Abstract

In automation of vehicles, the pose of the vehicle is very important. For a semitrailer the articulation angle describes the angle between the trailer and tractor. Having an accurate estimation of the articulation angle allows fine control of the semitrailer in intersections, which is essential in reversing, and can prevent jackknifing. The articulation angle sensors available today do not match the integrity classification required for safety related signals on a road vehicle. In this work an Inertial Measurement Unit (IMU), which has sufficient classification, is placed in the trailer.
Our goal is to evaluate the feasibility of a virtual sensor using the data from the sensor information already available on the vehicle combined with the IMU.

A basic kinematic single track model is developed and evaluated. Using this information a dynamic single track model is later developed. Two articulation angle estimators are derived using the developed models in a Unscented Kalman Filter (UKF) and compared to empirical data. By equipping a tractor and trailer with two highly accurate GNSS-aided inertial navigation systems the ground truth was obtained.

Both estimators were tested on data from approximately 30 minutes of real-world driving in varying situations. On this data the estimators manage to achieve a RMS error of 0.87 deg and 0.69 deg respectively. The maximum error is 6.88 deg and 3.54 deg respectively. A bi-product of the second estimator is an accurate lateral velocity estimator.

Overall, we conclude that a virtual sensor is deemed feasible but further analysis and extensive testing is required, in part to determine if there are any biases of the estimators towards the test-data. The accurate estimation of the lateral velocity gives the dynamic estimator a chance of being feasible.

Keywords: UKF, Kalman, Sensor fusion, Estimation, IMU, Trailer, Truck, Kinematic model, Forced based model.

Acknowledgements

First we would like to thank our supervisor at Chalmers, Mats Jonasson. For his assistance, fast responses to our questions and early meetings. We would also like to thank our supervisors at Volvo Trucks, Leon Henderson, Thorsten Helfrich and José Vilca who helped us during the entire duration of the thesis. Without these people, this project would not have been possible. Finally we would like to thank our examinor and his compendium, Bengt Jacobson.
We would also like to thank Volvo Trucks for the supply of coffee, it was much needed.

Axel Ceder
Jonathan Olsson
Gothenburg, June 2020

Contents

List of Figures

List of Tables

1
Introduction

Going into the 2020s more and more focus will be on automation of vehicles. As stated by Volvo, *Automation will revolutionize the transport industry – it will improve productivity, lower fuel consumption, and optimize traffic management and route planning among other things*[2]. To achieve this a precise knowledge of the vehicles pose is essential.

1.1 Background

Motion estimation for autonomous vehicles is concerned with extracting the dynamic characteristics and behavior of the whole vehicle combination. It has the task to provide accurate values in order to allow the control of motion actuators in a vehicle to perform safe and efficient maneuvers, e.g., follow the intended path along the road. One of the major challenges is to guarantee accurate and reliable values in real time, which is required for vehicles that are operated on public roads. To be able to make informed decision for controlling the vehicle, knowledge of the vehicles current pose is required. For a two unit semitrailer the pose mainly concerns the yaw-angle between the two units, the articulation angle. In the case of a semitrailer the larger the difference between the trailer's heading and the tractor's heading, the larger articulation angle.

In automotive systems there are areas of hazard involved. The ASIL [8] risk classification system is used to define integrity requirements on signals that can affect vehicle safety. ASIL-D is the most demanding rating, which is given to products using signals and systems that can result in dangerous situations that may be uncontrollable for the vehicle operator[13]. For these products to be considered safe to use in these environments, signals that have been assigned an ASIL rating need to be very rigorously tested and precise.

The connection point between tractor and trailer is the fifth wheel. On the trailers side the connection is called the kingpin. There exists sensors today that could be mounted on the kingpin to measuring the articulation angle. These sensors however have some drawback e.g. dead zones, latency in update or signals that are very noisy. Due to these drawbacks there are currently no sensors of this type matching the ASIL-D classification, which is typically applied to motion estimation related signals for highly automated vehicles. Other types of sensors with sufficient classification are available today. For pose estimation rotational and acceleration data

are important. This data is available in Inertial Measurement Units (IMUs). Many IMUs available are classed as ASIL-D.

Incorrect information of the vehicles state will lead to faulty decisions by the user. In autonomous vehicles the user is the path planner and motion controller. Accurate, robust and fast estimation are needed in order to provide sufficient information to the path planner and motion controller. High accuracy on the articulation angle is important in planning the required road-space, the space that the semi-trailer will occupy. Another large concern is jackknifing. Jackknifing is when the trailer pushes the tractor forward and causing it to rotate. This can often be prevented by detecting risks well in advance and then steered into a safe position. The risk here being a too large articulation angle.

One example where accurate pose estimation is required is when the semi-trailer needs to be parked. When parking accuracy is important, as the trailer needs to be driven into spaces with small margin of errors. Given that the position of the tractor is known, one degrees error of the articulation angle corresponds to about 10 cm uncertainty at the rear of the trailer for a trailer of set length. When parking in tight areas 10 cm is a large but still reasonable uncertainty. As parking will be one of the first steps in automating trucks an accurate articulation angle will be very beneficial.

In intersections it is not easy for the user to predict how the trailer will behave. As the front of the trailer tries to follow the tractor and cutting corners, the rear swings out and may occupy space outside of its own lane. If the user has information on the articulation angle, dangerous situation might be avoided. No matter if the user is a human or a autonomous system.

Figure 1.1: Example of how a human user might use Articulation Angle [19].

1.2 Related Work

Previous work has been done to estimate the articulation angle. In [5] a camera is used to determine the articulation angle. The system matches the image from the camera with a database containing warped images of the trailer with known articulation angles. From this the closest match was chosen as the current articulation, combining this with an Unscented Kalman Filter, maximum errors never exceeds 3 deg and the RMS resulted in $0.69 - 0.74$ deg. Although this system was not able to run in real-time it is the best estimator found for estimating the articulation angle. In [7] a model calculating the articulation angle from yaw-rate of the truck and steering angle is developed. The resulting error is at most 5.37 deg and has a standard deviation of 1.27 deg. Another study[6] uses a similar estimator, but does not present quantified errors. Observing the articulation angle from simulation and from estimate, the maximum error is around the value found in [7], 5 deg. However note that this is comparing a 20 DoF simulation, which may not match a real life situation.

1.3 Purpose

The aim of this Master Thesis is to design an virtual sensor that calculates the articulation angle. This sensor has to match the safety requirements ASIL-D. This is achieved by giving data, from actual sensors matching the safety requirements, as input to an estimator. To ensure accuracy of the estimator it will be compared to the ground truth from empirical data. A goal is set to maintain the angular error below one degree at all times.

1.3.1 Research Question

This project answers the following questions:

- How feasible is a virtual articulation sensor based on sensors matching the signal integrity requirements for safety critical vehicle functions?
- How can the error of such a virtual sensor be quantified?

1.4 Limitations

1. The estimation will only be done for one specific tractor and trailer combination. If possible, it would be a great asset to Volvo if the developed algorithms would be able applicable to different semitrailer combinations with a change in parameters. Limited to one tractor and one trailer.
2. The payload is assumed to be constant and not movable. This because a payload, like a water tank and will have a much higher complexity and needs more time to develop.
3. When predicting the state of the truck in the next time-step there are a many external conditions that may affect the prediction and thereby the performance of the estimation. A few example of these are wind, temperature, road incline.

If these conditions affects the estimator a decision will be taken on whether the condition needs to be taken into consideration to develop a robust and accurate estimation.

4. The estimator is required to run in real-time to give relevant data to the user. However, this report will not evaluate if the estimator is able achieve this.

2
Theory

In the following sections the necessary theory to understand the implementation of the developed estimators is presented.

2.1 Nomenclature

This thesis uses the vehicle dynamics sign convention according to ISO-8855[9]. This standard uses the right-handed axis system with the z-axis pointing up. Positive angles are defined as counter-clockwise around each axis. The articulation angle can be described as the steering angle of the trailer. A positive articulation angle means the tractor is to the left of the trailer, as seen in fig 2.1. In the figure below the most important parameters are shown. More parameters will be presented in this chapter when relevant.

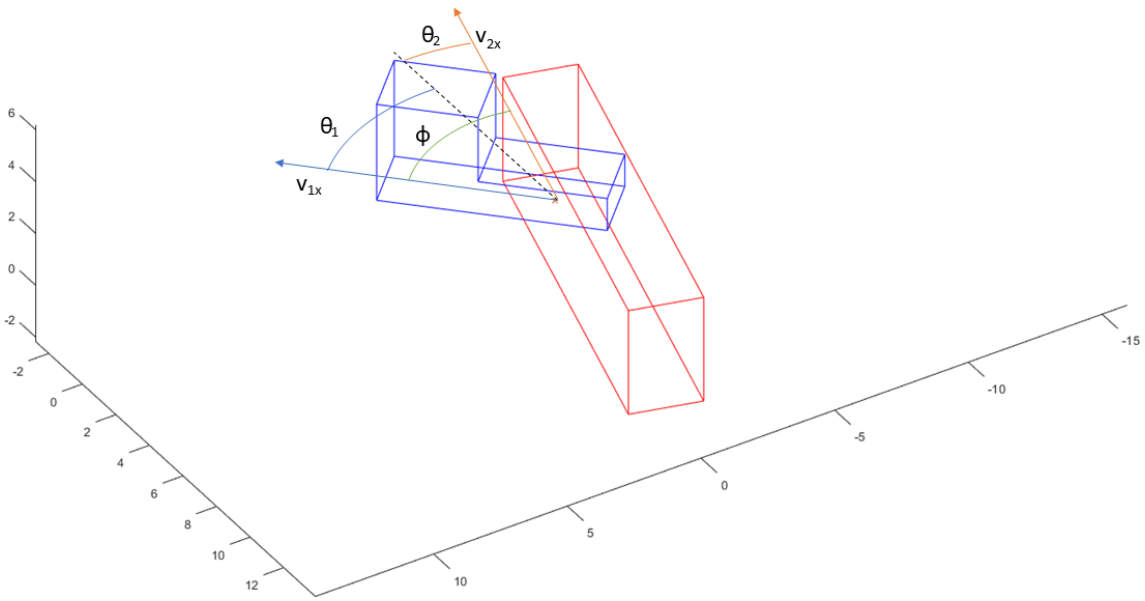

Figure 2.1: Visualisation of a tractor and trailer

2.2 Sensor

In this section the mathematical models of two sensors are described. They are later needed to calculate relevant data.

2.2.1 Speedometer

The centralized velocity of a vehicle can be described from the speed from two wheels on the same axle. The relevant parameters are visualised in figure 2.2 and presented in table 2.1.

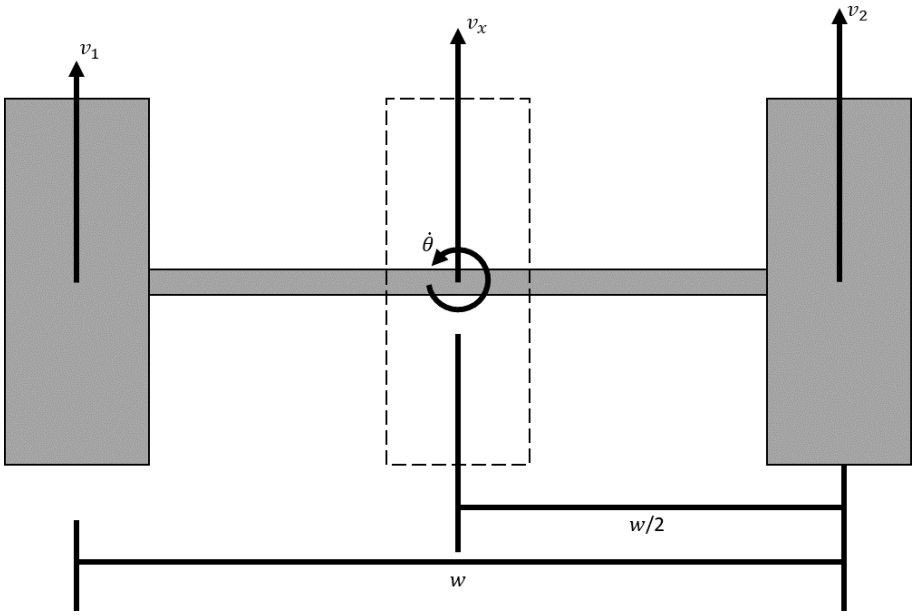

Figure 2.2: Wheel Speed Coordinate Systemq

v_x	Speed at the center of the axle
v_1	Left wheel hub speed
v_2	Right wheel hub speed
$\dot{\theta}$	Yaw-Rate of axle
w	Width of the wheelbase

Table 2.1: Variables used in the Speedometer section

The speed of the center of the axle, v_x, can be calculated as follows given the yaw rate, $\dot{\theta}_1$ and the hub speed of either wheel.

$$v_x = v_1 + \frac{\dot{\theta}_1 \cdot w}{2} \tag{2.1}$$

$$v_x = v_2 - \frac{\dot{\theta}_1 \cdot w}{2} \tag{2.2}$$

$$\tag{2.3}$$

Hence central speed can be calculated as the average of one wheel pair. This assumes there is no longitudinal slip on the wheels.

$$v_x = \frac{v_1 + v_2}{2} \tag{2.4}$$

2.2.2 Wire length to Articulation Angle

Some of test data given by Volvo is based on a system with two wires connecting the tractor and trailer. By measuring the length of these wires the articulation angle can be determined. The concept, with relevant variables, is illustrated in figure 2.3 and described in table 2.2

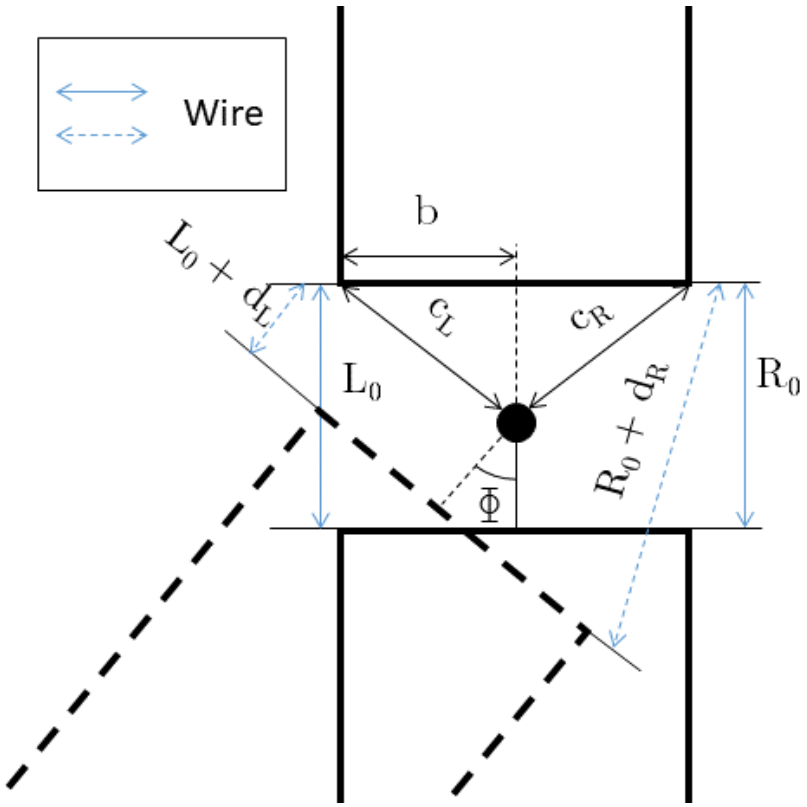

Figure 2.3: Setup of the wire sensor.

L_0	Length of left wire when the articulation angle is zero
R_0	Length of right wire when the articulation angle is zero
b	Orthogonal distance from articulation point to sensor
c_L	Diagonal distance from sensor to articulation point
c_R	Diagonal distance from sensor to articulation point
d_L	Extension of left-wire from L0
d_R	Extension of right-wire from L0
ϕ	Articulation angle

Table 2.2: Variables used in the Wire Length to Articulation Angle section.

The articulation angle, ϕ, can be calculated as follows if looking at the left wire.

$$\phi = \pi/2 - \cos^{-1}(T_L/N_L) \tag{2.5}$$

Where T_L and N_L are described below.

$$T_L = b^2 + (L_0 - d_L)^2 - c_L^2 \tag{2.6}$$
$$N_L = 2 \cdot b \cdot (L_0 - d_L) \tag{2.7}$$
$$\tag{2.8}$$

The right wire is uses the same algorithms and corresponding variables.

$$\phi = -\pi/2 + \cos^{-1}(T_R/N_R) \tag{2.9}$$
$$T_R = b^2 + (R_0 - d_R)^2 - c_R^2 \tag{2.10}$$
$$N_R = 2 \cdot b \cdot (R_0 - d_R) \tag{2.11}$$
$$\tag{2.12}$$

2.3 Estimation

This section gives a brief overview of the filters used in the project. These filters are the Kalman Filter, and its non-linear alternative, the Unscented Kalman Filter (UKF).

2.3.1 Kalman Filter

Kalman filters[12] uses Bayesian statistics[4] to, from previous knowledge, make a more accurate estimation of the current state. The state contains all of the variables that are of current interest, x_{k-1}. From the previous timestep knowledge of how uncertain the states are is available. These uncertainties are assumed to be of Gaussian distribution and describe the covariance of that Gaussian distribution. Through the motion model the state for the next time-step is predicted. By combining the current state and it's uncertainty with the measurements and knowledge of their noise a better estimation can be achieved. Under the assumption of the following.

- Measurement with Gaussian noise.
- The motion model is linear.
- The motion models noise is Gaussian.

Then the Kalman Filter is the optimal estimator.[20]. The relevant parameters are presented in table 2.3.

F_k	Motion model at time k
H_k	Measurement model at time k
$\hat{x}_{k\|k-1}$	Predicted state at time k, given state from time k-1, the prior
$\hat{x}_{k\|k}$	Updated state at time k, given measurements from time k, the posterior
$\hat{y}_k$	Estimated measurements at time k
y_k	Measurements at time k
v_k	Innovation at time k
S_k	Innovation Covariance at time k
K_k	Optimal Kalman gain at time k
$P_{k\|k-1}$	Predicted covariance at time k, the prior covariance
$P_{k\|k}$	Updated covariance at time k, the posterior covariance
Q_k	Motion model uncertainty at time k, normal distributions
R_k	Measurement model noise at time k, normal distributions

Table 2.3: Parameters used in the kalman filter

For the Kalman Filter each time-step contains two steps. These are the prediction step and the update step. A depiction of how the Kalman Filter functions is shown in figure 2.4.

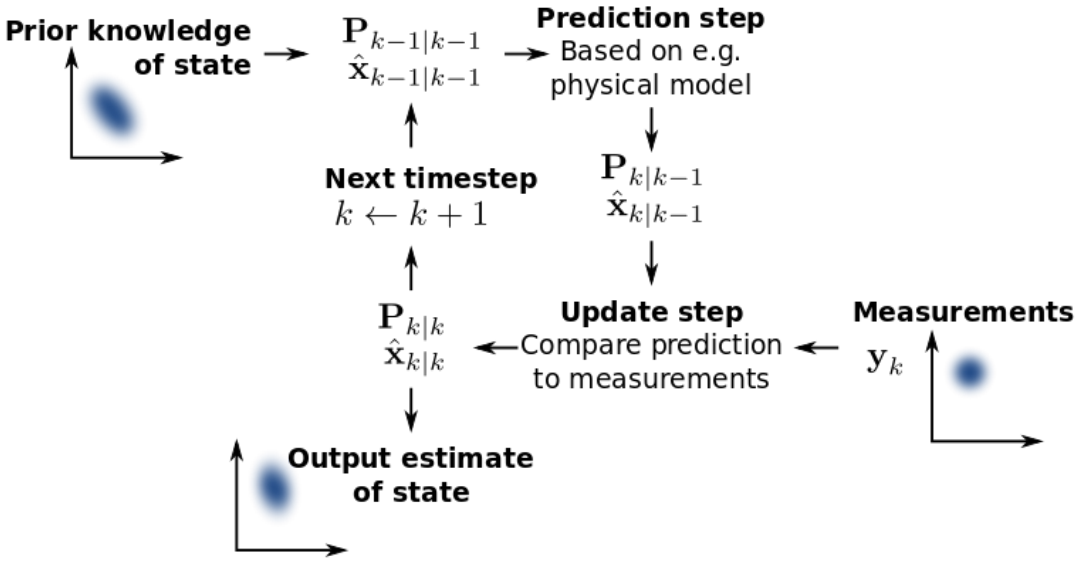

Figure 2.4: Basic Concept of Kalman Filtering[3]

The prediction step describes what the state at timestep k is predicted to be, $\hat{x}_{k|k-1}$. This is calculated from the previous timestep, $\hat{x}_{k-1|k-1}$, and the motion model, F_k. The motion is usually based on a physical model and describes how the state changes. The motion model can additionally use the user's input for the current state to assist in the prediction. The uncertainty of the state at timestep k, $P_{k|k-1}$, is calculated from the previous uncertainty, $P_{k-1|k-1}$, and the motion model. A process noise, Q_k, is added as no model describes the physical model perfectly. The prediction is

described below.

$$\hat{x}_{k|k-1} = F_k \hat{x}_{k-1|k-1} \tag{2.13}$$

$$P_{k|k-1} = F_k P_{k-1|k-1} F_k^T + Q_k \tag{2.14}$$

The update step uses the measurements from the actual data to refine the state. Through the measurement model, H_k, the predicted state describes the expected measurements, $\hat{y}_{k|k-1}$. The difference between the actual y_k and expected measurement is the innovation, v_k. For the uncertainty a innovation covariance, S_k is calculated from the predicted uncertainty, measurement model and measurement noise, R_k. The Kalman gain, K_k, is calculated and used to get the updated state, $\hat{x}_{k|k}$, and its uncertainty, $P_{k|k}$. These calculations are described by the equations are described in 2.15-2.20.

$$\hat{y}_{k|k-1} = H_k \hat{x}_{k|k-1} \tag{2.15}$$

$$v_k = y_k - \hat{y}_{k|k-1} \tag{2.16}$$

$$S_k = H_k P_{k|k-1} H_k^T + R_k \tag{2.17}$$

$$K_k = P_{k|k-1} H_k^T S_k^{-1} \tag{2.18}$$

$$\hat{x}_{k|k} = \hat{x}_{k|k-1} + K_k v_k \tag{2.19}$$

$$P_{k|k} = (I - K_k H_k) P_{k|k-1} \tag{2.20}$$

The Kalman Filter is limited to using linearized models around a certain point. In this thesis this won't suffice. A non-linear version of the kalman filter is required.

2.3.2 Unscented Kalman filter

The Unscented Kalman Filter[1] has the advantage of not requiring linearized models. When using a non-linear model, simply calculating the uncertainty as done in the Kalman Filter is not possible. To approximate the uncertainty a few methods are applicable. The one used in this thesis is the Uncented Kalman Filter, described in this section. The parameters used are described in Table 2.4.

f_k	Motion model at time k
h_k	Measurement model at time k
$\hat{x}_{k\|k-1}$	Predicted state at time k, given state from time k-1, the prior
$\hat{x}_{k\|k}$	Updated state at time k, given measurements from time k, the posterior
$\hat{y}_k$	Estimated measurements at time k
y_k	Measurements at time k
v_k	Innovation at time k
S_k	Innovation Covariance at time k
K_k	Optimal Kalman gain at time k
$P_{k\|k-1}$	Predicted covariance at time k, the prior covariance
$P_{k\|k}$	Updated covariance at time k, the posterior covariance
Q_k	Motion model uncertainty at time k, normal distributions
R_k	Measurement model noise at time k, normal distributions
$\mathbf{P_i}$	ith column of the covariance matrix
$\mathcal{X}^{(i)}$	i:th sigma point
W_i	Weight of sigma point i
n	Number of sigma points

Table 2.4: Notation

The simplified explanation of this method is as follows. Points, $\mathcal{X}_\rangle$, at the edge of the uncertainty around the estimated state are collected. Additionally a weight, W_i, for each point is calculated. Here n is two times the number of states plus one.

$$\mathcal{X}^{(0)} = \hat{\mathbf{x}} \tag{2.21}$$

$$\mathcal{X}^{(i)} = \hat{\mathbf{x}} + \sqrt{\frac{n}{1-W_0}\mathbf{P}_i^{1/2}}, \qquad \text{i = 1, 2,...,n} \tag{2.22}$$

$$\mathcal{X}^{(i+n)} = \hat{\mathbf{x}} - \sqrt{\frac{n}{1-W_0}\mathbf{P}_i^{1/2}}, \qquad \text{i = 1, 2,...,n} \tag{2.23}$$

$$W_0 = 1 - n/3 \tag{2.24}$$

$$W_i = \frac{1-W_0}{2n} \tag{2.25}$$

The prediction is done on each of these points. And a new uncertainty is calculated. The prediction model is here denoted $\mathbf{f}(x, u, T)$. The model takes in x, u and T, with x being the current state, u being the control inputs at current state and T

being how much time has passed between the two time-steps.

$$\hat{\mathbf{x}}_{k|k-1} = \sum_{i=0}^{2n} f(\mathcal{X}^{(i)}, T)W_i \tag{2.26}$$

$$s(i) = f(\mathcal{X}^{(i)}) - \hat{\mathbf{x}}_{k|k-1} \tag{2.27}$$

$$P_{k|k-1} = \mathbf{Q}_{k-1} + \sum_{i=0}^{2n}(s(i) \cdot W_i \cdot s^T(i)) \tag{2.28}$$

In the update step, just as in the prediction step, sigma points are calculated. Here $h(x)$ is the measurement model. P_{xy} is the measurement uncertainty. Except for this, the Unscented Kalman Filter is the same as the Kalman Filter.

$$\hat{y}_{k|k-1} = \sum_{i=0}^{2n} h(\mathcal{X}^{(i)})W_i \tag{2.29}$$

$$P_{xy} = \sum_{i=0}^{2n}(\mathcal{X}^{(i)} - \hat{x}_{k|k-1})(h(\mathcal{X}^{(i)}) - \hat{y}_{k|k-1})^T W_i \tag{2.30}$$

$$S_k = R_k + \sum_{i=0}^{2n}\Big((h(\mathcal{X}^{(i)}) - \hat{y}_{k|k-1})(h(\mathcal{X}^{(i)}) - \hat{y}_{k|k-1})^T\Big)W_i \tag{2.31}$$

$$v = y_k - \hat{y}_{k|k-1} \tag{2.32}$$

$$\hat{\mathbf{x}}_{k|k} = \hat{\mathbf{x}}_{k|k-1} + P_{xy}S^{-1}v \tag{2.33}$$

$$P_{k|k} = P_{k|k-1} - P_{xy}S^{-1}P_{xy}^T \tag{2.34}$$

2.4 Model

The motion model of a tractor-semitrailer's yaw motion can be either kinematic or dynamic. All three models presented in this thesis all depend on two simplifications. The first simplification being that each wheel pair has been simplified to one central wheel, a so called single-track model. The second simplification is a replacement of the three axles on the trailer to one axle, and replacement of the two rear axles on the tractor to one axle, these replacements are called the equivalent wheel axles. The replacement axle on the tractor is placed at the distance L_1 from the front axle. On the trailer, the replacement axle is placed at the distance L_2 from the articulation point, P.

2.4.1 Kinematic model

The least complicated of these models is the single track kinematic model. This model assumes that there is no slip in any of the wheels. Which in turn results in no lateral velocity at the equivalent wheel base.

P	The articulation point, fifth wheel, where the trailer connects to the tractor.
β	Slip-angle at articulation point between tractor and trailer.
δ	Steering angle on front axle of the truck.
$v_x^{(1)}$	Longitudinal speed of the tractor.
$v_x^{(2)}$	Longitudinal speed of the trailer.
$v_y^{(2c)}$	Lateral speed of the trailer at the articulation point.
$\dot{\theta}_1$	Yaw-rate of the tractor.
$\dot{\theta}_2$	Yaw-rate of the trailer.
ϕ	Articulation angle between trailer and tractor.
L_1	Distance from front axle to equivalent tractor rear axle.
L_2	Distance from articulation point to equivalent trailer rear axle.
R_t	Distance from center of trailer to the common pivot point, O_2.
a	Distance from articulation point to first real axle on trailer.
e	Distance between real axles on trailer.
b	Distance between equivalent axle and articulation point on tractor.

Table 2.5: Variables used in the kinematic model.

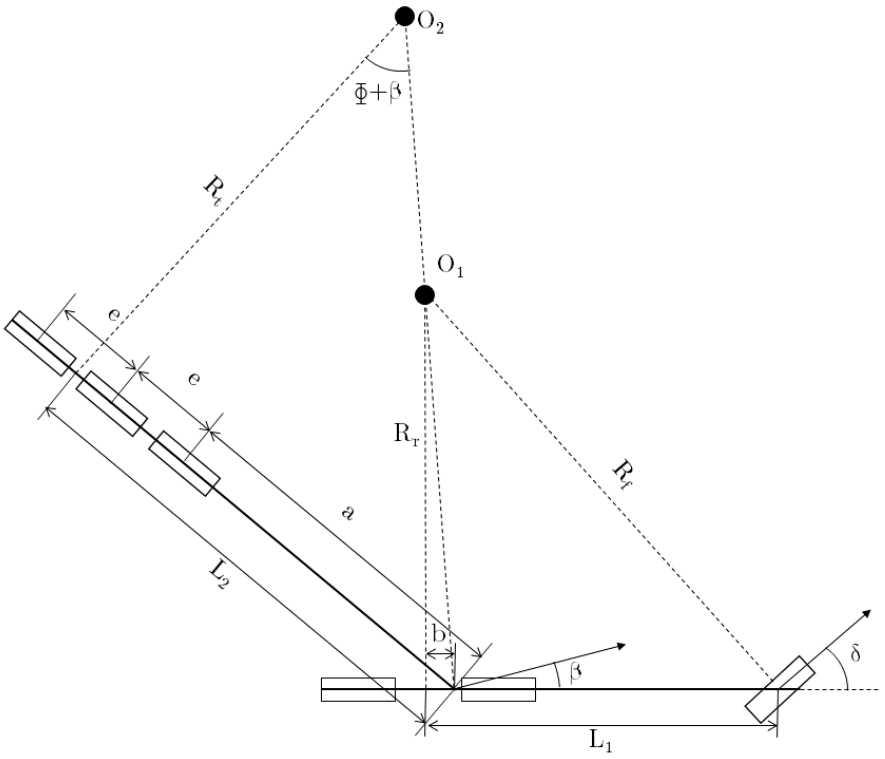

Figure 2.5: Kinematic model for tractor and trailer.

In a paper by B. Källstrand he presents how the variables of one unit can be described by variables from the other unit. [11]. This model assumes Ackermann steering introduced in 1818[15].

The Ackermann steering describes where the rotation point of a vehicle is, based on its steering angle. To begin with, the yaw-rate of the trailer can be described

as the longitudinal velocity, divided by the lateral distance to the rotation point. Using trigonometry, the articulation angle can be connected to the distances to the equivalent wheelbase and the lateral distance to the rotation point.

$$\dot{\theta}_2 = \frac{v_{x2}}{R_t} \tag{2.35}$$

$$tan(\phi + \beta) = \frac{L_2}{R_t} \tag{2.36}$$

Through manipulation of equations (2.35)-(2.36), the yaw-rate of the trailer can be described as follows.

$$\dot{\theta}_2 = \frac{v_x^{(2)}}{L_2} tan(\phi + \beta) \tag{2.37}$$

Remaining variable β, is the slip-angle of the vehicle at the articulation point. This variable can be calculated in at least two methods. Motivation for the first method is as follows. The slip-angle at a certain point of the vehicle is the angle from the x-axis of the vehicle to the actual velocity of said point. As described earlier, slip-angle in the equivalent wheel base is zero. With no slip angle on any of the wheels, the slip angle at the front of the trailer is the steer angle. As the tractor is a rigid body, the lateral velocity is linear along the vehicle, depending on the yaw-rate.

$$\kappa = \tan^{-1}\left(\frac{v_y^{(\kappa)}}{|v_x|}\right) \tag{2.38}$$

The slip angle is here defined as κ and the lateral velocity at this point is $v_y^{(\kappa)}$. With this equation and previous motivation, a formula for β can be derived.

$$\beta = tan^{-1}\left(\frac{tan(\delta)b}{L_1}\right) \tag{2.39}$$

The second method is based on that the lateral velocity at a any given point of the vehicle is dependent on the yaw-rate and distance to the equivalent wheel-base.

$$\beta = tan^{-1}\left(\frac{\dot{\theta}_1 b}{|v_x^{(1)}|}\right) \tag{2.40}$$

The longitudinal velocity is equal along the length of the trailer. Each method has its drawback. With the first method any slip on the front wheels is discarded, which might affect the results. The second method relies on a division by the longitudinal velocity. If this velocity is close to zero, the result becomes very unreliable.

To completely define the yaw-rate of the trailer with variables of the tractor, the longitudinal velocity, $v_x^{(2)}$, can be described as a coordinate change from the longitudinal velocity of the tractor. The lateral velocity at the articulation point has been described earlier.

$$\begin{bmatrix} v_x^{(2)} \\ v_y^{(2c)} \end{bmatrix} = \begin{bmatrix} cos(\phi) & -sin(\phi) \\ sin(\phi) & cos(\phi) \end{bmatrix} \begin{bmatrix} v_x^{(1)} \\ v_x^{(1)} tan(\beta) \end{bmatrix} \tag{2.41}$$

From this rotational coordinate change $v_x^{(2)}$ can be expressed through $v_x^{(1)}$.

$$v_x^{(2)} = v_x^{(1)}(cos(\phi) - sin(\phi)tan(\phi)) \tag{2.42}$$

Using (2.42) in (2.37) gives the following.

$$\dot{\theta}_2 = \frac{v_x^{(1)}}{L_2}(sin\phi + cos\phi tan\beta) \tag{2.43}$$

Using (2.43) and (2.39) $\dot{\theta}_2$, can instead be described with $\dot{\theta}_1$, v_{x1}, ϕ.

$$\dot{\theta}_2 = \frac{v_x^{(1)}}{L_2}\left(sin\phi + cos\phi\frac{\dot{\theta}_1 b}{v_x^{(1)}}\right) \tag{2.44}$$

Equation (2.44) depends on two parameters, L_2 and b. From analysing the equation it's evident that L_2 will affect the estimator's behavior, especially the magnitude of the articulation angle. The two distances describe the distance from the articulation point to the equivalent wheelbase. A simple solution is to place the equivalent axle in the center between the two actual axles. Another way to perform this is to calculate the torque equilibrium.

Torque Equilibrium at Point P1

The torque equilibrium assumes steady state. This section goes through the necessary equation to calculate where the equivalent wheelbase is in this situation. The tire model used here is described in the Vehicle Dynamics Compendium [10].

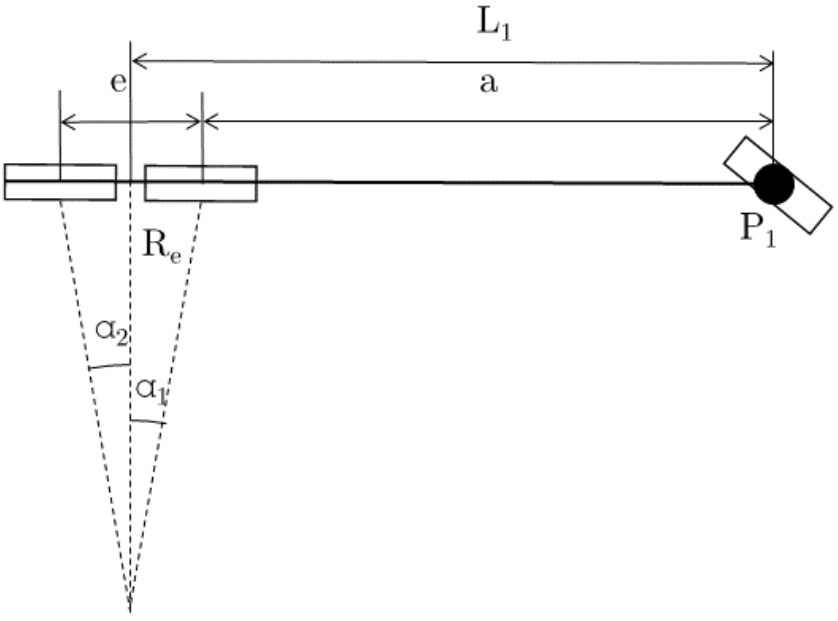

Figure 2.6: A simple force model for tractor.

Figure 2.6 shows parameters used in this section.

$$C_i = C_{Ci} F_{zi} \tag{2.45}$$

C_i is the cornering stiffness and C_{ci} is the cornering coefficient. Geometric relationships gives the following.

$$tan(\alpha_1) = \frac{L_1 - a}{R_e}, tan(\alpha_2) = \frac{L_1 - e - a}{R_e} \tag{2.46}$$

In this case steady state, means there is a constant yaw rate. The change in moment inertia is zero. The torque equilibrium is calculated in point P_1. By calculating the torque here, any forces on the front axle is canceled out.

$$\circlearrowleft + P_1 = C_1 tan(\alpha_1)(a) + C_2 tan(\alpha_2)(a + e) = 0 \tag{2.47}$$

Using equation (2.45) and (2.47):

$$C_{C1} F_{z1} tan(\alpha_1)(a) + C_{C2} F_{z2} tan(\alpha_2)(a + e) = 0 \tag{2.48}$$

Combine equation (2.46) and (2.48):

$$C_{C1} F_{z1} \frac{L_1 - a}{R_e} a + C_{C2} F_{z2} \frac{L_1 - a - e}{R_e} (a + e) = 0 \tag{2.49}$$

As the rear axles of the vehicle are of the same type, it can be assumed that $C_{C1} = C_{C2}$, this allows a few simplifications.

$$L_1 a + L_1 (a + e) = a^2 + (a + e)(a + e) \tag{2.50}$$

$$L_1 = \frac{F_{z1} a^2 + F_{z2} (a + e)(a + e)}{F_{z1} a + F_{z2} (a + e)} \tag{2.51}$$

If the normal forces are assumed to be equal, $F_{z1} = F_{z2}$, the resulting equation is the following. The closer the axles are two eachother, this statement becomes more realistic.

$$L_1 = \frac{a^2 + (a + e)(a + e)}{a + (a + e)} \tag{2.52}$$

There are two additional assumptions used in this model, they are, no lateral slip on the front wheels and that the forces in the articulation point are negligible. A more developed model is theoretical move front wheel axle forward to match the steering angle with actual movement [21]. The affect of the two assumptions are not investigated in this report.

Torque Equilibrium at Point P2

Just as in the calculation for L_1, an equation for L_2 could be derived with the same approach.

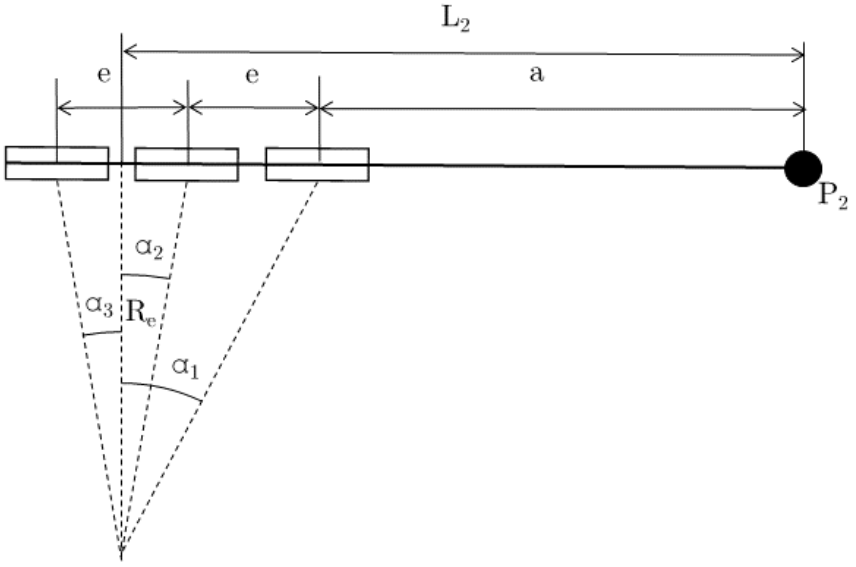

Figure 2.7: A simple force model for trailer.

$$tan(\alpha_1) = \frac{L_2 - a}{R_e}, tan(\alpha_2) = \frac{L_2 - a - e}{R_e}, tan(\alpha_3) = \frac{L_2 - 2e - a}{R_e} \tag{2.53}$$

Assuming steady state, in this case constant yaw rate. The point P_2 is chosen as the forces on P_2 is irrelevant for this calculation.

$$\circlearrowleft + P_2 = C_1 tan(\alpha_1)(a) + C_2 tan(\alpha_2)(a + e) + C_3 tan(\alpha_3)(a + 2e) = 0 \tag{2.54}$$

Using equation (2.54) and (2.54):

$$C_{C1} F_{z1} tan(\alpha_1)(a) + C_{C2} F_{z2} tan(\alpha_2)(a + e) + C_{C3} F_{z3} tan(\alpha_3)(a + 2e) = 0 \tag{2.55}$$

Assume $C_{C1} = C_{C2} = C_{C3}$ and combine equation (2.53) and (2.55):

$$F_{z1} \frac{L_2 - a}{R_e} a + F_{z2} \frac{L_2 - a - e}{R_e} (a + e) + F_{z3} \frac{L_2 - a - 2e}{R_e} (a + 2e) = 0 \tag{2.56}$$

$$F_{z1} L_2 a - F_{z1} a^2 + F_{z2} L_2 (a+e) - F_{z2} (a+e)^2 + F_{z3} L_2 (a+2e) - F_{z3} (a+2e)^2 = 0 \tag{2.57}$$

$$L_2 = \frac{F_{z1} a^2 + F_{z2} (a + e)^2 + F_{z3} (a + 2e)^2}{F_{z1} a + F_{z2} (a + e) + F_{z3} (a + 2e)} \tag{2.58}$$

Assume F_{z1}, F_{z2} and F_{z3} are equal results in the following equation.

$$L_2 = \frac{a^2 + (a + e)^2 + (a + 2e)^2}{a + (a + e) + (a + 2e)} \tag{2.59}$$

2.4.2 Kinematic Model with Lateral Velocity

While the kinematic model assumes no lateral velocity in the equivalent wheel base, this is not true for an actual vehicle. This model uses the vehicle description in

section 2.4.1, with the addition of a known lateral velocity. The point O_1 and O_2 are fixed points on the vehicle. If a angle-rate change from moment equality is to be added, these points should be placed in the Center of Gravity (CoG) of each unit. Figure 2.8 presents the parameters, and table

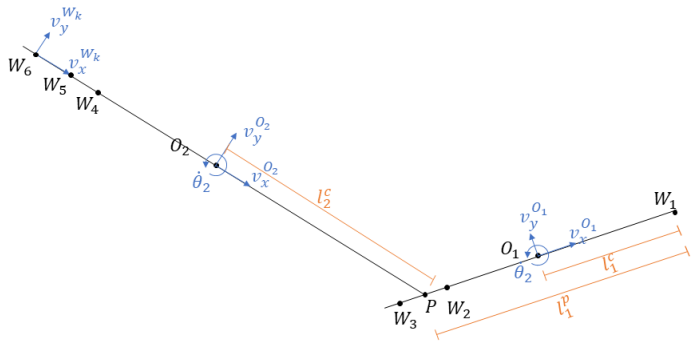

Figure 2.8: Kinematic model for tractor and trailer with lateral velocity.

P	The articulation point, fifth wheel, where the trailer connects to the tractor.
$v_x^{(1)}$	Longitudinal speed of the tractor.
$v_x^{(2)}$	Longitudinal speed of the trailer.
$v_y^{P_1}$	Lateral speed of the tractor in the articulation point.
$v_y^{P_2}$	Lateral speed of the trailer in the articulation point.
$v_y^{P_1}$	Lateral speed of the tractor in the O_1 point.
$v_y^{P_2}$	Lateral speed of the trailer in the O_2 point.
$\dot{\theta}_1$	Yaw-rate of the tractor.
$\dot{\theta}_2$	Yaw-rate of the trailer.
ϕ	Articulation angle between trailer and tractor.
l_1^c	Distance to the O_1 point from the front axle of the tractor
l_1^f	Distance to the articulation point from the front axle of the tractor
l_2^c	Distance to the O_2 point from the articulation point.

Table 2.6: Variables used in the kinematic model.

$$v_x^{P_1} = v_x^{O_1} \tag{2.60}$$
$$v_y^{P_1} = v_y^{O_1} - \dot{\theta}_1(l_1^p - l_1^c) \tag{2.61}$$
$$v_x^{P_2} = v_x^{O_2} \tag{2.62}$$
$$v_y^{P_2} = v_y^{O_2} + \dot{\theta}_2 l_2^c \tag{2.63}$$
$$\tag{2.64}$$

Shown in equation (2.60)-(2.63), along the length of the vehicle, the lateral velocity changes, the longitudinal velocity does not. The change of lateral velocity is distance multiplied by the yaw-rate. The point P has the same velocity for each unit, but with different coordinate systems, rotated ϕ degrees. Performing the rotation results in the following relationship.

$$v_x^{P_2} = v_x^{P_1} cos(\phi) - v_y^{P_1} sin(\phi) \tag{2.65}$$
$$v_y^{P_2} = v_y^{P_1} cos(\phi) + v_x^{P_1} sin(\phi) \tag{2.66}$$
$$v_x^{P_1} = v_x^{P_2} cos(-\phi) - v_y^{P_2} sin(-\phi) \tag{2.67}$$
$$v_y^{P_1} = v_y^{P_2} cos(-\phi) + v_x^{P_2} sin(-\phi) \tag{2.68}$$
$$\tag{2.69}$$

From the lateral velocity description a formula for the yaw-rate can be derived.

$$\dot{\theta}_1 = \frac{v_y^{O_1} - v_y^{P_1}}{l_1^P - l_1^O} \tag{2.70}$$
$$\dot{\theta}_2 = \frac{v_y^{P_2} - v_y^{O_2}}{l_2^O} \tag{2.71}$$
$$\tag{2.72}$$

Finally, let's describe the longitudinal velocity and the yaw-rate in terms of the velocities of the opposite unit.

$$v_x^{P_1} = v_x^{P_2} cos(-\phi) - v_y^{P_2} sin(-\phi) \tag{2.73}$$
$$v_x^{P_2} = v_x^{P_1} cos(\phi) - v_y^{P_1} sin(\phi) \tag{2.74}$$
$$\dot{\theta}_1 = \frac{v_y^{O_1} - v_x^{P_2} sin(-\phi) + v_y^{P_2} cos(-\phi)}{l_1^P - l_1^O} \tag{2.75}$$
$$\dot{\theta}_2 = \frac{v_x^{P_1} sin(\phi) + v_y^{P_1} cos(\phi) - v_y^{O_2}}{l_2^O} \tag{2.76}$$

2.4.3 Dynamic Based Model

The Dynamic Model described here is a Single-Track Model. The two rear axles on the Tractor simplified with one axle, and the three axles of the trailer simplified to one. The simplified axle is placed in the middle of the replaced axles, with an added torque. The Dynamic Model is based on the Kinematic Model, with additional equations explaining where each velocity originates from, how the forces affects the vehicle. With these equations the lateral velocity can be determined and thereby using the equations from Kinematic Model with Lateral Velocity, from section 2.4.2. To achieve this a few additional equations are added.

- Constitution for axles on 1^{st} unit
- Compatibility, shifting lateral velocity within 1^{st} unit

- Constitution for axles on 2^{nd} unit
- Compatibility, within 2^{nd} unit
- Equilibrium of coupling
- Constitution for coupling
- Dynamic Equilibrium of 1^{st} unit
- Dynamic Equilibrium of 2^{nd} unit

A few new notations are needed.

P	The articulation point, fifth wheel, where the trailer connects to the tractor.
δ	Steering angle on front axle of the truck.
$v_x^{(k)}$	Longitudinal speed of unit k.
$v_y^{(k)}$	Lateral speed of unit k in CoG.
$v_y^{(kh)}$	Lateral speed of unit k in point h
$s_h^{(k)}$	Slip-angle in point h of unit k
$C_h^{(k)}$	Cornering stiffness in point h of unit k
$M^{(k)}$	Torque from simplifying axles in unit k
$F_y^{(kh)}$	Lateral force of unit k at point h
$F_z^{(kh)}$	Vertical force of unit k at point h
$\dot{\theta}_k$	Yaw-rate of unit k.
ϕ	Yaw angle between trailer and tractor.
J_k	Inertia of unit k
m_k	Mass of unit k

Table 2.7: Variables used in the kinematic model

2.4.4 Constitution for axles on 1^{st} unit

Each axle has it's own slip-Angle. As small slip-angles are assumed, $a \approx \tan^{-1}(a)$

$$s_f^{(1)} = \frac{v_y^{(1f)}}{|v_x^{(1)}|} \tag{2.77}$$

$$s_r^{(1)} = \frac{v_y^{(1r)}}{|v_x^{(1)}|} \tag{2.78}$$

The cornering stiffness is linearly dependant on load on each axles, the normalised cornering coefficient is a constant, that can be assumed to be around $C_c \in [5, 10]1/\text{rad}$ [10].

$$C_f^{(1)} = F_z^{(1f)} \cdot C_c \tag{2.79}$$

$$C_r^{(1)} = F_z^{(1f)} \cdot C_c \tag{2.80}$$

The lateral forces are then calculated from Cornering Stiffness and slip angle

$$F_y^{(1f)} = -C_f^{(1)} \cdot s_f^{(1)} \tag{2.81}$$

$$F_y^{(1r)} = -C_r^{(1)} \cdot s_r^{(1)} \tag{2.82}$$

$$\tag{2.83}$$

Remaining Torque From Simplifying to One Axle

When simplifying the multiple axles into a single axis, there is a resulting force and a resulting torque. The torque varies depending on where the resulting force is placed. This torque is calculated from the lateral force shown earlier.

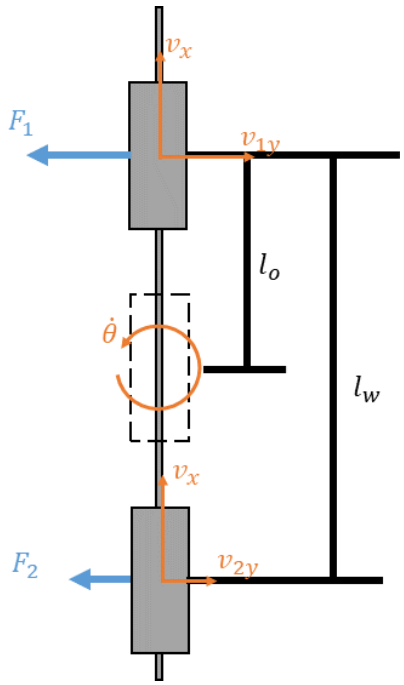

Figure 2.9: Simplification of axles to one axle.

Additional variables used here to explain the torque that are only used within this section.

v_{1y}	Lateral velocity of the first rear axle
v_{2y}	Lateral velocity of the second rear axle
F_1	Lateral force from first rear axle
F_2	Lateral force form second rear axle
l_o	Distance to the simplified axle, from the first axle
l_w	Distance between the axles.

Table 2.8: Variables for remaining torque.

First describe the lateral forces.

$$F_1 = -\frac{C_{1r} v_{1y}}{|v_x|} \tag{2.84}$$

$$F_2 = -\frac{C_{2r} v_{2y}}{|v_x|} \tag{2.85}$$

Compatibility within rear axle.

$$v_{1y} = v_y^{(1r)} + l_o \cdot \dot{\theta}_1 \tag{2.86}$$
$$v_{2y} = v_y^{(1r)} - (l_w - l_o) \cdot \dot{\theta}_1 \tag{2.87}$$

Now calculate the torque in the simplified axle.

$$M^{(1)} = F_1 l_o - F_2(l_w - l_o) \tag{2.88}$$
$$M^{(1)} = \frac{C_{1r} \cdot (v_y^{(1r)} + l_o \cdot \dot{\theta}_1) \cdot l_o - C_{2r} \cdot (v_y^{(1r)} - (l_w - l_o) \cdot \dot{\theta}_1) \cdot (l_w - l_o)}{|v_x|} \tag{2.89}$$

As the axles are close to each other, the load on each axle is similar. From the load the cornering stiffness is calculated. Assume the difference between the two cornering stiffness is negligible. Additionally placing the simplified axle in the middle allows the resulting torque equation to be very simplified.

$$M^{(1)} = \frac{\dot{\theta}_1 (\frac{l_w^1}{2})^2}{2|v_x^1|} \tag{2.90}$$

Compatibility within 1^{st} unit

Longitudinal velocity is the same over length of the unit. Lateral is linearly dependant on lateral velocity in CoG and yaw-rate

$$v_{ry}^{(1)} = v_y^{(1)} - \dot{\theta}_1 l_r^{(1)} \tag{2.91}$$
$$v_{fy}^{(1)} = v_y^{(1)} + \dot{\theta}_1 l_f^{(1)} \tag{2.92}$$
$$v_{cy}^{(1)} = v_y^{(1)} - \dot{\theta}_1 l_c^{(1)} \tag{2.93}$$

Constitution for axles on 2^{nd} unit

Each axle has it's own Slip-Angle.

$$s_r^{(2)} = \frac{v_{y_r}^{(2)}}{|v_x^{(2)}|} \tag{2.94}$$

The cornering stiffness is linearly dependant on load on each axles, the cornering coefficient is a constant, that can be assumed to be around $C_c \in [5, 10]1/\text{rad}$ [10].

$$C_r^{(2)} = F_{z_r}^{(2)} \cdot C_c \tag{2.95}$$

The lateral forces are then calculated from Cornering Stiffness and slip angle

$$F_y^{(2r)} = -C_r^{(2)} \cdot s_r^{(2)} \tag{2.96}$$
$$\tag{2.97}$$

Remaining Torque From Simplifying to One Axle

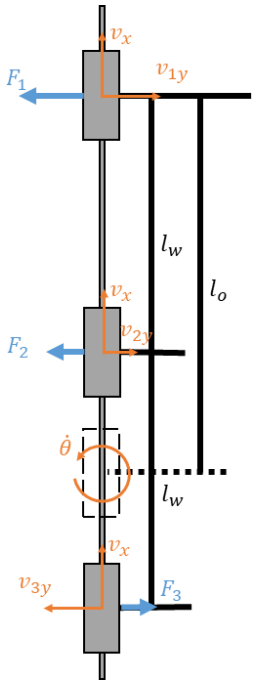

Figure 2.10: Simplification of axles to one axle.

Additional variables used here to explain the torque that are only used within this section.

v_{1y}	Lateral velocity of the first rear axle
v_{2y}	Lateral velocity of the second rear axle
v_{3y}	Lateral velocity of the second rear axle
F_1	Lateral force from first rear axle
F_2	Lateral force form second rear axle
F_3	Lateral force form third rear axle
l_o	Distance to the simplified axle, from the first axle
l_w	Distance between the axles.

Table 2.9: Variables for remaining torque.

First describe the lateral forces.

$$F_1 = -\frac{C_{1r} v_{1y}}{|v_x^{(1)}|} \tag{2.98}$$

$$F_2 = -\frac{C_{2r} v_{2y}}{|v_x^{(1)}|} \tag{2.99}$$

$$F_3 = -\frac{C_{3r} v_{3y}}{|v_x^{(1)}|} \tag{2.100}$$

Compatibility within rear axle.

$$v_{1y} = v_y^{(2r)} + l_o \cdot \dot{\theta}_1 \tag{2.101}$$

$$v_{2y} = v_y^{(2r)} - (l_w - l_o) \cdot \dot{\theta}_1 \tag{2.102}$$

$$v_{3y} = v_y^{(2r)} - (l_w - l_o) \cdot \dot{\theta}_1 \tag{2.103}$$

Now calculate the torque in the simplified axle.

$$M^{(2)} = F_1 l_o + F_2(l_o - l_w) - F_3(2l_w - l_o) \tag{2.104}$$

$$\tag{2.105}$$

As the axles are close to each other, the load on each axle is similar. From the load the cornering stiffness is calculated. Assume the difference between the two cornering stiffness is negligible. Additionally placing the simplified axle in the middle allows the resulting torque equation to be very simplified.

$$M^{(2)} = \frac{2\dot{\theta}_2 (l_w^{(2)})^2}{3|v_x^{(2)}|} \tag{2.106}$$

Compatibility, within 2^{nd} unit

Longitudinal velocity is same over length of the unit.

$$v_y^{(2r)} = v_y^{(2)} - \dot{\theta}_2 l_r^{(2)} \tag{2.107}$$

$$v_y^{(2c)} = v_y^{(2)} + \dot{\theta}_2 l_c^{(2)} \tag{2.108}$$

Constitution for coupling

The force in the coupling is calculated as a dampener between the two units, where the force is linearly dependant on the difference in velocity between the two units.

$$P_x^{(2)} = d \cdot (v_x^{(1)}\cos(\phi) - v_y^{(1)}\sin(\phi) - v_x^{(1)}) \tag{2.109}$$

$$P_y^{(2)} = d \cdot (v_x^{(1)}\sin(\phi) + v_y^{(1)}\sin(\phi) - v_x^{(2)}) \tag{2.110}$$

Equilibrium of coupling

Express the relationship between forces in the two units.

$$P_x^{(2)} + \cos(\phi)P_x^{(1)} - \sin(\phi)P_y^{(1)} = 0 \tag{2.111}$$

$$P_y^{(2)} + \sin(\phi)P_x^{(1)} + \cos(\phi)P_y^{(1)} = 0 \tag{2.112}$$

Dynamic Equilibrium of 1^{st} unit

$$m_1 \cdot (\dot{v}_x^{(1)} - \dot{\theta}_1 \cdot v_y^{(1)}) = F_x^{(1fv)} + F_x^{(1r)} - P_x^{(1)} \tag{2.113}$$
$$m_1 \cdot (\dot{v}_y^{(1)} + \dot{\theta}_1 \cdot v_x^{(1)}) = F_y^{(1fv)} + F_y^{(1r)} - P_y^{(1)} \tag{2.114}$$
$$J_1 \ddot{\theta}_1 = F_y^{(1v)} l_f^{(1)} - F_y^{(1r)} l_r^{(1)} - P_y^{(1)} l_c^{(1)} - M^{(1)} \tag{2.115}$$

Dynamic Equilibrium of 2^{nd} unit

$$m_2 \cdot (\dot{v}_x^{(2)} - \dot{\theta}_2 \cdot v_y^{(2)}) = F_x^{(r2)} + P_x^{(2)} \tag{2.116}$$
$$m_2 \cdot (\dot{v}_y^{(2)} + \dot{\theta}_2 \cdot v_x^{(2)}) = F_y^{(r2)} + P_y^{(2)} \tag{2.117}$$
$$J_2 \ddot{\theta}_2 = F_y^{(2r)} l_r^{(2)} + P_y^{(2)} l_c^{(2)} - M^{(2)} \tag{2.118}$$

3

Method

To achieve the goal of this project, to estimate the yaw-angle between tractor and trailer within one degrees certainty, an initial concept for an estimator is designed and evaluated. The purpose of this concept being to gain understanding of the problems faced when estimating the articulation angle. To evaluate in what conditions the performance is robust and precise the estimator is verified both on empirical data and on simulated data from Volvo's in house simulator, VTM, which will be described in depth in section 3.3.

Verification pointed towards some situations where the performance of the estimator was not up to standard, which is taken into consideration to develop a second and improved estimator. Finally their performances are evaluated and compared. Figure 3.1 depicts the work process. The result of the research is presented in the Theory chapter.

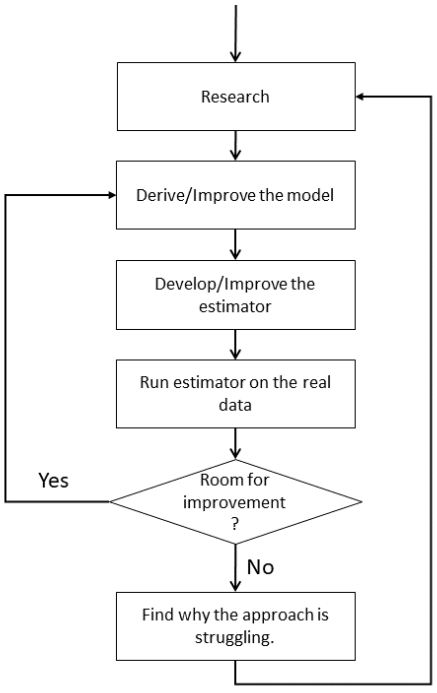

Figure 3.1: The project's process.

3.1 Kinematics Based Estimator

The first estimator is the Kinematic Based Estimator, it uses the Unscented Kalman Filter (UKF) described in section 2.3.2 to filter the signals. The UKF requires a motion model and atleast one measurement model, these are described in this section. This estimator consists of 4 states and uses 3 sensors for measurements. The state vector, x, and measurement vector, y, are shown in equations (3.1) and (3.2). Parts of the filter is linear, but as one of the measurement models is non-linear, the filter chosen is is the UKF.

$$x = \begin{bmatrix} v_x^{(1)} \\ \dot{\theta}_1 \\ \phi \\ \dot{\theta}_2 \end{bmatrix} \tag{3.1}$$

$$y = \begin{bmatrix} v_x^{(1)} \\ \dot{\theta}_1 \\ \dot{\theta}_2 \end{bmatrix} \tag{3.2}$$

3.1.1 Prediction

In the Kinematic Estimator's prediction step a constant velocity model is used. This means it assumes that the change in velocity and yaw-rates are uncertain, specified by the process noise, Q. The distribution of this uncertainty is calculated from changes in each state from the provided data. Given the difference between yaw-rate of tractor and trailer, the change in articulation angle is calculated. T describes the time between each time step.

$$A = \begin{bmatrix} 1 & 0 & 0 & 0 \\ 0 & 1 & 0 & 0 \\ 0 & T & 1 & -T \\ 0 & 0 & 0 & 1 \end{bmatrix} \tag{3.3}$$

$$x_{k+1} = Ax_k + q_k, q_k \sim \mathcal{N}(0, Q) \tag{3.4}$$

3.1.2 Update

For this estimator two update steps were required, the first update step directly uses the measurements to update the yaw-rates and velocity.

$$\hat{y} = \begin{bmatrix} v_1 \\ \dot{\theta}_1 \\ \dot{\theta}_2 \end{bmatrix} = \begin{bmatrix} x(1) \\ x(2) \\ x(4) \end{bmatrix} \tag{3.5}$$

In section 2.4.2 a relationship between the tractor and trailer is described. The second update step's measurement model utilizes that the trailer's yaw-rate can be described as a function depending on the articulation angle as seen in equation (2.43).

$$\hat{y} = \dot{\theta}_2 = \frac{x(1) \cdot sin(x(3)) + x(2) \cdot b \cdot cos(x(3))}{L_2} \tag{3.6}$$

In equation (3.6), $\dot{\theta}_2$ is described from 3 states, $x(1) = v_x^{(1)}$, $x(2) = \dot{\theta}_1$ and $x(3) = \phi$. The two first of these three has been updated to have a lower uncertainty in the previous update step. By running through the update step described in the UKF, seen in equations (2.29)-(2.34), all the states used in the measurement model is changed in the direction of the innovation. This change is scaled by the Kalman gain. The state with the highest uncertainty is the most affected.

3.2 Dynamics Based Estimator

The Dynamic Based Estimator is an Unscented Kalman Filter, just as the Kinematic Estimator. However it uses a dynamic model in it's prediction step. This allows more accurate estimation of the yaw-rate and a estimation of the lateral velocity. For this estimator seven states, and the data from four sensors are used.

$$x = \begin{bmatrix} v_x^{(1)} \\ v_y^{(1)} \\ v_x^{(2)} \\ v_y^{(2)} \\ \theta_1 \\ \dot{\theta}_2 \\ \phi \end{bmatrix} \tag{3.7}$$

$$y = \begin{bmatrix} v_x^{(1)} \\ v_x^{(2)} \\ \dot{\theta}_1 \\ \dot{\theta}_2 \end{bmatrix} \tag{3.8}$$

3.2.1 Prediction

The motion model for the Dynamic Estimator predicts the next time step by calculating what the resulting forces are from the current states and inputs. The inputs here are steering angle, driving torque and brake forces on each axle, found in vector u. Together they allow for an accurate prediction of the next state. The equations described in section 2.4.3 can be used to create a function, f, describing the change in state from state ($\mathbf{x}$), input ($\mathbf{u}$) and length of time step (T), $\dot{x} = \mathbf{f}(x, u, T)$. Calculating this f and making the function discrete results in equations (3.9).

$$x_{k+1} = x_k + T \begin{bmatrix} (F_x^{(1v)} + u(2) + u(3) + P_x^{(1)})/m_1 + x_k(5) \cdot x_{k-1}(2) \\ (F_y^{(1v)} + F_y^{(1r)} + P_y^{(1)})/m_1 - x_k(5) \cdot x_k(1) \\ (u(4) + P_x^{(2)})/m_2 + x_k(6) \cdot x_k(4) \\ (F_y^{(2r)} + P_y^{(2)})/m_2 + x_k(6) \cdot x_k(3) \\ (F_y^{(1v)} l_f^{(1)} - F_y^{(1r)} l_r^{(1)} - P_y^{(1)} l_c^{(1)} + M^{(1)})/J_1 \\ (P_y^{(2)} l_c^{(2)} - F_y^{(2r)} + M^{(2)})/J_2 \\ x_k(6) - x_k(5) \end{bmatrix} \tag{3.9}$$

3.2.2 Update

Just as the Kinematic Estimator, the Dynamic Estimator consists of two update steps, one direct and one indirect. Both of these update steps uses measurement models that describes all of the measurements.

Direct Measurement Model

The direct measurement model describes four of the states directly, these states are the longitudinal velocities and the yaw-rates of each unit. By using these measurements in the Kalman Filter each of these states are directly updated and provides a more accurate prediction for the following time step.

$$\hat{y} = \begin{bmatrix} v_x^{(1)} \\ v_x^{(2)} \\ \dot{\theta}_1 \\ \dot{\theta}_2 \end{bmatrix} \tag{3.10}$$

Indirect Measurement Model

The indirect measurement model uses the same measurements as the direct measurement model, but here the measurements are described with states from the opposite unit. By including this measurement model the lateral velocities and articulation angle does not only rely on the integrated value calculated in the motion model.

In equations (3.11) and (3.12) the lateral velocity in the connection point is described.

$$v_y^{(1c)} = v_y^{(1)} - \dot{\theta}_1 l_c^{(1)} \tag{3.11}$$

$$v_y^{(2c)} = v_y^{(2)} - \dot{\theta}_2 l_c^{(2)} \tag{3.12}$$

Then the measurements can be described by states of the opposite unit. The derivation of these equations can be found in section 2.4.2

$$\hat{y} = \begin{bmatrix} v_x^1 \\ v_x^2 \\ \dot{\theta}_1 \\ \dot{\theta}_2 \end{bmatrix} = \begin{bmatrix} v_x^{(2)} cos(-\phi) - v_y^{(2c)} sin(-\phi) \\ v_x^{(1)} cos(\phi) - v_y^{(1c)} sin(\phi) \\ \frac{v_y^{(1)} - (v_x^{(2)} \sin(-\phi) + v_{cy}^{(2)} \cos(-\phi))}{l_c^{(1)} - l_f^{(1)}} \\ \frac{-v_y^{(1)} + (v_x^{(2)} \sin(\phi) + v_y^{(1c)} \cos(\phi))}{l_c^{(2)}} \end{bmatrix} \tag{3.13}$$

3.3 Verification

To determine the performance of the estimators a few performance metrics are looked at. These metrics are:

- A distribution chart for how the error is spread over all available tests.
- The mean of the absolute error determines how far off the average error is.
- Root Mean Square Error, RMSE, with no bias is equivalent to the standard deviation of the error.

- Observe the time where the angular error is outside the acceptable error of one degree.
- The maximum absolute error.
- The 3-Sigma uncertainty will be compared to the error, if the error is within the uncertainty at 99.7% of the time, the uncertainty is able to capture the error.

3.4 Verification Data

In a collaboration between Volvo Trucks and Chalmers Revere, vehicle tests with a tractor-semitrailer combination were conducted. Chalmers Revere's states "The aim of Revere is to provide a research platform for the development and verification of theoretical models, algorithms and technologies using real vehicles in real or conditioned traffic environments."[18]. The test vehicles were equipped with a few very precise sensors to measure the articulation angle, these sensors will be further described in section 3.4.3. The vehicle tests covered a wide range of different challenging driving situations. This empirical data is used to both develop and test the estimators. This data was also used to verify the performance of the estimators.

As a distribution chart for the estimators error for the entire set will be presented, the distribution of the articulation angles for the entire data set is here presented in figure 3.2 as a reference.

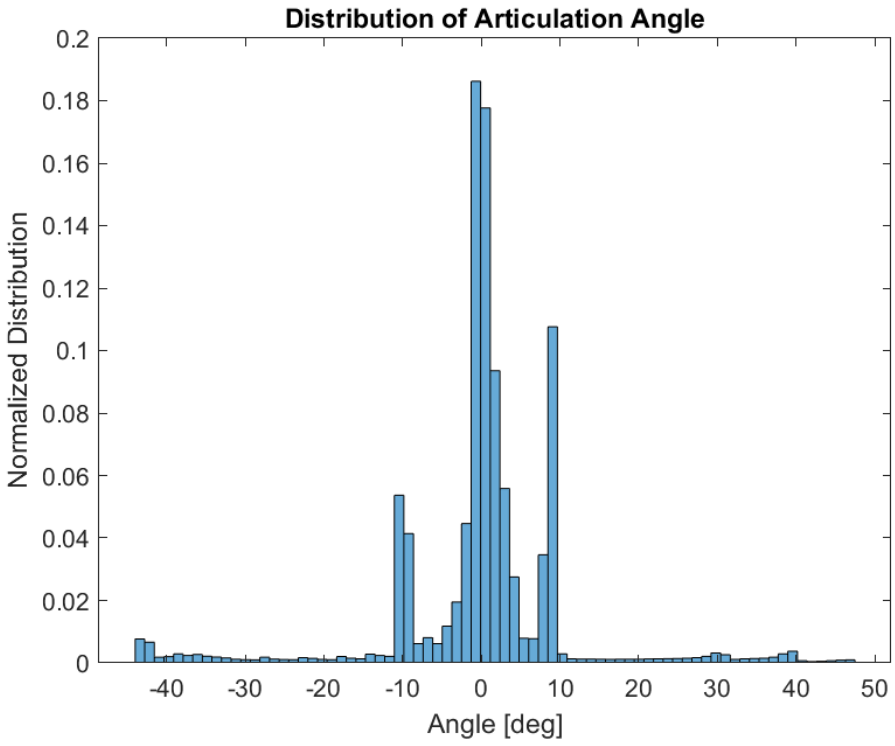

Figure 3.2: Distribution of articulation angle in the data set.

In addition to the empirical data a simulator was available. This is an in house simulator provided by Volvo, called VTM. It has a very high number of degrees of freedom. However it is hard to use this with roadbank and does not capture all the discrepencies in a real system.

3.4.1 Manoeuvres

Some driving situations to be evaluated are:

1. Driving in low speed and straight forward and backward, < 20 km/h
2. Driving in high speed and straight forward, > 50 km/h
3. Driving forward and backward with high articulation angle, articulation angle > 25 degrees
4. Driving on road that with high roughness, e.g. gravel in both high speed and low speed.

Described in this section are some of the most interesting manoeuvres found in the data set, these capture the desired driving situations. These include high articulation angles, fast changes in articulation angle and periodical changes in articulation angle. Each manoeuvre used is described below, with a graph showing the equirectangular position from longitude and latitude for the entire time sequence.

Fast Straight, with Evasion

This test shows how the estimator handles sudden jolts in articulation angle. Going at a average speed of 54 km/h and obstacles are avoided by the driver. This manoeuvre is relevant when considering driving situation 2.

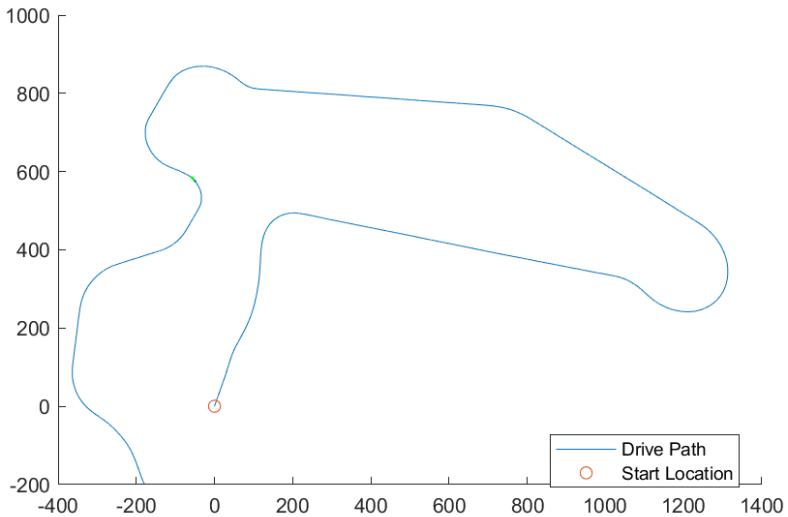

Figure 3.3: Fast Straight, with Evasion

Small Eights Fast

This test shows how the estimator handles high lateral forces and scrubbing. Here the tractor makes very tight curves in the shape of eights with a average speed of 14 km/h. This manoeuvre is relevant when considering driving situation 1 and 3.

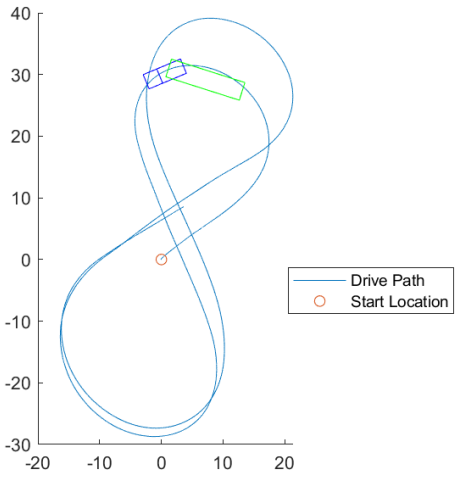

Figure 3.4: Small Eights Fast

Highway Driving with Low Frequency Sine Steering

This test shows how the estimator handles periodical turns. From these tests any phase delays in the estimator will be made clear. The tractor is driven in a periodical motion. In a controlled and slow fashion the driver alternates between turning left and right with a frequency of 0.2 Hz at a speed of 50 km/h. This manoeuvre is relevant when considering driving situation 2. But also gives a introspect into phase delays of the system.

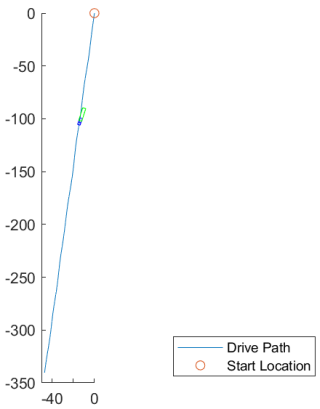

Figure 3.5: Highway driving with Low Frequency Sine Steering

Highway driving with High Frequency Sine Steering

This test shows how the estimator handles faster periodical turns. In a faster motion than Low Frequency Sine Steering the tractor is now alternates between left and right turn with a frequency of 0.5 Hz at a speed of 50 km/h. This manoeuvre is relevant when considering driving situation 2. But also gives a introspect into phase delays of the system.

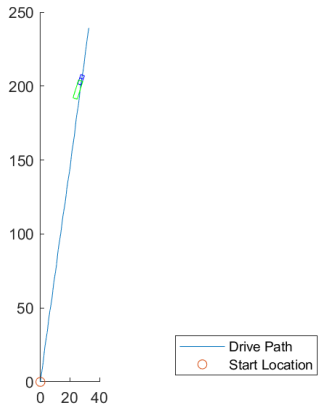

Figure 3.6: Highway driving with High Frequency Sine Steering

Fast on Low Friction Surface

This test shows how the estimator handles surfaces with lower tyre-road friction. To test the semi-trailer on low friction, test was done while driving on gravel. Providing less friction than driving on roads. This manoeuvre is relevant when considering driving situation 4.

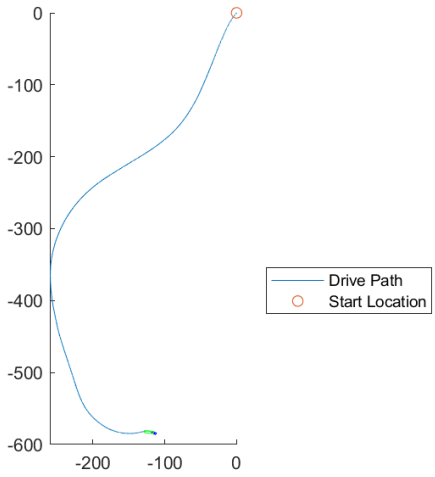

Figure 3.7: Fast on Low Friction Surface

Uphill with Turn

This test shows how the estimator handle roads with a different inclination. There is also a stop in the middle of the test. This manoeuvre is relevant when considering driving situation 2. Also tests the estimator when an unknown inclination and bank is present.

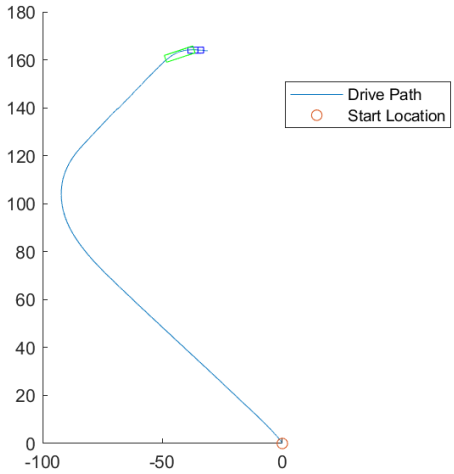

Figure 3.8: Uphill with Turn

Reversing with High Articulation Angle

This test shows how the estimator handles driving in reverse. The semi-trailer is driven so a high articulation is achieved. This manoeuvre is relevant when considering driving situation 3.

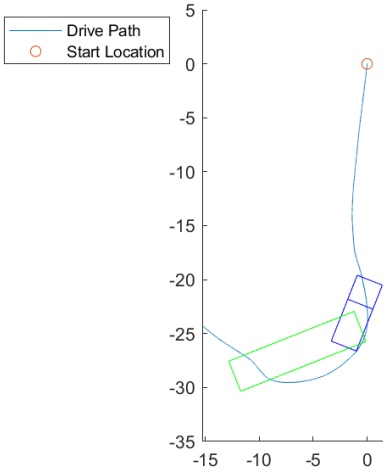

Figure 3.9: Reversing with High Articulation Angle

3.4.2 Sensors

Wheel speed sensors

The velocity of the vehicle needs to be calculated from the wheel speed. On the trailer the average wheel hub speed and difference between the wheels are available. In the truck however the individual wheel hub speeds are available. From these, the vehicle's longitudinal speed at the centre of each axle can be calculated. Described in section 2.2.1

IMU - Tractor

From the brake-system in the tractor some measurements are available. One of these is the yaw-rate. This sensor is however filtered. As the signal is filtered, its measurements are no longer time-invariant, which is nessecary for a Kalman filter to operate optimally. This accuracy reduction can be reduced by using a more advanced filter [14], but this will not be covered in this thesis.

IMU - Trailer

In the trailers of today, IMU is not the standard, a lateral accelerometer is common, however a gyro for yaw-rate is very rare. In the provided data for this thesis an IMU was attached to the trailer. The sensor has a 3 DoF accelerometer and a 3 DoF gyroscope.

3.4.3 Ground Truth

The estimated articulation angle is compared to three different ground truths made available. These thruths will be described in this section.

GPS Heading

On the test vehicle two very precise GNSS-aided Inertial Navigation Systems called RT3000[17] were installed, one on each unit. Each of these sensors are a combination of a GNSS and an IMU. The output is improved by using sensor fusion between the internal components[16]. The RT3000 have very accurate measurements, one of these measurements is the heading of the sensor. To acquire the articulation angle the trailer's heading is subtracted from the tractor's heading. This resulting articulation angle is the ground truth used in this report.

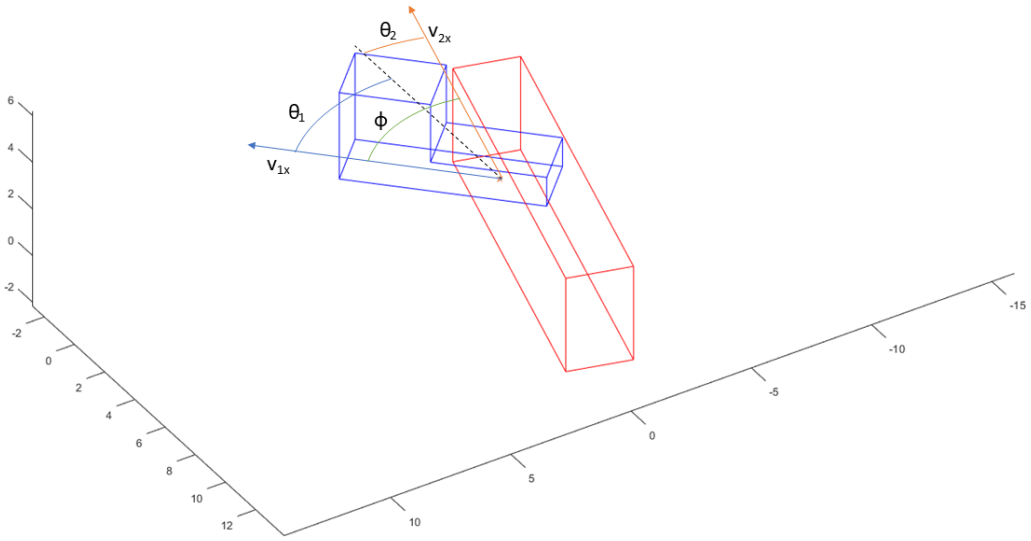

Figure 3.10: Setup of the test truck.

$$\phi = \theta_1 - \theta_2 \tag{3.14}$$

Draw-Wire Based Articulation Angle Measurement

Along each side of the truck a wire has been placed. One end of the wire is connected to the trailer, the other end is connected to a draw-wire displacement sensor on the tractor. These sensor are very precise with very high resolution. From the displacement of these wires the articulation angle is calculated, as described in section 2.2.2

Due to issues in higher articulation angles, these sensors are not used for the results for the estimator. They are used in evaluating the articulation angle from the RT3000.

Trailer kingpin articulation angle sensor

A commercially available articulation angle sensor was fitted to the trailer, used in the data provided. This sensor is mounted on the trailer's kingpin and measures the relative angle between the kingpin and the tractor's fifth wheel coupling. This sensor has a few issues: It is not classified to a high enough signal integrity classification and can therefore not be used in safety critical functions. Additionally, with fast changes in the articulation angle, this sensor is not able to track the true value. The estimators will be compared to this sensor in the results.

4

Performance: Kinematic Based Estimator

This chapter presents the performance of the Kinetic Based Estimator. First the overall result is presented. Then the estimators result for each manoeuvre described in section 3.4.1 is presented. The accuracy of this estimator is described. Finally from these results, the Dynamic Based Estimator is motivated.

4.1 Results

By observing the figure 4.1, a skew towards the left of the figure can be seen. This shows that the estimator has a negative bias of the articulation angle for this test. Stated goal for this thesis was to estimate the articulation angle within one degree of the ground truth. The Kinematic Based Estimator manages to achieve this for 87 % of the time according to table 4.1. However the Root Mean Square Error seen here is below said goal. Here it is also shown that the uncertainty of the filter does not capture the error as well as it should do.

Time	1848 s
RMS Err	0.87 deg
Mean Abs Err	0.57 deg
Max Abs Err	6.88 deg
Within 1 deg	87 %
Within 3-Sigma	71 %

Table 4.1: Result table of kinematic based estimator.

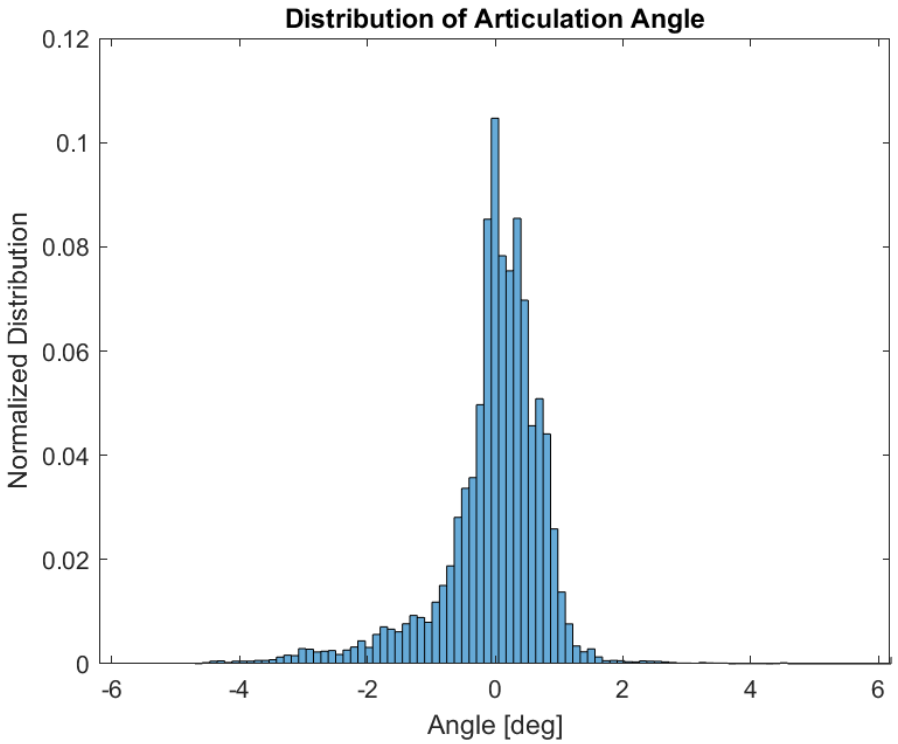

Figure 4.1: Difference between estimated articulation angle and actual articulation angle.

In the following sections the result of each maneuver will be presented with a figure and a short description of what can be observed in the figure. Each figure consists of four plots each. These plots are, in order of up to down and left to right:

1. All articulation angle data.
2. Error in articulation angle estimation, and uncertainties.
3. Yaw rate of the tractor and the trailer.
4. Speed of the tractor.

The articulation angle figure contains three lines: Estimation, this is the estimated value coming from the Estimator. GPS Heading, this signal is used as the ground truth described in section 3.4.3. Kingpin Sensor, this sensor used as a comparison to the estimator as it is a commercially available sensor.
The second plot consists of three lines: Diff heading, this is the absolute difference between GPS Heading and Estimation. 3-sigma line, this is the uncertainty of the estimation from the UKF. Estimated error is an error estimation that will be describe in section 4.2.
The last two plots are self explanatory.

4.1.1 Fast Straight, With Evasion

The plots presented in this section were acquired by testing the kinematic estimator on data from the tractor driving at high speed, around a test track while evading obstacles, the manoeuvre is described in section 3.4.1.

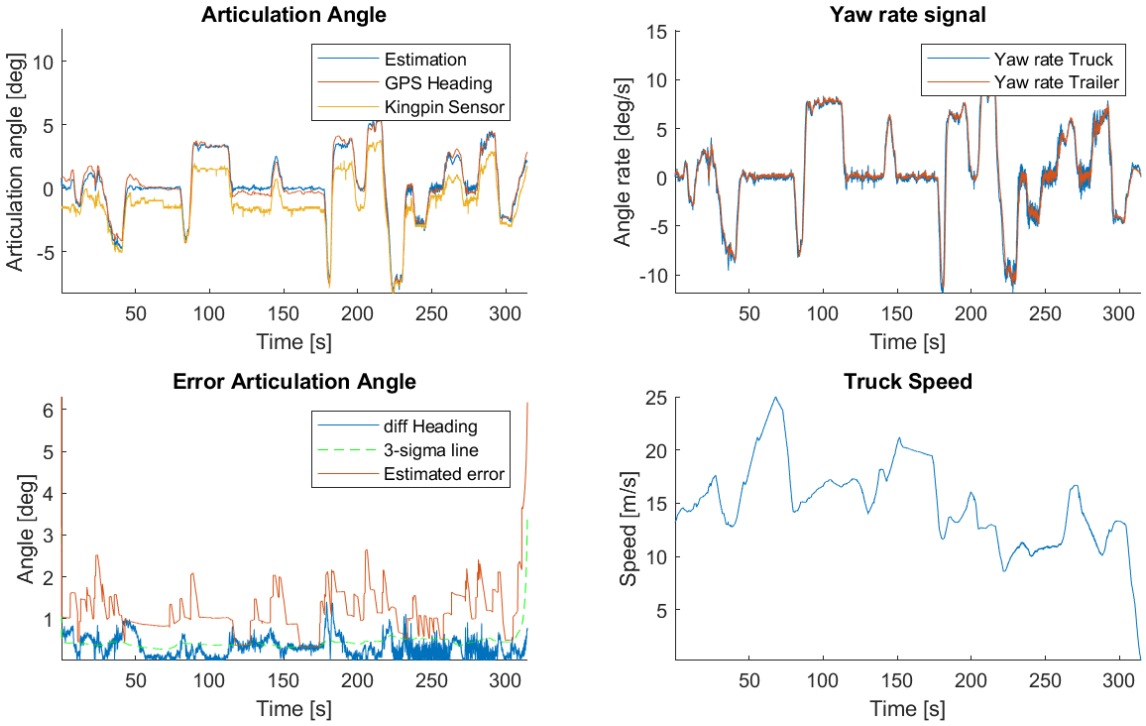

Figure 4.2: Results of estimating articulation angle when driving in high speed, in a straight line with evasion.

Time	332 s
RMS Err	0.47 deg
Mean Abs Err	0.38 deg
Max Abs Err	2.00 deg
Within 1 deg	98 %
Within 3-Sigma	54 %
Within Error Estimation	99 %

Table 4.2: Result table for kinematic based estimator on maneuver, Fast Straight, With Evasion.

The estimated articulation angle has an error more than one degree at a very small portion of the time. It follows the fast changes in the articulation angle well. The Kingpin Sensor has a bias when driving straight, but matches up in some turns.

4.1.2 Small Eights Fast

The plots presented in this section were acquired by testing the kinematic estimator on data from the tractor while making hard turns in the shape of eights, the manoeuvre is described in section 3.4.1.

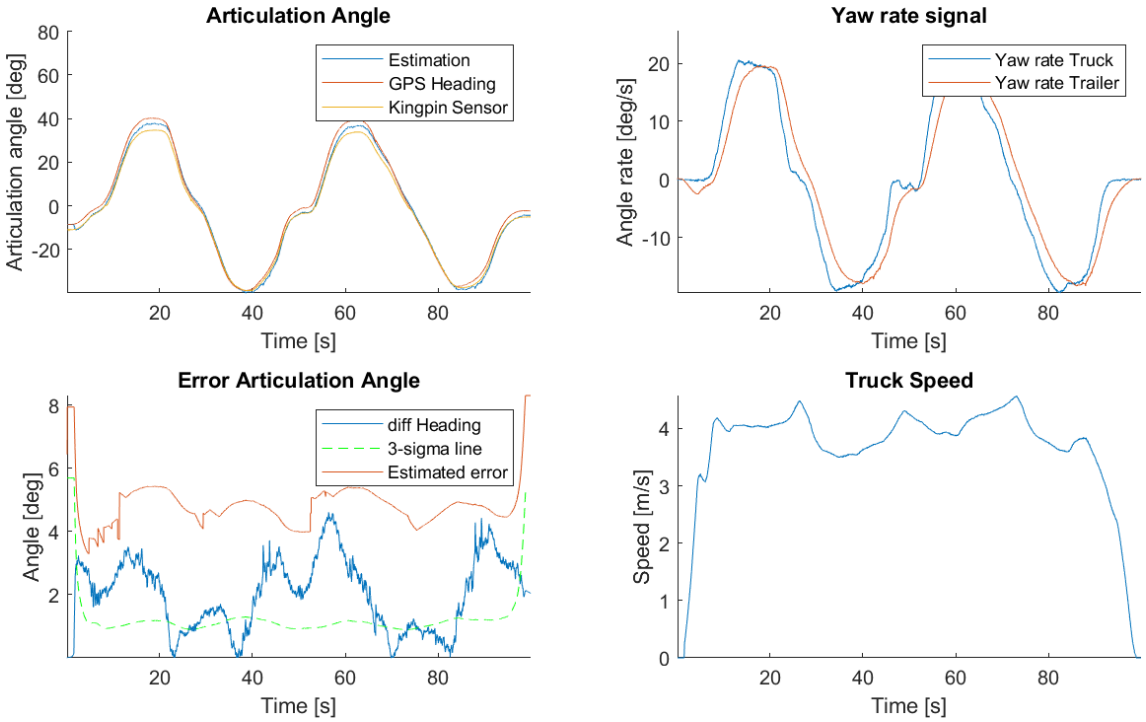

Figure 4.3: Results of estimating articulation angle when driving in small eights

Time	100 s
RMS Err	2.31 deg
Mean Abs Err	2.01 deg
Max Abs Err	4.60 deg
Within 1 deg	26 %
Within 3-Sigma	28 %
Within Error Estimation	100 %

Table 4.3: Result table for kinematic based estimator on maneuver, Small Eights Fast.

The estimator is struggling in this maneuver and gives a maximum error that is higher than 4 degrees. In this test the vehicle was subjected to high lateral forces. However, it is not always at these points in time that the estimator struggles, observe the data at 50s.

4.1.3 Highway Driving with Low Frequency Sine Steering

The plots presented in this section were acquired by testing the kinematic estimator on data from the tractor while driving straight with a sinusoidal steering angle, the manoeuvre is described in section 3.4.1.

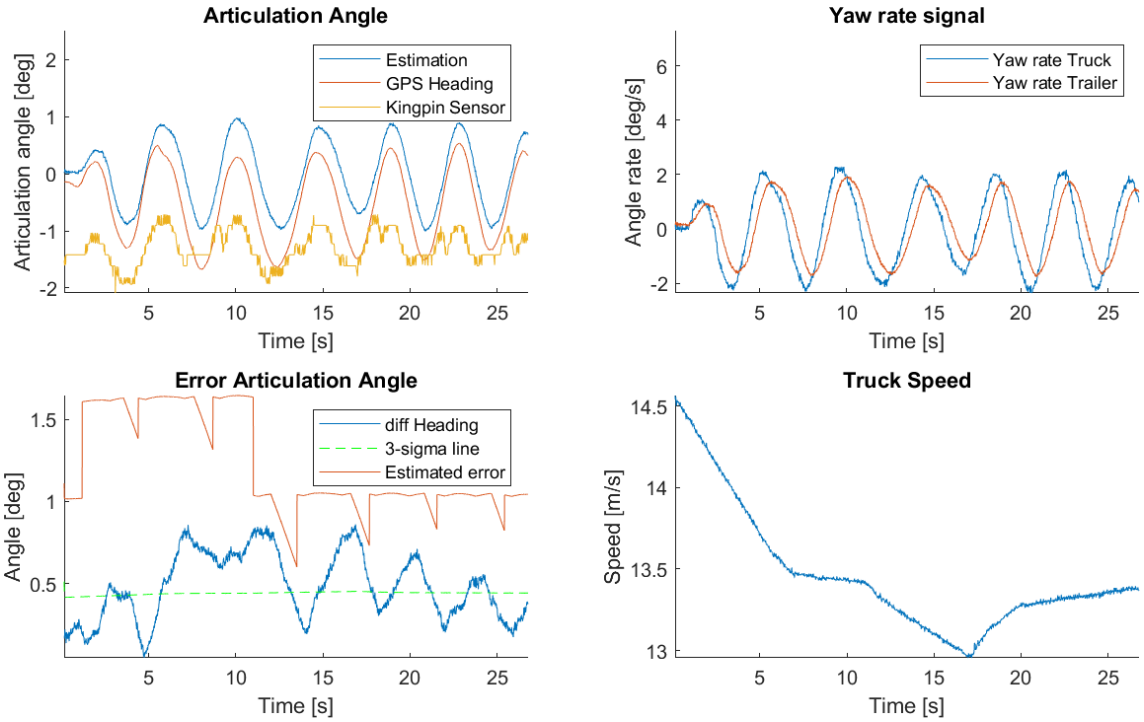

Figure 4.4: Results of estimating articulation angle when driving with sine steering low frequency

Time	27 s
RMS Err	0.52 deg
Mean Abs Err	0.48 deg
Max Abs Err	0.86 deg
Within 1 deg	100 %
Within 3-Sigma	45 %
Within Error Estimation	100 %

Table 4.4: Result table for kinematic based estimator on maneuver, Highway Driving with Low Frequency Sine Steering.

In this situation, the kingpin sensor produces a large error and does not seem to handle fast changes in the articulation angle. The estimator however manages to estimate the angle within one degree at all time. The error stems from a phase delay.

4.1.4 Highway Driving with High Frequency Sine Steering

The plots presented in this section were acquired by testing the kinematic estimator on data from the tractor while driving straight with a sinusoidal steering angle, the manoeuvre is described in section 3.4.1.

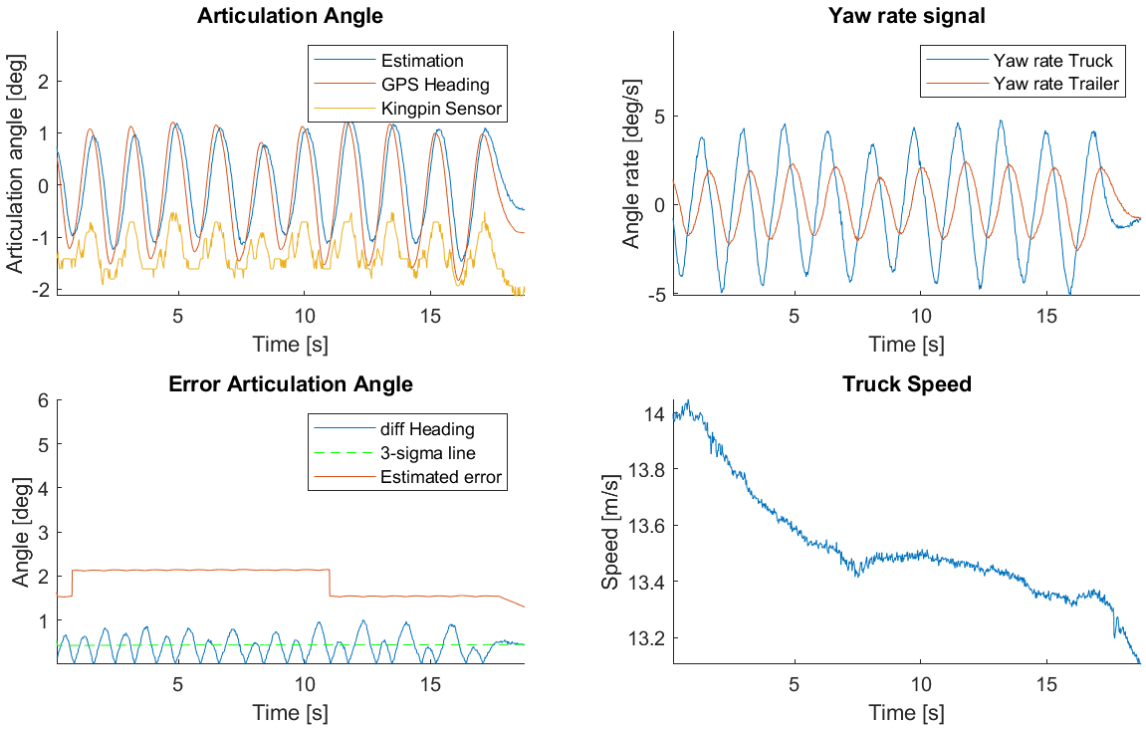

Figure 4.5: Results of estimating articulation angle when driving with sine steering high frequency

Time	19 s
RMS Err	0.48 deg
Mean Abs Err	0.41 deg
Max Abs Err	1.01 deg
Within 1 deg	100 %
Within 3-Sigma	54 %
Within Error Estimation	100 %

Table 4.5: Result table for kinematic based estimator on maneuver, Highway Driving with High Frequency Sine Steering.

Just as the ”Low Frequency Sine Steering” case, the kingpin sensor produces a large error. The estimator produces an error that is larger than one degree for a very brief moment, and with a phase delay.

4.1.5 Fast on Low Friction Surface

The plots presented in this section were acquired by testing the kinematic estimator on data from the tractor while driving around a track on gravel, the manoeuvre is described in section 3.4.1.

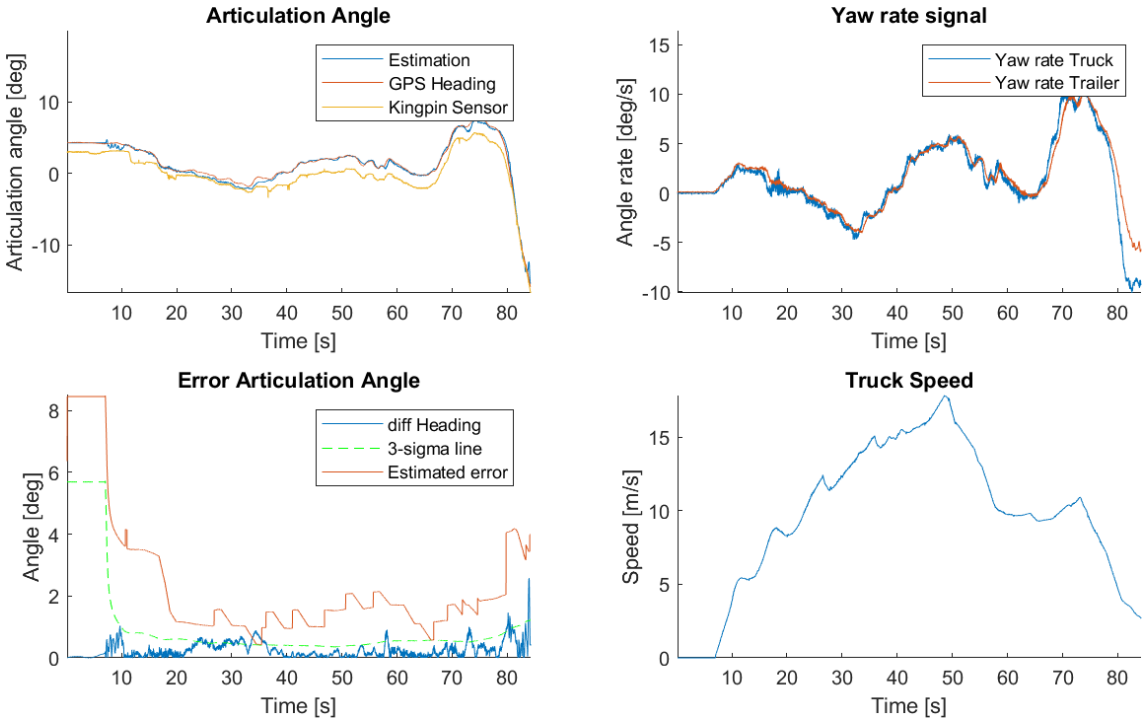

Figure 4.6: Results of estimating articulation angle when driving fast on surface with lower friction

Time	84 s
RMS Err	0.36 deg
Mean Abs Err	0.25 deg
Max Abs Err	2.58 deg
Within 1 deg	99 %
Within 3-Sigma	88 %
Within Error Estimation	98 %

Table 4.6: Result table for kinematic based estimator on maneuver, Fast on Low Friction Surface.

Just as the ”Fast Straight, With Evasion” manoeuvre, the estimator stays below one degrees error when the vehicle is driving at higher speed.

4.1.6 Uphill With Turn

The plots presented in this section were acquired by testing the kinematic estimator on data from the tractor while driving up a small hill and turning, the manoeuvre is described in section 3.4.1.

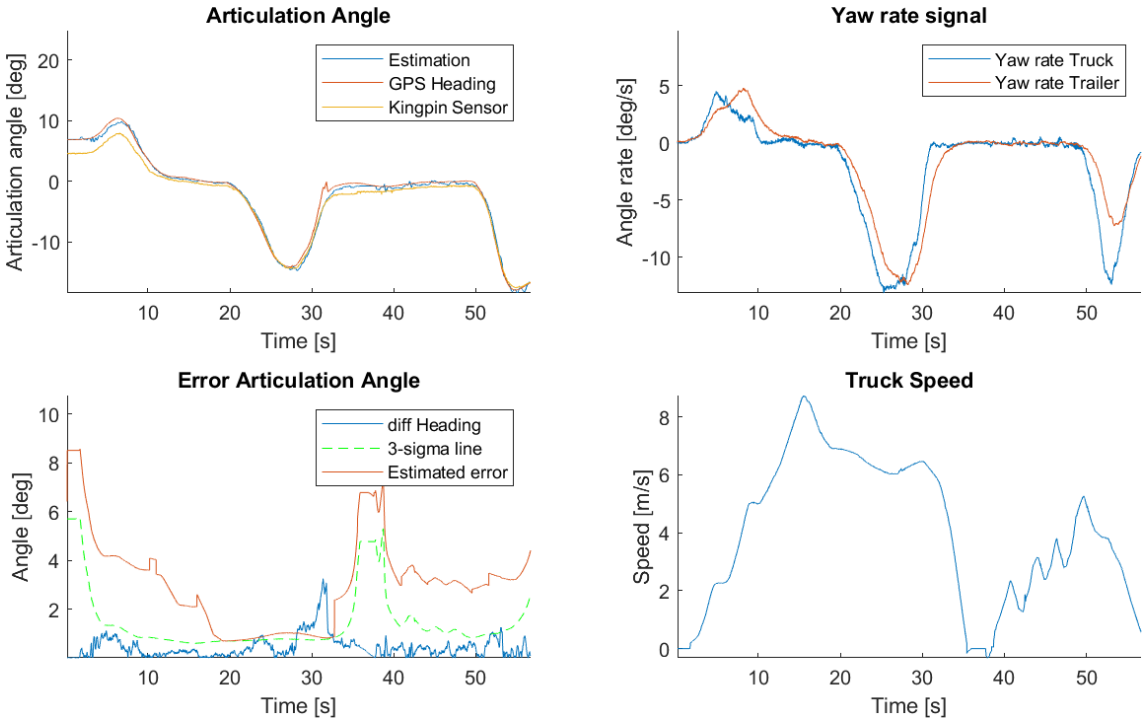

Figure 4.7: Results of estimating articulation angle when driving up a road with 12 degrees slope, continuously turning.

Time	57 s
RMS Err	0.64 deg
Mean Abs Err	0.44 deg
Max Abs Err	3.25 deg
Within 1 deg	92 %
Within 3-Sigma	90 %
Within Error Estimation	91 %

Table 4.7: Result table for kinematic based estimator on maneuver, Uphill With Turn.

At 30 seconds in the plot, the ground truth, GPS Heading, is giving a faulty value. This may be due to connection being broken between those. The uncertainty from Kalman filter, 3-sigma line, is increasing when the speed decrease.

4.1.7 Reversing With High Articulation Angle

The plots presented in this section were acquired by testing the kinematic estimator on data from the tractor while driving up a small hill and turning, the manoeuvre is described in section 3.4.1.

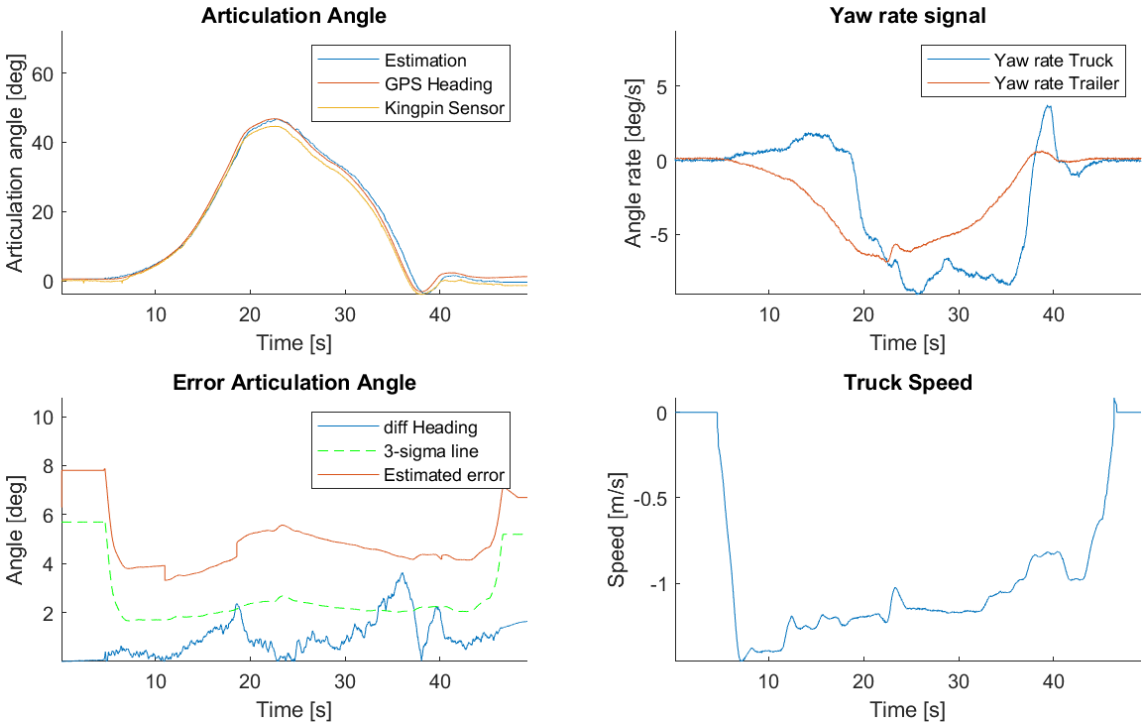

Figure 4.8: Results of estimating articulation angle when driving reversing with large articulation angle

Time	49 s
RMS Err	1.22 deg
Mean Abs Err	0.95 deg
Max Abs Err	3.63 deg
Within 1 deg	63 %
Within 3-Sigma	91 %
Within Error Estimation	100 %

Table 4.8: Result table for kinematic based estimator on maneuver, Reversing With High Articulation Angle.

Reversing is a difficult situation for the estimator, resulting in a maximum error of around 4 degrees and overall large error. With the shifting yaw rate at 38s, the estimator struggles.

4.2 Conclusion on Error Estimation

The accuracy of the estimator is very important. In addition to describing the articulation angle, the estimator needs to know when the error might be larger, and when the estimator is certain of it's estimation. A Kalman Filter outputs the uncertainty for each of it's state. The estimation should produce an uncertainty that is as small as possible, but not lower than the actual error at the percent of time the measured sigma notation describes. In a normal distribution 3-sigma, three standard deviations from the mean, is the value where 99.7% of the error is within. From the table 4.1 it is clear that only using 3-sigma as accuracy is not enough. Therefore, an error estimation was developed, and a goal was set to capture the error at 95% of the time.

The correlation between the true error and different state of the vehicle was analysed to find what kind of situation results in a higher error for the kinematic estimator. This analysis did not find one state that was the sole source of the error. By combining different signals that had a correlation to a larger error in some of the situation the new error estimation could be derived. The raw signals are noisy and contains spikes, the spikes often correlate to a higher error. A simple algorithm was developed that looks for spikes, increasing the estimated error at that time instant, and then converging the error estimation to zero, or until another spike is found. Table 4.9 shows the gain and threshold for each states that is used. When the state gives a value over threshold, the error estimator adds the gain value to its output.

State	Symbol	Threshold	Gain [degree]
$\frac{d}{dt}$ Yaw rate truck	$\ddot{\theta}_1$	0.1	0.5
Yaw rate truck	$\dot{\theta}_1$	0.28	1.5
Pitch rate truck	$\dot{\theta}_{p1}$	2.5	0.55
Steering angle	δ	0.005	0.59
Acceleration x times speed	$a_{x1}v_{x1}$	7	0.55

Table 4.9: State contribution to error estimation

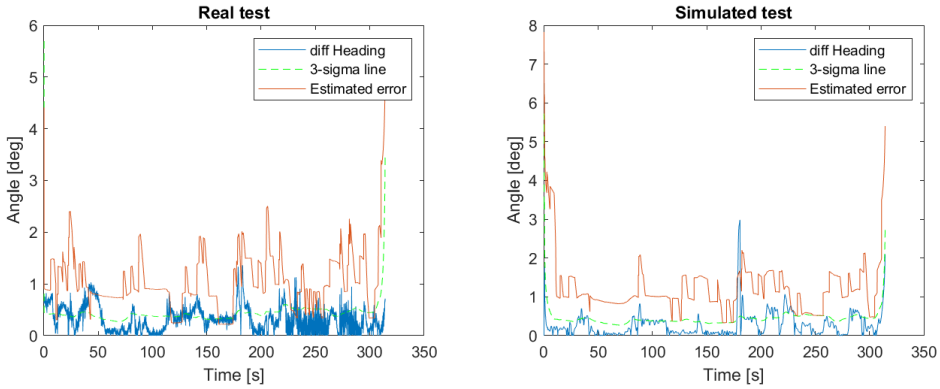

Figure 4.9: Error Estimation for real test versus simulator for similar maneuver

Figure 4.9 shows the result of the estimated error for real test versus a simulation in the VTM for a similar manoeuvre. In the simulator the signals does not contain any disturbances, however the surface is assumed to be flat and therefore the manoeuvre is not equal. The figure shows that this new error estimator manages to estimate the error almost the entire sequence. After running through the entire data set, the estimator is shown to overestimate the error with a mean of 1.7 degree but at 98.4 % of the time it encapsulates the error. That meets the set goal for the error estimation, but there is room for improvement. There might be other manoeuvres this error estimation does not perform as well, more testing needs to be done.

4.3 Conclusion on Model Accuracy

The estimator manages to be be within one degree of the true articulation angle at a majority of the time. As seen in figure 4.1 the error of the estimator is rarely over two degrees, but even with . The estimator is still not correct. This points towards the model used not being accurate enough. Using (2.76) a new estimator can be made. Figure 4.10 shows comparison of this new and the previously estimator with the test where the truck was driven in small eights fast 4.3.

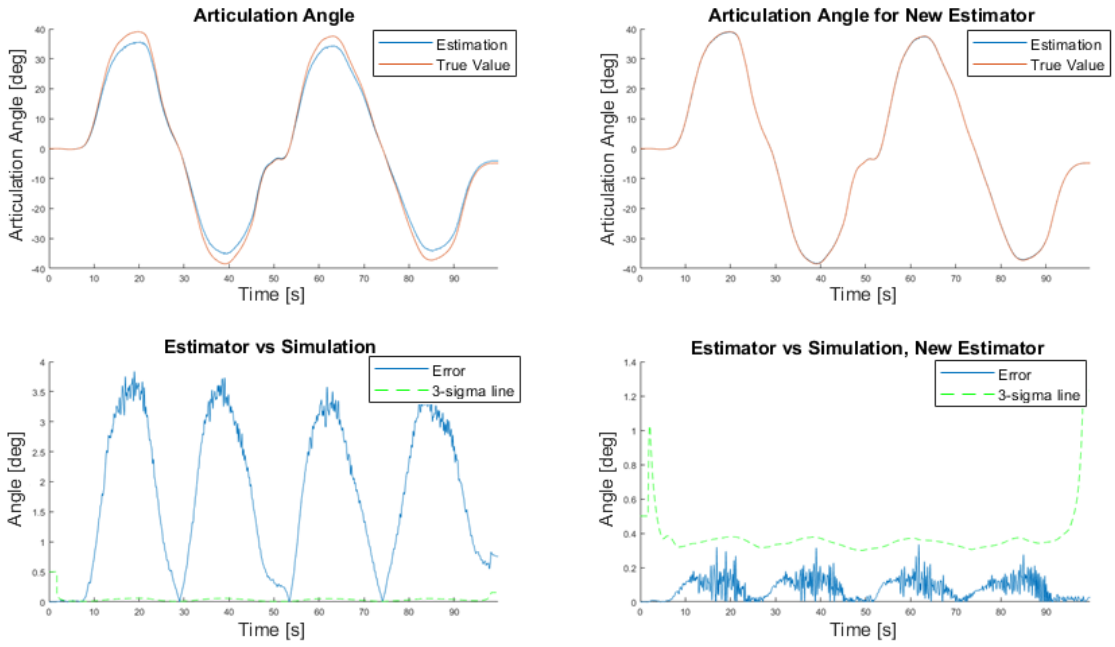

Figure 4.10: Comparison between different models.

This estimator is able to remove some of the error and is not overestimating it is certainty as estimator concept 1 does. The model of the estimator concept 1 is assumed zero lateral velocity in the equivalent wheel axle. According to figure 4.11 the actual lateral velocity is not zero.

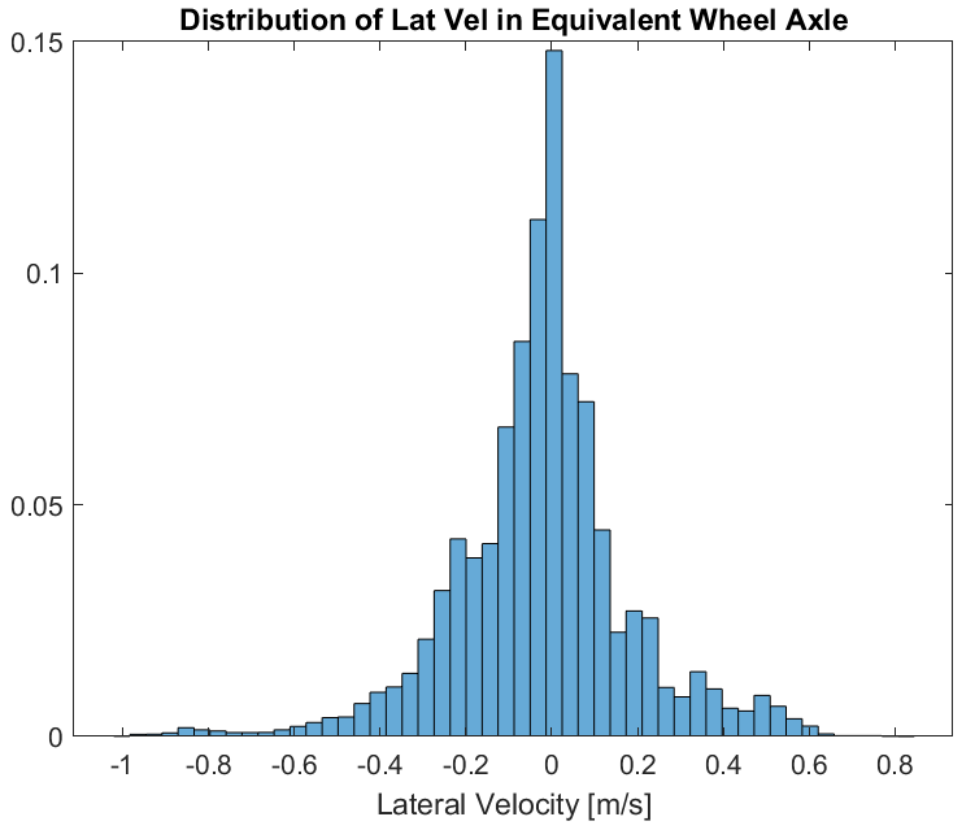

Figure 4.11: Distribution of the lateral velocity in the equivalent wheel axle.

This shows that a new estimator should be developed there lateral velocity should take into consideration. The estimator used for this comparison is however not the answer as it is very sensitive to noise in v_y, which is a very hard variable to estimate.

5

Performance: Dynamics Based Estimator

This chapter presents the performance of the Dynamic Based Estimator. First the overall result is presented. Then the estimators result for each manoeuvre described in section 5.1 is presented. The accuracy of this estimator is described. As a part of the dynamic estimator is the lateral velocity, the estimation of lateral velocity is also presented in section 5.3. Finally the estimator is evaluated when the yaw-rate of the trailer is excluded.

5.1 Results

The figure 5.1 shows that the estimator has a negative bias of the articulation angle. The Dynamic Estimator estimates the articulation angle within one degree for 90% of the time, as shown in table 5.1. While the 3-Sigma encapsulates the error for 98% of the time it does not match what 3-Sigma represents, that will say 99.7%.

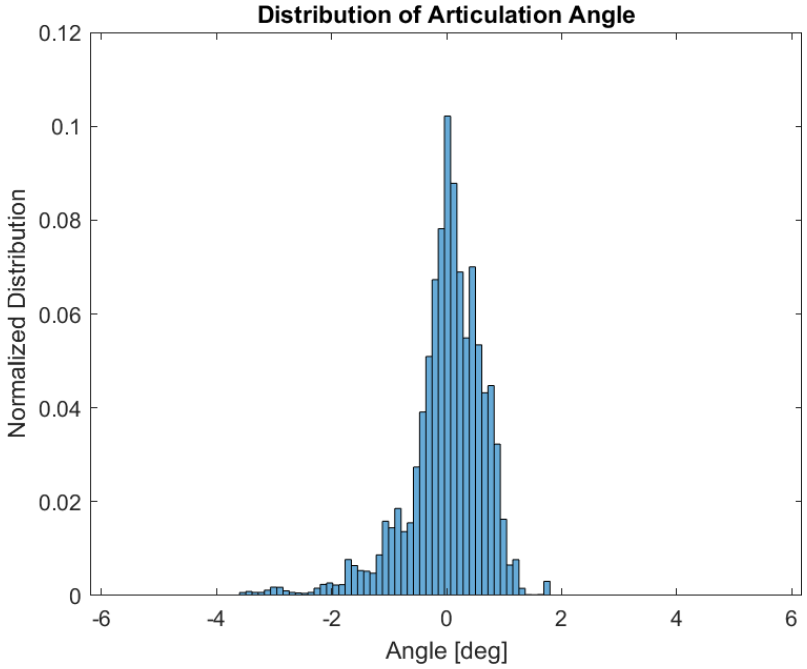

Figure 5.1: Difference between actual estimated articulation angle and actual articulation angle.

Time	1848 s
RMS Err	0.69 deg
Mean Abs Err	0.49 deg
Max Abs Err	3.54 deg
Within 1 deg	90 %
Within 3-Sigma	98 %

Table 5.1: Result table of Dynamic Based Estimator

Worth to note is loading each file, filtering and producing data for all of the 1848s of run time takes about 170s on a stationary computer. These results will show the estimators result, the articulation angle from the RT3000s as GPS heading and kingpin sensor.
The following sections presents the performance of the Dynamic Estimator on the manoeuvres described in 3.4.1. The layout of the plots in these subsections are the same as described in section 4.1.

5.1.1 Fast Straight, With Evasion

The plots presented in this section were acquired by testing the dynamic estimator on data from the tractor driving at high speed, around a test track while evading obstacles, the manoeuvre is described in section 3.4.1.

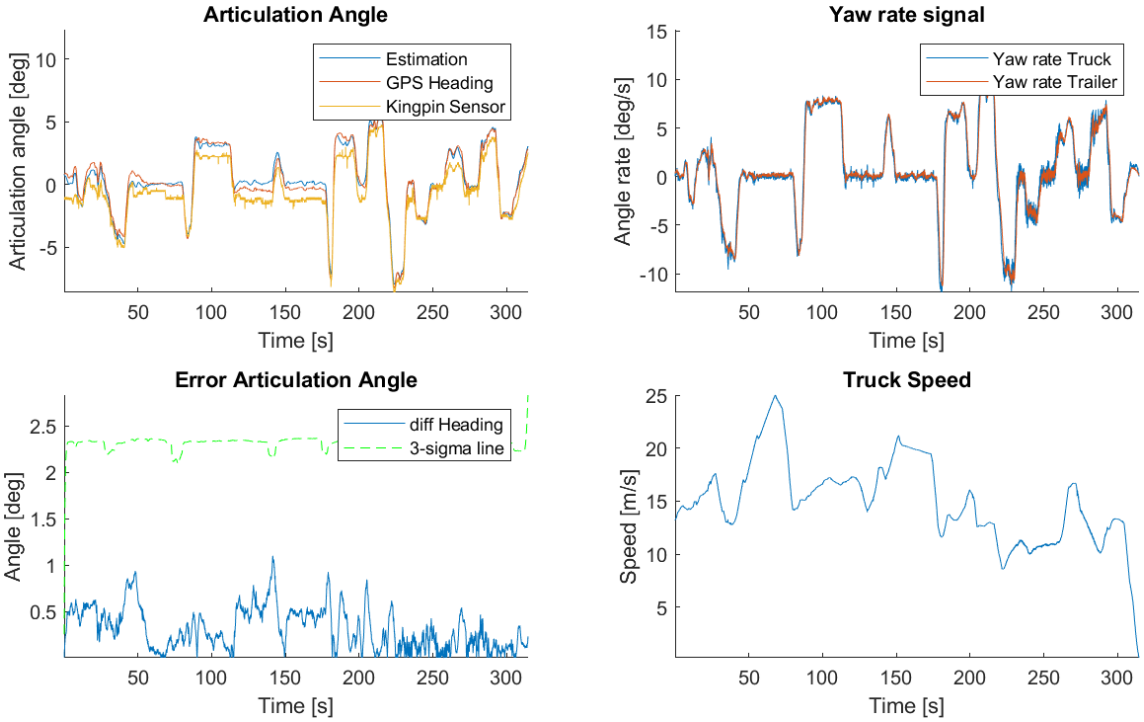

Figure 5.2: Results of estimating articulation angle when driving in high speed straight with evasion

Time	332 s
RMS Err	0.44 deg
Mean Abs Err	0.35 deg
Max Abs Err	1.13 deg
Within 1 deg	98 %
Within 3-Sigma	100 %

Table 5.2: Result table for kinematic based estimator on maneuver, Fast Straight, With Evasion.

The estimator never underestimates the error, but it highly overestimates the error. This will be present in most of the manoeuvres, but will not be mentioned in the rest.

5.1.2 Small Eights Fast

The plots presented in this section were acquired by testing the dynamic estimator on data from the tractor while making hard turns in the shape of eights, the manoeuvre is described in section 3.4.1.

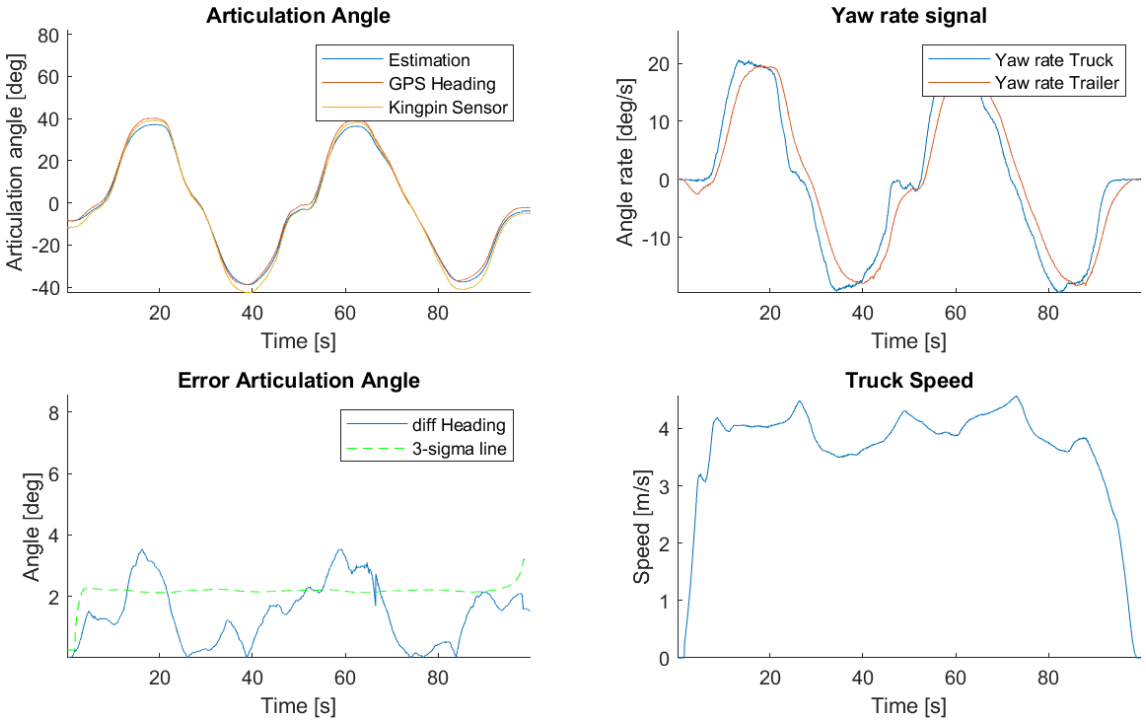

Figure 5.3: Results of estimating articulation angle when driving in small eights

Time	100 s
RMS Err	1.77 deg
Mean Abs Err	1.46 deg
Max Abs Err	3.54 deg
Within 1 deg	35 %
Within 3-Sigma	77 %

Table 5.3: Result table for kinematic based estimator on maneuver, Small Eights Fast.

The estimator performs a lot better when turning in one direction, to the right. And underestimates the articulation angle when turning left. Here the estimated error is surpassed by the error.

5.1.3 Highway Driving with Low Frequency Sine Steering

The plots presented in this section were acquired by testing the dynamic estimator on data from the tractor while driving straight with a sinusoidal steering angle, the manoeuvre is described in section 3.4.1.

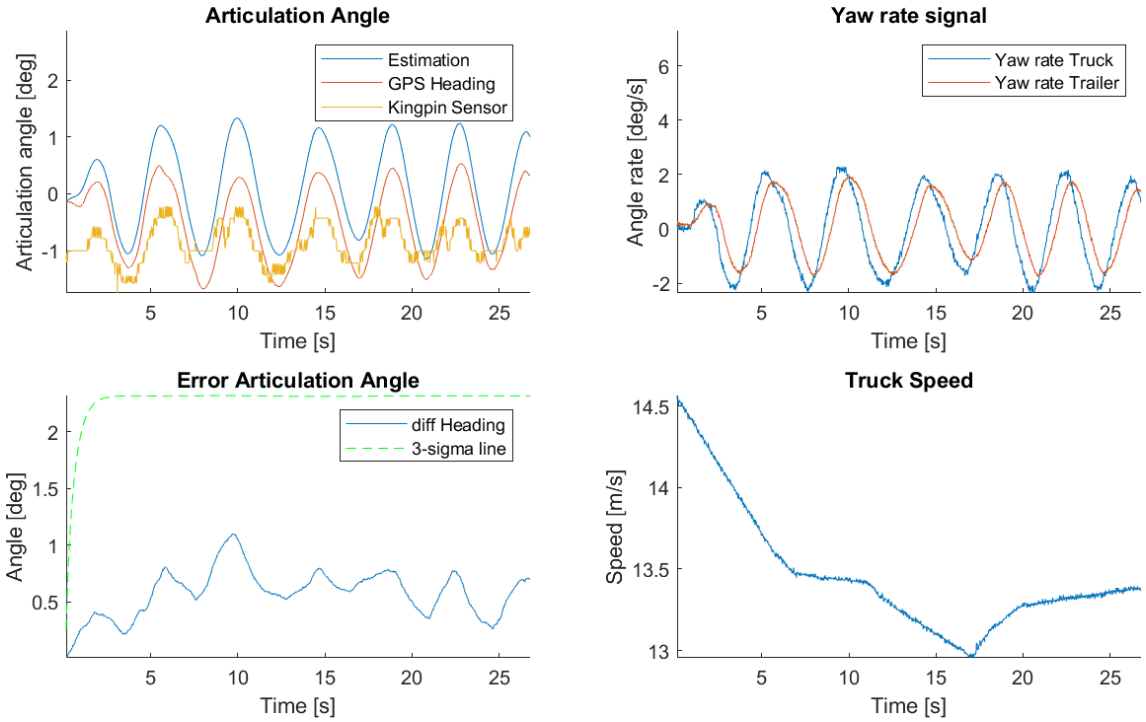

Figure 5.4: Results of estimating articulation angle when driving with sine steering low frequency

Time	27 s
RMS Err	0.62 deg
Mean Abs Err	0.58 deg
Max Abs Err	1.10 deg
Within 1 deg	96 %
Within 3-Sigma	99 %

Table 5.4: Result table for kinematic based estimator on maneuver, Highway Driving with Low Frequency Sine Steering.

A bias and phase delay is present for the estimator on this test. The phase delay is smaller than the kinematic estimator.

5.1.4 Highway Driving with High Frequency Sine Steering

The plots presented in this section were acquired by testing the dynamic estimator on data from the tractor while driving straight with a sinusoidal steering angle, the manoeuvre is described in section 3.4.1.

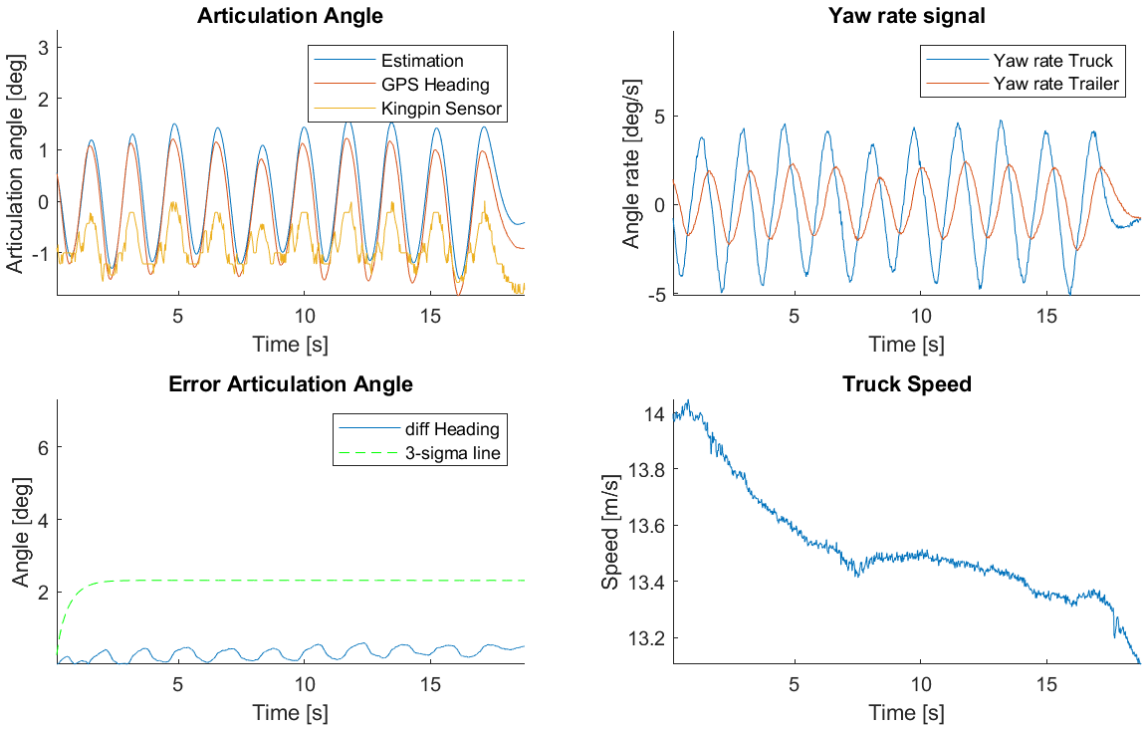

Figure 5.5: Results of estimating articulation angle when driving with sine steering high frequency

Time	19 s
RMS Err	0.34 deg
Mean Abs Err	0.30 deg
Max Abs Err	0.59 deg
Within 1 deg	100 %
Within 3-Sigma	99 %

Table 5.5: Result table for kinematic based estimator on maneuver, Highway Driving with High Frequency Sine Steering.

The estimator underestimates the articulation angle in left turns, but accurately estimates the angle in right turns.

5.1.5 Fast on low friction surface

The plots presented in this section were acquired by testing the dynamic estimator on data from the tractor while driving around a track on gravel, the manoeuvre is described in section 3.4.1.

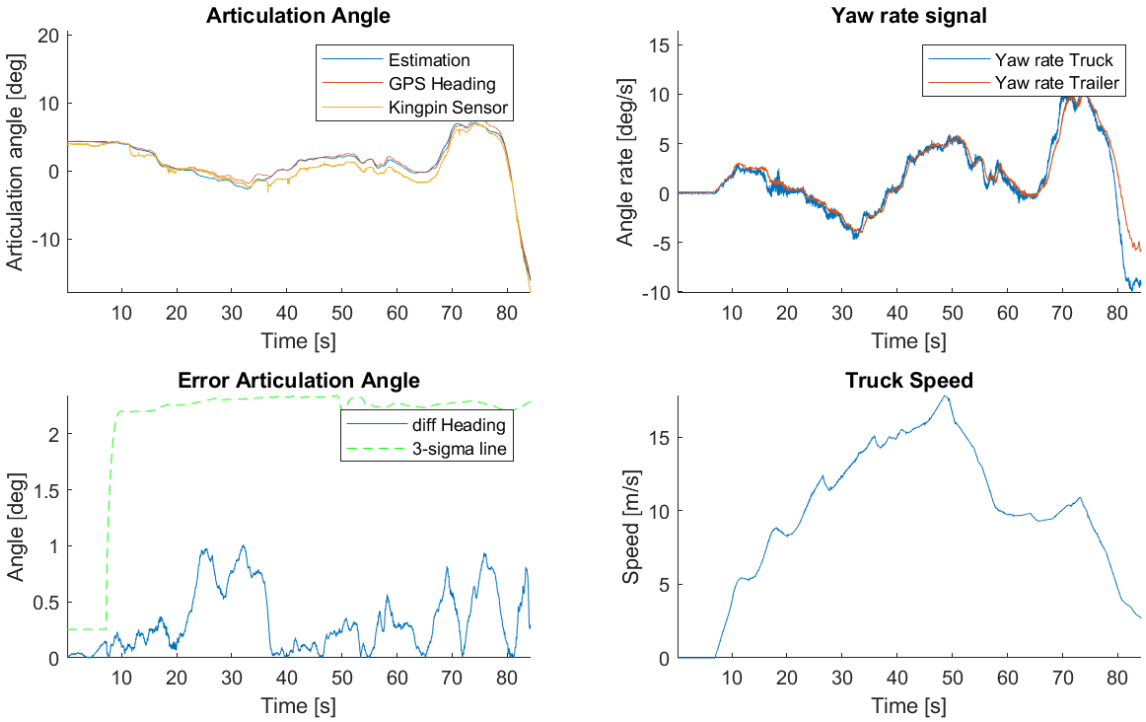

Figure 5.6: Results of estimating articulation angle when driving fast on surface with lower friction

Time	84 s
RMS Err	0.43 deg
Mean Abs Err	0.33 deg
Max Abs Err	1.01 deg
Within 1 deg	100 %
Within 3-Sigma	100 %

Table 5.6: Result table for kinematic based estimator on maneuver, Fast on low friction surface.

The estimated angle is more than one degree off at a very brief period of time. It also manages to estimate the angle at low speeds.

5.1.6 Uphill With Turn

The plots presented in this section were acquired by testing the dynamic estimator on data from the tractor while driving up a small hill and turning, the manoeuvre is described in section 3.4.1.

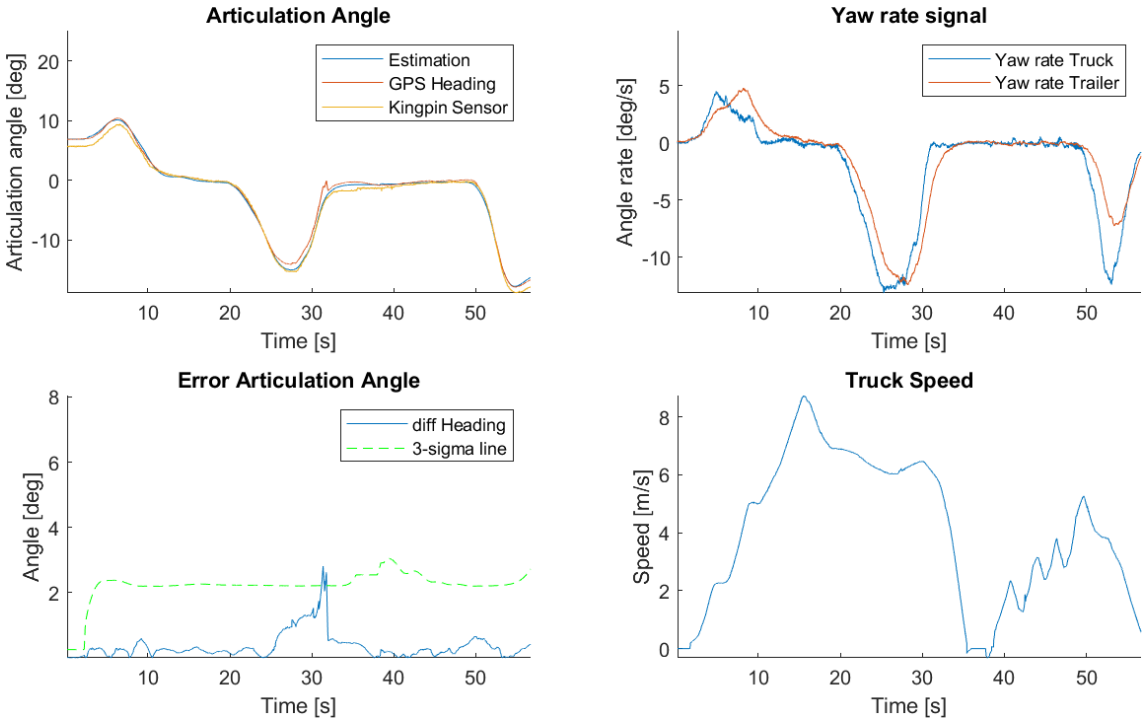

Figure 5.7: Results of estimating articulation angle when driving up a road with 12 degrees slope, continuously turning.

Time	57 s
RMS Err	0.52 deg
Mean Abs Err	0.35 deg
Max Abs Err	2.81 deg
Within 1 deg	92 %
Within 3-Sigma	99 %

Table 5.7: Result table for kinematic based estimator on maneuver, Uphill With Turn.

In Figure 5.7 the error visible at 30s is due to a fault in the RT3000 and not in the estimation. Outside of the time period around the fault, the error is below one degree.

5.1.7 Reversing with High Articulation Angle

The plots presented in this section were acquired by testing the dynamic estimator on data from the tractor while driving up a small hill and turning, the manoeuvre is described in section 3.4.1.

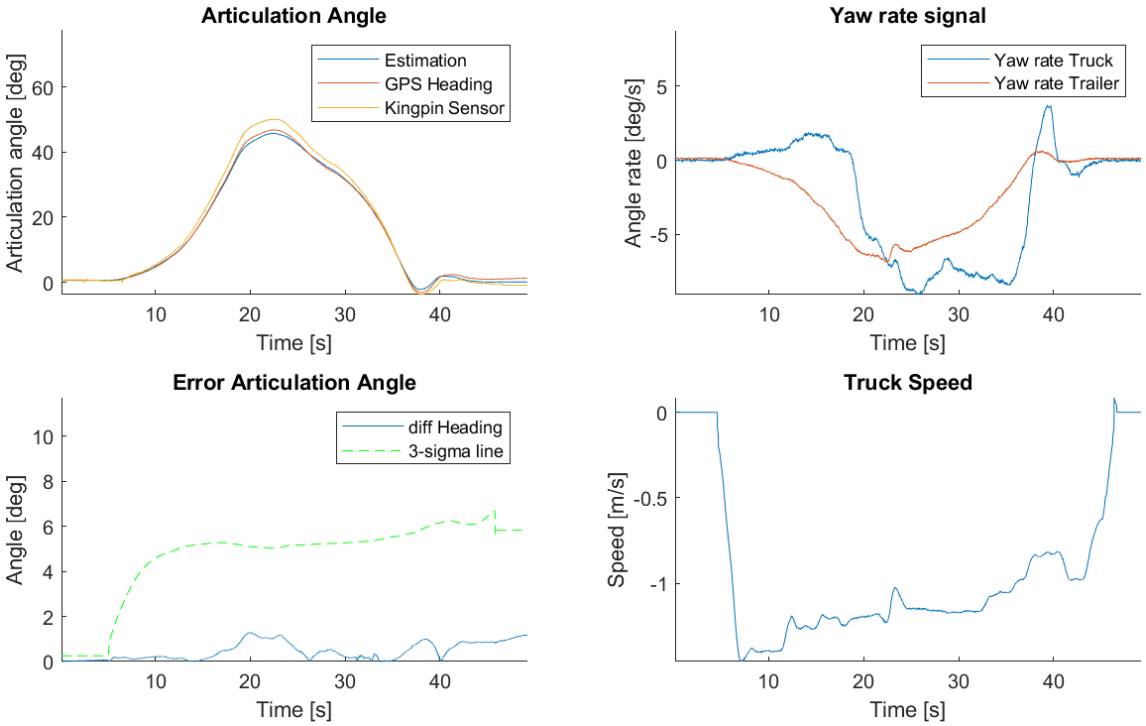

Figure 5.8: Results of estimating articulation angle when driving reversing with large articulation angle

Time	49 s
RMS Err	0.60 deg
Mean Abs Err	0.46 deg
Max Abs Err	1.28 deg
Within 1 deg	87 %
Within 3-Sigma	100 %

Table 5.8: Result table for kinematic based estimator on maneuver, Reversing with High Articulation Angle.

The maximum error is very low, but as previously mentioned the estimated error is a lot higher.

5.2 Accuracy of the Dynamics Based Estimator

The model used in dynamics based estimator is closer to reality than the model used in kinematic based estimator. As the Kalman Filter does not take into account that the model itself might be inaccurate the error estimation is less accurate the larger the difference there is between model and reality. The error between the estimated articulation angle and that measured from the RT3000s is within the 3-sigma 98 % of the time wish is close to the 99.7 % were it should be.

5.3 Lateral Velocity

A bi-product of the force-based estimator is an estimation of the lateral velocity. Comparing the lateral velocity estimate at the CoG to that measured by the RT3000s of each units results in the following histograms.

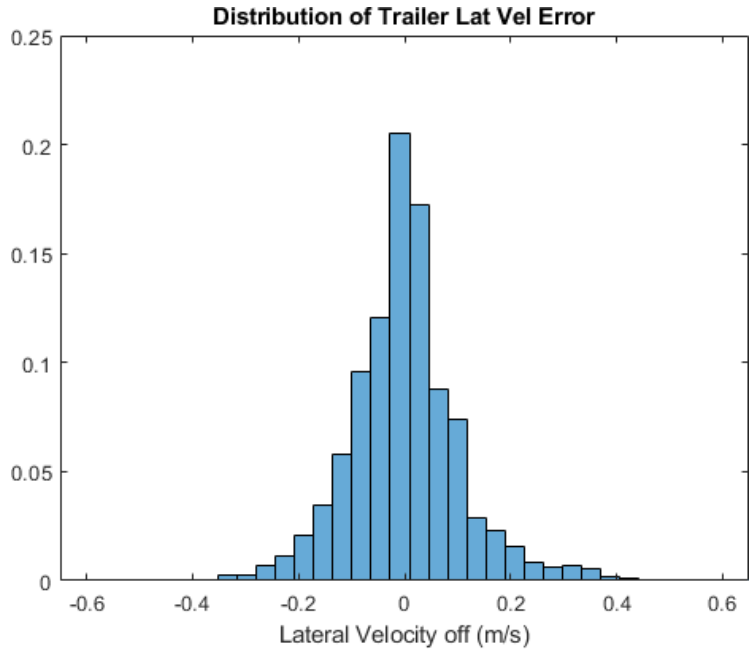

Figure 5.9: Difference between estimated lateral velocity and lateral velocity from RT3000 on the Trailer.

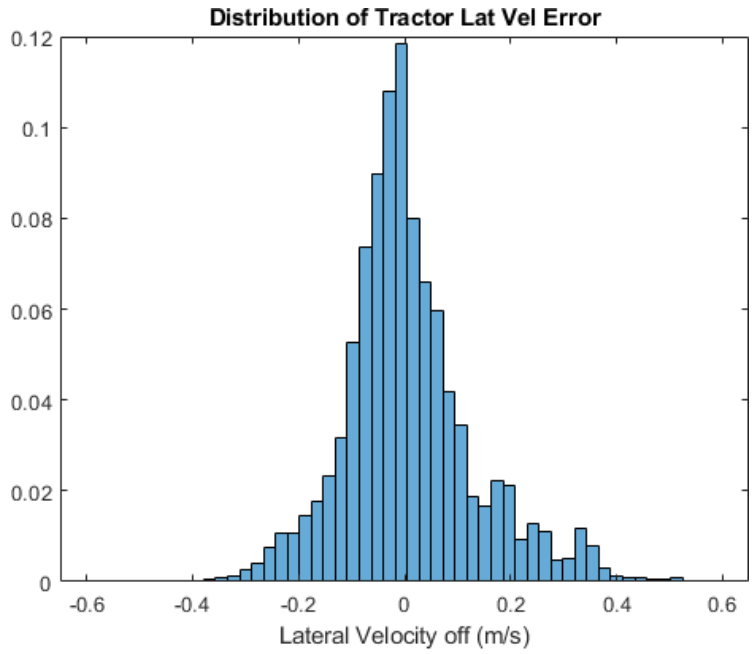

Figure 5.10: Difference between estimated lateral velocity and lateral velocity from RT3000 on the Tractor.

The lateral velocity error of the tractor is slightly higher than in figure 2.8. That however measures the lateral velocity in the equivalent wheelbase, where as here the lateral velocity is described in the CoG.

Looking at some example the estimated lateral velocity can be more directly compared to the real lateral velocity. The green dashed line is the uncertainty from estimator 3σ.

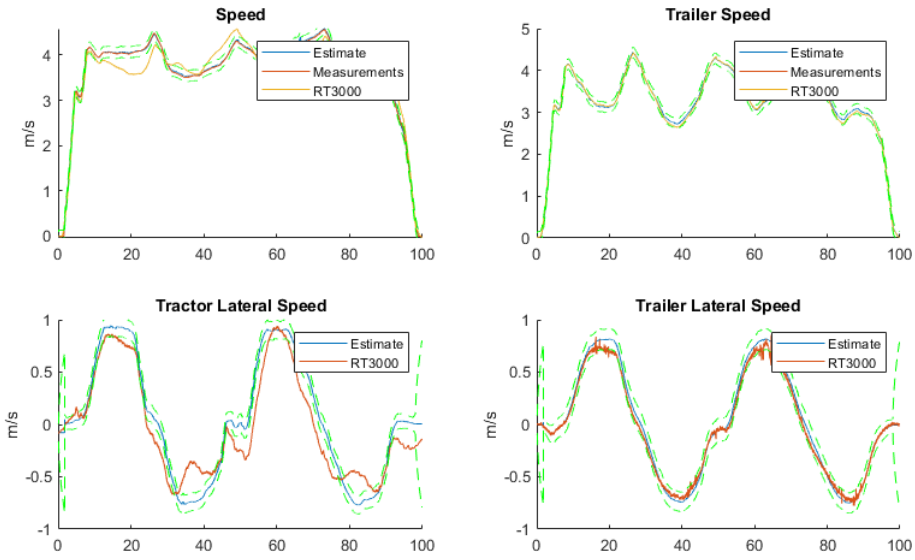

Figure 5.11: Velocities for driving in eights.

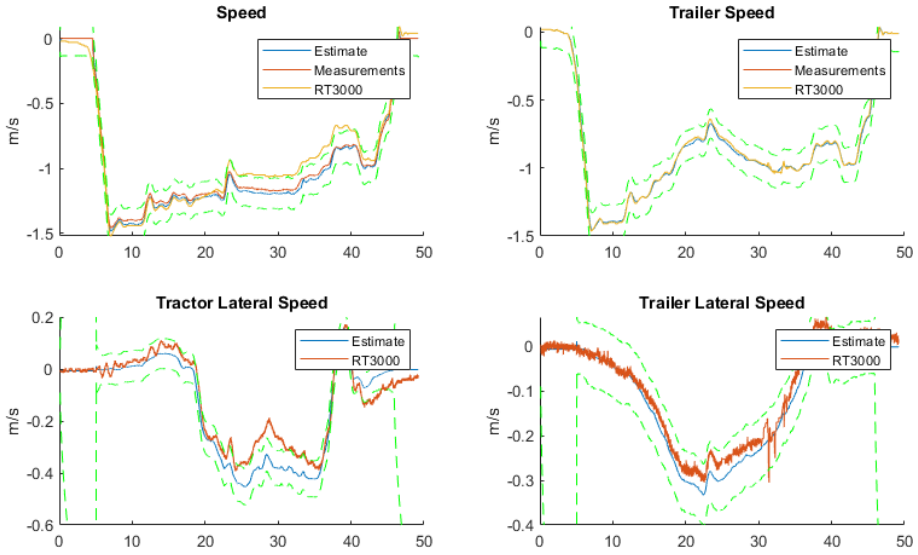

Figure 5.12: Velocities for driving in reverse.

5.4 Estimator without Yaw-Rate on trailer

Since the trailer are not usually equipped with an IMU it is interesting to see what result it is possible to get without it. The kinematic model that was used in this project needs yaw rate of the trailer, but the force based model can run without it. To test this, the measurement model is adapted. The new measurement will be the same but without $\dot{\theta}_2$ like it is presented in equation (5.1). The result from not using these measurements are presented in figure 5.13 and 5.14. Worth to note is that the yaw-rate of the trailer could be estimated with the difference in wheel speed between left and right side of the trailer.

$$y = \begin{bmatrix} v_x^{(1)} \\ v_x^{(2)} \\ \dot{\theta}_1 \end{bmatrix} \tag{5.1}$$

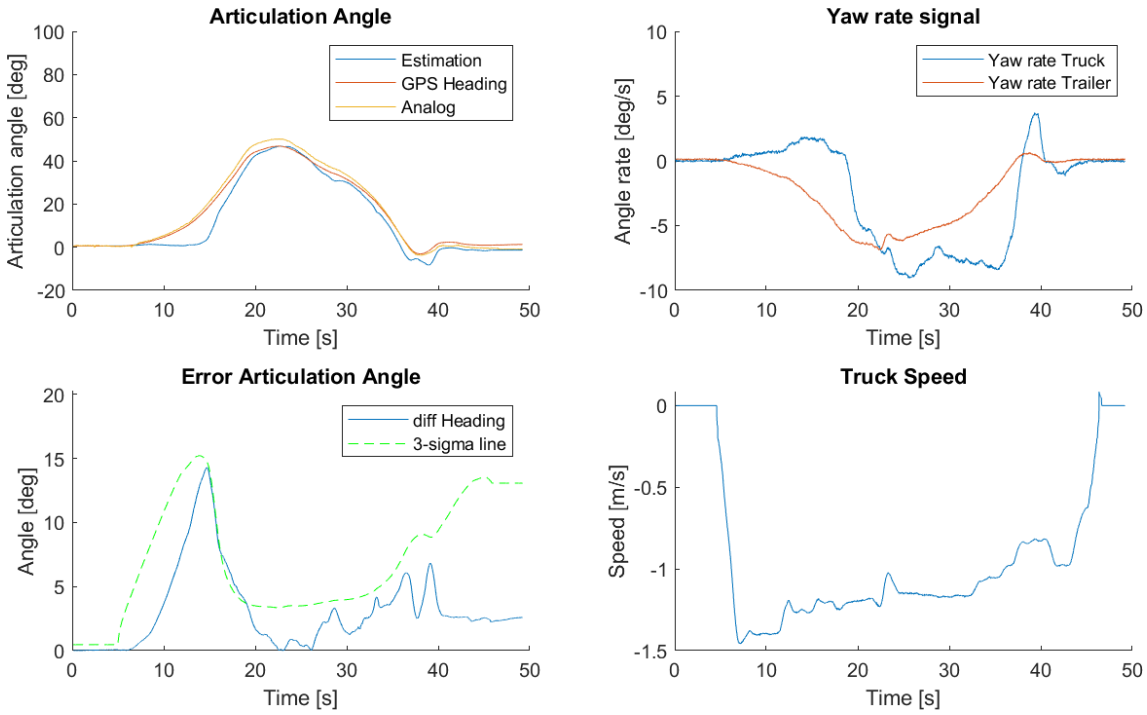

Figure 5.13: Results of estimating articulation angle when driving reversing with large articulation angle without gyro on trailer

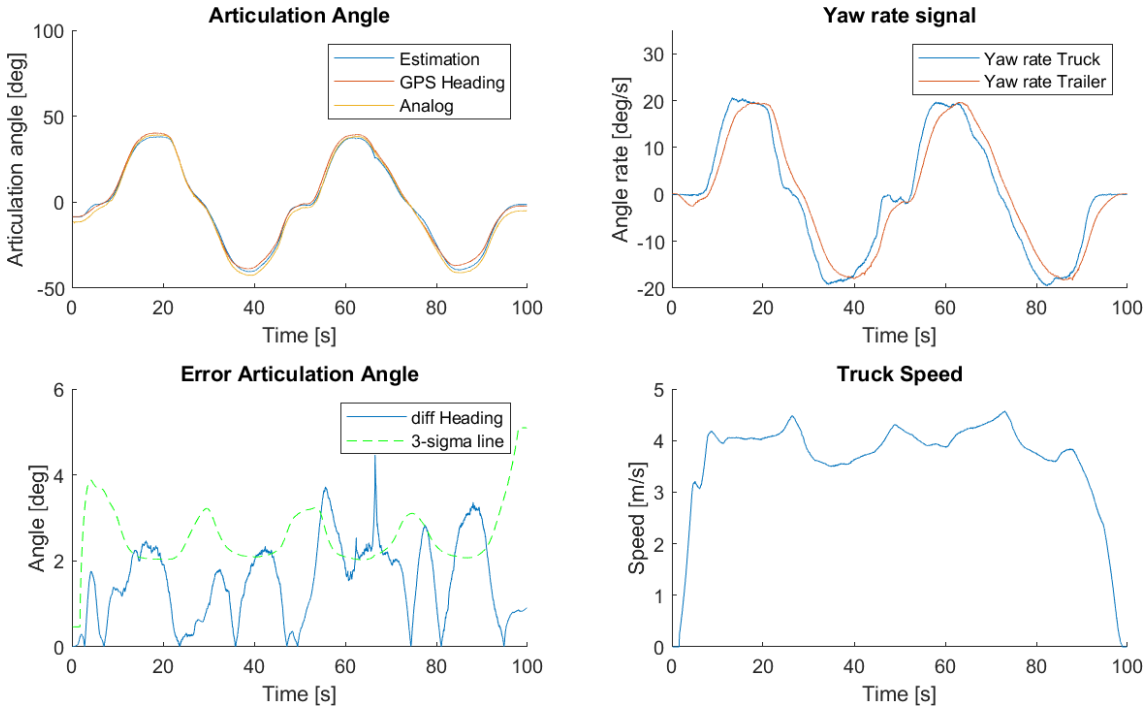

Figure 5.14: Results of estimating articulation angle when driving with sine steering low frequency without gyro on trailer

6

Discussion

This thesis covers two models with an estimator for each. The discussion will split into covering each estimator and then comparing the estimators against each other.

6.1 Performance of the Kinematic Based Estimator

As seen in 4.1 the RMS error of the Kinematic Estimator is below the goal of one degree's error set in the Research Questions in section 1.3.1, which is a very positive result. However, the maximum error is 6.88 deg, which in turns corresponds to the rear of a 11 m long trailer being 1.38 m offset of estimated position, this result is not as promising. Looking at the next value in the table, we are back at a positive result. At only 13% of the time, the estimator is more than one degree off from the actual articulation angle. With the test being focused on situations with intense maneuvers it can be argued that the estimator performs very well in low intensity situations, this can also be seen in figures 4.4, 4.5 and 4.7. Even in figure 4.2, where quick jolts are applied to the steering to simulate evasion the estimator performs within the 1 deg. The issues appear when a larger steering angle is applied. This can be seen in figures 4.8 and 4.3. Due to the higher lateral forces in this situation the assumption that there is no lateral velocity at the equivalent rear axle is increasingly inaccurate. Removing the results with large steering angles, will then result in an even lower mean.

6.1.1 Accuracy Estimation of Kinematic Based Estimator

The Kinematic Estimator cannot by itself give a good value of accuracy with the model uncertainty. Therefore, an additional accuracy estimator was needed. The result of the accuracy estimation was that 98.4 % of the time it gives a correct value but overestimated with a mean of 1.7 degree. Result is meeting the low requirement with manage to give a correct value higher than 95 % of the time. There was no set requirement for preventing overestimation.

6.2 Performance of the Dynamic Based Estimator

The Dynamic Estimator has both a mean and RMS error below the one degree's error. This matches the goal that was set in the Research Questions in section 1.3.1. However, the maximum error is 3.54 deg, which in turns corresponds to the rear of a 11 m long trailer being 0.68 m offset of estimated position. For 90% of the time the estimator is within one degree which is an improvement over the Kinematic Estimator.
The Dynamic Estimator has an advantage of being able to run without the IMU on the trailer. The error is increasing compare to with IMU but since the trailer are normally not equipped with IMU this is a good property. Figure 5.13 shows that the estimator is having a hard time when reversing without the IMU. This might be due to tuning errors.

Due to unforeseen circumstances, real-time tests was not able to be performed. Both estimators were developed and tested on only one data-set, with only one occurrence of each situation. Due to this, it is possible that the estimators could be over tuned for the data acquired. More vehicle tests would need to be carried out to verify that the accuracy seen here is realistic.

In an effort to try and define the complexity of the required calculations we looked at the run time of the filters. As mentioned in section **??** the time it took to run the filter over the entire data-set is about 170s. This is just under 11 times faster than the 1848s that the data set consists of. The on board computer on a tractor would not run this code as fast. But on the other hand, the code is not optimized and there is a lot of code that runs before filtering in those 170s. A few of these tasks were to load files, load parameters and save data. With this said, there is a high chance that the algorithm could be run in real-time on a platform.

6.3 Lateral Velocity Estimator

As the Dynamic Estimator is a force based model, it inherently estimates the lateral velocity in addition to the articulation angle. The performance of this estimation is surprisingly precise, it is never more than 0.4 m/s off in either tractor or trailer. This is more than can be said for the longitudinal velocity when comparing the velocity from RT3000 and the wheel hub speed. Thanks to the connection between the two units the lateral velocity is measured as mentioned earlier. Doing this without a trailer connected to the tractor would not allow these measurements. This should be explored further, as some of the lateral data was not reliable.

6.4 Comparison Between Estimators

Overall, the Dynamic Estimator outperforms the Kinematic Estimator. In more difficult maneuver, the Dynamic Estimator is better which the "Max Abs Err" in

the tables 4.1 and 5.1 shows. In the maneuver, fast with low and high frequency sine steering, there is some other improvements. The Kinematic Estimator has a small phase delay, which the Dynamic Estimator handles better. Looking at the case with high frequency, figures 4.5 and 5.6, the magnitude is better estimate in the Kinematic Estimator, but the Dynamic Estimator manages the phase delay better. But they both concepts outperform the kingpin sensor that struggle a lot in this manoeuvre.

The Dynamic Estimator has three additional states, and requires more computational power. If computational time is a very hard, small limit, the Kinematic Estimator, with it's weaknesses shuold be chosen.

6.5 Comparison to Similar Work

The estimators outperforms many of the estimators in similar works. The works using state observers[6][7] has similar maximum error to the Kinematic Estimator. The performance here is expected as the models used are similar. The maximum error of Dynamic Estimator is however a lot lower, indicates that the lateral velocity is an important variable when estimating the articulation angle. Standard deviation, RMS, of both Estimators is below the state observers seen in literature. There is a probability that this improvement is from using a Kalman filter to filter the signals. In accuracy. both estimators are outperformed by the camera based model in Christopher de Saxe report[5]. The Dynamic Estimator has similar RMS, but a higher maximum error. This might be due to chosen manoeuvre. As suggested by de Saxe, the camera based estimator might be combined with an estimator of our kind to minimize the computation time.

6.6 Reflection on Project

6.6.1 Method

The method of first evaluating a simple estimator was very beneficial. Not only did it prove to be an estimator that was within one degree 87 % of the time, but it allowed us to see what is required to advance the estimator. We did however get stuck for too long on trying to find if there were any more sources of the error. This was done by studying the correlation between the error and different state available to us. These states covered all the states in RT3000 and a few from internally in the truck, but to no avail.

It was a bit late in the project when the decision to make Estimator Concept 2 a kinetic one. This caused us to not find the most optimal parameters. It also forced us to not be able to evaluate what the next largest source of error is to the degree we had hoped.

6.6.2 Results

The results are a bit mixed, the kinematics based estimators perform better than we expected. It performs well in the situations with low steering angles and handles the larger steering angles fine enough. Estimator Concept 2 however does not match our expectations. Even with a rather accurate estimation for lateral velocity, it's performance is mostly outdone by Estimator Concept 1 as can be seen in how much of the time the first estimator is within one degree, the mean and rms of said estimator. In certain situations, the data of the RT3000 in the tractor appears to be off, taking a look at figure 5.11, the longitudinal velocity does not match up with the sensors in the tractor. The lateral velocity also behaves erratically here. The lateral velocity of the trailer matches, but in the tractor it does not. There is also the question if the lateral velocity should decrease such an amount while in a sharp turn? Nothing confirmed but we have a suspicion that the equipment being placed in the cabin of the tractor may have affected the data. With higher lateral forces the roll of the cabin will increase and changing the RT3000s reference coordinates. The springing of the cabin might also have an effect. The wires were ultimately not giving as good result as was hoped for. As the linear sensor measuring the length of the wires, our hopes were that this would give very accurate data. But the wires seemed to be hooked onto some part of the trailer skewing the data.

6.6.3 Future Work

The accuracy estimation can be improve. It depends on several parameters that was set to match the requirement without any algorithm for finding a more optimized estimation. To improve the parameters an iterative run of different value could be done to see what parameter gives the best result. This requires high calculation power since every iteration has to go through all data and will be time expansive. But only optimize the parameter will not add or remove any state. Another approach of estimate the accuracy is using a neural network were input could be several states and output a value of the error. But to be able to get a good result from this is, lot of data is needed. This is as well time expensive to try different size of the network and try different state. Which state that should be used could be determent from the covariance check of different state and the error.

Going forward with the project, new tests should be run. Both to store new data, but also to assess whether the estimators can be run in real-time. As mentioned, we have some suspicions on the validity of the data on RT3000, a better placement for this equipment would be required. While the wire solution can result in a great ground truth, but must be improved.

7
Conclusion

The research question stated in section 1.3.1 are the following.

- How feasible is a virtual articulation sensor based on sensors matching the signal integrity requirements for safety critical vehicle functions?
- How can the error of such a virtual sensor be quantified?

These questions have been central during the project.

The error estimation of the estimators is currently not very accurate, neither well quantified. The special error estimation created for the Kinematic Estimator managed to estimate the maximum error at 98.4% of the time, but it still largely over estimates the error. For the Dynamic Estimator the inherent uncertainty from the Kalman Filter is used. This uncertainty over estimates the accuracy and fails to estimate a high error enough when the estimator has larger errors, some tuning in retrospect of it's uncertainty is required. The estimator could benefit greatly from a method that can change the process noise over time.

We would say that it is feasible to estimate the articulation angle to match the safety requirements. But more work would have to be done on identifying the errors in Dynamic Estimator. New tests should be conducted to ensure the estimators are not over-tuned to the given tests, favorably with a wire solution with higher accuracy. Doing this would greatly assist in determining the source of error of the estimator.

The estimators perform well when comparing them to existing sensors, actual and virtual. Dynamic Estimator was within one degree's error at 90% of the time. As seen in the report, it is very possible that this estimator would be able to provide the required information for a motion controller when parking.

Bibliography

[1] Eric A Wan and Rudolph van der Merve. *The Unscented Kalman Filter for Nonlinear Estimation*. Oregon, 2000. URL: https://www.seas.harvard.edu/courses/cs281/papers/unscented.pdf.

[2] AB Volvo. *About Us - Automation*. 2020. DOI: 10.1017/CBO9781107415324.004. URL: https://www.volvotrucks.com/en-en/about-us/automation.html.

[3] Petteri Aimonen. *Basic Concept of Kalman Filter*. 2011. URL: https://en.wikipedia.org/wiki/File:Basic_concept_of_Kalman_filtering.svg.

[4] A.L. Barker, D.E. Brown, and W.N. Martin. "Bayesian estimation and the Kalman filter". In: *Computers & Mathematics with Applications* 30.10 (Nov. 1995), pp. 55–77. ISSN: 0898-1221. DOI: 10.1016/0898-1221(95)00156-S. URL: https://www.sciencedirect.com/science/article/pii/089812219500156S?via%3Dihub#aep-bibliography-id11.

[5] David Cebon Christopher de Saxe. "A Visual Template-Matching Method for Articulation Angle Measurement". In: *Intelligent Transportation Systems (ITSC), 2015 IEEE 18th International Conference on*. IEEE, 2015, pp. 626–631. URL: https://www.christopherdesaxe.com/publications/2015_ITSC.pdf.

[6] Liang Chu et al. "Estimation of articulation angle for tractor semi-trailer based on state observer". In: *2010 International Conference on Measuring Technology and Mechatronics Automation, ICMTMA 2010*. Vol. 2. 2010, pp. 158–163. ISBN: 9780769539621. DOI: 10.1109/ICMTMA.2010.342.

[7] T Ehlgen, T Pajdla, and D Ammon. "Eliminating Blind Spots for Assisted Driving". In: *IEEE Transactions on Intelligent Transportation Systems* 9.4 (2008), pp. 657–665.

[8] ISO. *Road vehicles — Functional safety — Part 9: Automotive Safety Integrity Level (ASIL)-oriented and safety-oriented analyses*. 2011. URL: https://www.iso.org/obp/ui/#iso:std:iso:26262:-9:ed-1:v1:en.

[9] ISO/TC 22/SC 33 Vehicle dynamics and chassis components. *ISO 8855:2011*. 2011.

[10] Bengt Jacobson. *Vehicle Dynamics Compendium*. Chalmers, 2019. URL: https://research.chalmers.se/publication/513850.

[11] Björn Källstrand. *Path generation and Path following approaches*. Tech. rep. 2018.

[12] Rudolph Emil Kalman. "A New Approach to Linear Filtering and Prediction Problems". In: *Transactions of the ASME–Journal of Basic Engineering* 82.Series D (1960), pp. 35–45.

[13] Matthijs Klomp et al. “Trends in vehicle motion control for automated driving on public roads”. In: *Vehicle System Dynamics* 57.7 (July 2019), pp. 1028–1061. ISSN: 0042-3114. DOI: 10.1080/00423114.2019.1610182. URL: https://doi.org/10.1080/00423114.2019.1610182.

[14] Zhaoming Li, Wenge Yang, and Dan Ding. “Time-Varying Noise Statistic Estimator Based Adaptive Simplex Cubature Kalman Filter”. In: *Mathematical Problems in Engineering* 2017 (2017). Ed. by Ton D Do, p. 5349879. ISSN: 1024-123X. DOI: 10.1155/2017/5349879. URL: https://doi.org/10.1155/2017/5349879.

[15] William Norris. *Modern steam road wagons*. London, New York, Bombay, Longmans, Green, and co., 1906, pp. 63–67. URL: https://archive.org/details/modernsteamroadw00norrrich/page/62/mode/2up.

[16] NovAtel Inc. *An Introduction to GNSS*. 2015. URL: https://en.calameo.com/read/00191579602f9b13b088e?authid=9leJ1niQkK75.

[17] OXTS. *RT3000 specifications*. 2019. URL: https://www.oxts.com/products/rt3000/.

[18] Page manager. *Chalmers Revere, About Us*. 2018. URL: https://www.chalmers.se/en/researchinfrastructure/revere/AboutUs/Pages/default.aspx.

[19] Panoha. *Modified Image of File:Inside FH16 Mk2.JPG*. 2009. URL: https://commons.wikimedia.org/wiki/File:Inside_FH16_Mk2.JPG.

[20] Richard M. Murray. *State Estimation - Optimality*. 2007. URL: https://www.cds.caltech.edu/~murray/wiki/images/b/b3/Stateestim.pdf.

[21] Christopher B Winkler and John Aurell. “ANALYSIS AND TESTING OF THE STEADY-STATE TURNING OF MULTIAXLE TRUCKS”. In: 1998.

A

Parameters Estimator:Kinematic

The content of this appendix has been removed due to secrecy considerations.

B

Parameters Estimator:Dynamics Based

The content of this appendix has been removed due to secrecy considerations.

C

Correlation Between States and Diff Heading:Kinematic

File	mean_error_deg	art_heading	art_analog	time	x_speed	x_yaw_tract	articulation	x_yaw_trail	heading	steering	tractor_acc_x	tractor_acc_y	trailer_conti_acc_x
162129_Standing_still_on_levelled_surface.mat	0,035521712	-0,99999994	0,079945907	-0,359807193	-0,044490874	-0,057404216		-0,034260601	0,978023946	2,98033E-07	2,00273E-07	-0,03933261	-0,000422358
162346_EuroComb_Hallered_2020_01_14.mat	0,256099433	-0,758815348	-0,571084321	-0,756944835	0,202077955	-0,781925976	-0,6103449119	-0,653449833	0,702518523	-0,722468793	0,318239391	-0,404537678	0,211369112
162842_Eight_with_small_radius_start_left.mat	2,009322882	-0,262486666	-0,223185614	-0,052376643	0,145889431	-0,473239928	-0,197627202	-0,224983469	0,307702363	-0,493753016	-0,069300555	-0,423151284	0,083385043
163216_Driving_in_reverse_direction_slowly.mat	0,945155799	0,021722639	0,029099414	-0,04852663	-0,198112428	-0,668639362	0,092956781	-0,087900303	0,138607249	0,653418958	0,1688568	0,39851436	-0,119109765
163818_Radius_45m_increase_speed_stand-still_max_speed_left.mat	0,235286772	-0,734825492	0,000731838	0,045188457	-0,42932573	-0,423850358	0,184838057	-0,425606161	-0,031197792	-0,25757575	-0,348738998	-0,460880011	0,016192026
164228_Radius_45m_increase_speed_stand-still_max_speed_right.mat	0,55482322	-0,483156979	-0,220422342	-0,603136539	-0,546501517	0,507505357	-0,132660612	0,515874863	0,145827338	0,173149422	0,174038008	0,604444504	0,394493222
165218_Radius_45m_speed_30mps_counterclockwise.mat	0,734605134	-0,621951818	-0,062073319	0,214048356	-0,040644787	-0,042312231	0,586109281	-0,040646665	-0,021541156	-0,043996386	-0,335704952	-0,205456004	-0,32146436
165515_Radius_1250cm_outerwheel_low_speed.mat	1,663054347	-0,221253887	-0,220190361	0,385744095	-0,374845386	0,302573502	-0,128689766	0,328763962	-0,010608604	-0,245426863	-0,186560959	0,103210717	0,07226263
170544_Acc_2mps2_stand-still_80kmh_decc_2mps2_stand-still.mat	0,49103266	-0,895832896	-0,60470438	0,741868973	0,757903278	-0,006434912	0,132574528	0,050462518	0,778356612	-0,186768621	-0,387153298	-0,170281366	-0,403234094
172134_ABS_braking_50kmh.mat	0,871138215	-0,987389982	0,055927973	0,721646547	0,707704306	-0,203972027	-0,130149782	-0,272151887	0,729406536	-0,030597966	-0,555152059	-0,123077616	-0,366479635
172301_EuroComb_Hallered_2020_01_14.mat	0,315711439	0,648090601	0,753277957	-0,646957576	0,569921315	-0,045205168	0,972257376	-0,027225116	-0,828642309	0,551196814	0,235228747	0,074408308	0,052418292
172424_Drive_straight_50kmh_sine_steering_low_freq.mat	0,483936012	-0,456766576	-0,229358256	0,024205506	-0,452978879	-0,515537739	-0,169733122	-0,194821611	-0,317458302	-0,617037594	0,497969896	-0,522736013	0,236123592
172642_Drive_straight_50kmh_sine_steering_high_freq.mat	0,412457377	-0,513207912	-0,497366965	0,173458278	-0,178279787	-0,94984448	-0,011572198	-0,111681439	0,054142211	-0,84146142	0,304615468	-0,93280524	-0,080364421
172921_Double_lange_change_80kph.mat	0,51759553	-0,620441914	-0,56786561	-0,099048242	0,278137118	-0,743020058	-0,258660585	-0,280287266	-0,183281809	-0,78989011	0,504604757	-0,588129759	0,105061881
173614_Uphill_12perc_start_bottom_with_stop_start_middle.mat	0,436444908	-0,083295435	-0,024580255	0,009322067	0,009440877	-0,270398974	0,001668922	0,056320306	0,320209533	-0,292809159	-0,00963526	-0,223766729	-0,050556932
174114_EuroComb_Hallered_2020_01_14.mat	0,427717417	0,323626071	0,501724482	0,579299867	-0,292366505	-0,084012985	0,939005077	-0,023750633	0,145987079	0,08673726	-0,143597275	-0,178055793	0,209700853
174226_EuroComb_Hallered_2020_01_14.mat	0,454211473	-0,60450983	0,672420681	0,552452564	-0,712357998	-0,100099444	0,871146679	0,470495582	0,251996875	0,097661369	0,063995905	-0,297308892	0,222737551
174801_Gravel.mat	0,252516508	-0,094812207	-0,122338317	0,248110026	-0,202169046	-0,061305363	0,008179963	0,08667551	-0,303145617	-0,188096687	-0,398263186	-0,151755139	-0,525390208
175103_Landsvagsbanan_1lap_hitting hinders.mat	0,31954217	-0,207436502	-0,108272657	0,267912924	0,111013323	-0,125626311	-0,052734256	-0,044739064	0,455442816	-0,151303008	-0,264474332	-0,085586898	-0,242940307
180531_Roundabout_left_normal_driving.mat	1,041603565	-0,768514931	-0,762818456	0,235270143	0,408344924	-0,830778062	-0,733348727	-0,617868602	0,32096684	-0,920984387	-0,312836945	-0,667643309	-0,080014393
180714_Acceleration_stand-still_turn_in_junction_left.mat	0,686305523	-0,539844751	-0,548049808	0,221946582	0,116822504	-0,816586733	-0,48525852	-0,418666035	-0,338803142	-0,908424735	-0,459840506	-0,776671231	-0,205170751
180834_Acceleration_stand-still_turn_in_junction_right.mat	1,29595983	0,053224612	0,151435077	-0,685203911	-0,161447585	-0,40540731	0,19609338	0,127016172	-0,830584466	-0,462124854	0,398174882	-0,420653731	0,28493464
181021_Full_throttle_from_stand-still.mat	0,408044279	-0,259669513	0,011438215	0,591220379	0,52099508	-0,463080823	0,079536468	-0,38787654	0,343002707	-0,385400832	-0,291602612	-0,43796128	-0,339758098
181210_Hard_brake_evasive_50kph.mat	0,31871894	-0,334711313	-0,256002367	0,459987044	0,006990535	-0,760985553	-0,114185333	-0,207253247	-0,253054619	-0,835530877	-0,459698558	-0,711942077	-0,351394296
181359_Smooth_double_lane_change_60kph.mat	0,230594471	-0,677301526	-0,590147138	-0,765549719	0,767929494	-0,551665008	-0,454618871	-0,343799591	0,40471518	-0,578840673	0,776067019	-0,306024581	0,573663712
181655_Handlingbana2_moderate_braking_end.mat	0,378265321	-0,25324139	-0,13883847	0,357433498	0,232750461	-0,325111151	-0,101796269	-0,223817706	0,129667118	-0,298353404	-0,245968819	-0,374907821	-0,241114601
Total	0,567217946	-0,05633267	-0,004995763	0,124462791	0,139571205	-0,180444688	0,020769164	-0,067449532	0,100763574	-0,063141279	-0,083623029	-0,132214263	-0,032230567

File	trailer_conti_acc_y	trailer_conti_acc_z	tractor_angrate_forward	tractor_angrate_lateral	tractor_angrate_down	trailer_angrate_forward	trailer_angrate_lateral	trailer_angrate_down	tractor_vel_forward
162129_Standing_still_on_levelled_surface.mat	-0,358332217	-0,015537837	-0,011147493	-0,002089896	-0,013073392	0,022437824	-0,00999484	0,054587122	-0,230388001
162346_EuroComb_Hallered_2020_01_14.mat	-0,431282192	0,152750105	-0,088845521	0,070370816	-0,777859151	-0,017955035	0,042049166	-0,639248371	0,200310811
162842_Eight_with_small_radius_start_left.mat	-0,365912288	0,00539633	-0,363361686	0,014831479	-0,477448553	-0,171143457	0,067947559	-0,223180488	0,138216689
163216_Driving_in_reverse_direction_slowly.mat	0,453828275	0,035535939	0,162052408	-0,055651169	-0,663342774	0,026559478	0,197749138	-0,097420923	-0,131705269
163818_Radius_45m_increase_speed_stand-still_max_speed_left.mat	-0,466767609	0,027426956	-0,020214632	-0,016671926	-0,424585462	-0,022895142	-0,007861548	-0,424151272	-0,428251207
164228_Radius_45m_increase_speed_stand-still_max_speed_right.mat	0,603880703	0,111824572	-0,042506155	-0,003936274	0,50395596	-0,04558127	0,023203423	0,517962992	-0,54606986
165218_Radius_45m_speed_30mps_counterclockwise.mat	-0,213919044	-0,00947102	-0,011280019	0,056576144	-0,042497829	-0,011434228	-0,034868337	-0,039485849	-0,036627561
165515_Radius_1250cm_outerwheel_low_speed.mat	0,121161908	-0,015860863	0,038181707	-0,035570834	0,302565008	0,019071722	0,06127004	0,328466088	-0,352452397
170544_Acc_2mps2_stand-still_80kmh_decc_2mps2_stand-still.mat	-0,085398279	-0,113873437	0,00233551	0,011187366	-0,02155547	-0,001061749	0,00793799	0,015950069	0,764699876
172134_ABS_braking_50kmh.mat	-0,081120171	0,016238363	0,133364409	-0,064979404	-0,170618981	-0,02244791	-0,01852748	-0,171557769	0,728568971
172301_EuroComb_Hallered_2020_01_14.mat	0,029004667	-0,009237108	0,026532749	0,149257928	-0,014638323	0,015133922	-0,064135067	-0,012217903	0,572010577
172424_Drive_straight_50kmh_sine_steering_low_freq.mat	-0,465032518	-0,039674472	-0,216190934	0,047332548	-0,534647584	-0,292297035	0,029539153	-0,183401585	-0,456320643
172642_Drive_straight_50kmh_sine_steering_high_freq.mat	-0,817191601	0,013109265	0,056198951	0,367500544	-0,968102455	-0,792213619	0,026974855	-0,104406975	-0,139545932
172921_Double_lange_change_80kph.mat	-0,486870676	0,014493895	-0,461349219	0,18195039	-0,772915065	-0,783919811	0,060377818	-0,269557655	0,291156113
173614_Uphill_12perc_start_bottom_with_stop_start_middle.mat	-0,10721536	-0,059734058	-0,04372051	0,084227182	-0,280887008	-0,089728758	0,306196719	0,131842896	0,003081499
174114_EuroComb_Hallered_2020_01_14.mat	0,10452459	-0,094429605	-0,013315043	-0,058338415	-0,062090237	0,100640543	0,093712077	-0,017152714	-0,287949532
174226_EuroComb_Hallered_2020_01_14.mat	0,081109688	0,034861095	0,27912125	-0,137525976	0,093354948	-0,025252169	0,012826985	0,401089936	-0,695814669
174801_Gravel.mat	-0,111875258	-0,013211647	-0,090979576	-0,02769373	-0,068233527	-0,071763583	0,045691472	0,08667551	-0,185205325
175103_Landsvagsbanan_1lap_hitting hinders.mat	-0,073702835	0,012641585	-0,041559167	-0,055738356	-0,13228029	0,039090134	-0,004291814	-0,042104438	0,11337468
180531_Roundabout_left_normal_driving.mat	-0,644378304	0,139006183	0,049949672	-0,511566579	-0,834688365	0,15641591	-0,532947361	-0,617609918	0,42311275
180714_Acceleration_stand-still_turn_in_junction_left.mat	-0,720777392	0,038082719	-0,082892247	-0,160550117	-0,825250208	0,280737549	-0,140396804	-0,415045142	0,136669353
180834_Acceleration_stand-still_turn_in_junction_right.mat	-0,375438243	0,03502446	-0,255096614	0,140420571	-0,418190718	-0,340731204	0,372292042	0,138492331	-0,234900981
181021_Full_throttle_from_stand-still.mat	-0,410500675	-0,070516065	-0,077756703	0,112075053	-0,47421509	0,0042075	-0,062994711	-0,38750878	0,528449357
181210_Hard_brake_evasive_50kph.mat	-0,667110205	-0,081625171	0,167905509	-0,070517257	-0,780671954	-0,145092353	-0,054334629	-0,155987874	0,007025586
181359_Smooth_double_lane_change_60kph.mat	-0,281039596	0,134315759	-0,134996414	-0,091195248	-0,563238561	0,000763689	-0,169196561	-0,334423751	0,766392708
181655_Handlingbana2_moderate_braking_end.mat	-0,357073963	0,015901195	-0,157613948	-0,041081436	-0,331394583	0,045675121	-0,018749801	-0,222992286	0,242123842
Total	-0,115253776	0,004604013	-0,054050814	-0,024720652	-0,183765888	-0,007445938	-0,007476143	-0,065689743	0,140623614

File	tractor_vel_lateral	trailer_vel_forward	trailer_vel_lateral	trailer_angroll	trailer_angpitch	tractor_angroll	tractor_angpitch	tractor_curvature	tractor_vel_lateral_p	calc_error
162129_Standing_still_on_levelled_surface.mat	0,055096705	-0,037206139	0,565235436	-0,393907219	-0,54400605	-0,396446824	-0,273498565	0	0,01654204	0,087894432
162346_EuroComb_Hallered_2020_01_14.mat	-0,79462558	0,19544439	0,593075752	-0,533876419	0,179086849	-0,168703124	-0,171106458	-0,776201665	0,065733843	-0,215617254
162842_Eight_with_small_radius_start_left.mat	-0,496104628	0,220223665	0,200412989	0,696570933	-0,037638694	-0,175191447	0,022322254	-0,476935148	0,218481809	-0,113408871
163216_Driving_in_reverse_direction_slowly.mat	-0,63622272	-0,22327067	0,093498431	0,161366358	-0,174151585	-0,164390564	-0,25049004	0,711647332	0,489216983	-0,084842771
163818_Radius_45m_increase_speed_stand-still_max_speed_left.mat	-0,411193103	-0,42980057	0,416452736	-0,436956614	0,063429601	-0,440651625	0,404199779	0,030333208	0,368674874	0,270409077
164228_Radius_45m_increase_speed_stand-still_max_speed_right.mat	0,378317922	-0,547043622	-0,557040036	0,598298848	-0,174177706	0,603904188	-0,092823431	-0,179618344	-0,530630589	0,19020462
165218_Radius_45m_speed_30mps_counterclockwise.mat	0,056831308	-0,040987641	0,073852189	-0,199812271	-0,16109331	-0,198753551	0,458909333	0,083559744	0,377414912	-0,369149029
165515_Radius_1250cm_outerwheel_low_speed.mat	0,212193131	-0,327997684	-0,32893917	-0,224446148	-0,337793291	-0,014201225	-0,133945271	0,047503289	-0,300142676	0,504728615
170544_Acc_2mps2_stand-still_80kmh_decc_2mps2_stand-still.mat	0,877609551	0,7659657	-0,718589246	-0,434256673	0,272653699	-0,614141703	0,411602736	0,043006234	0,87381798	-0,58210808
172134_ABS_braking_50kmh.mat	-0,433256954	0,735748708	-0,924063981	-0,429288536	-0,418442488	-0,514511228	-0,069848366	-0,076803878	-0,423671842	-0,82221967
172301_EuroComb_Hallered_2020_01_14.mat	-0,250284016	0,572329283	-0,170549303	0,265564144	0,198650971	0,423590571	-0,215126038	-0,075959876	-0,231934711	-0,725166738
172424_Drive_straight_50kmh_sine_steering_low_freq.mat	-0,621777236	-0,443264604	-0,001672838	-0,560415089	0,033830825	-0,571488798	-0,313341886	-0,521270156	0,424881876	0,048760191
172642_Drive_straight_50kmh_sine_steering_high_freq.mat	-0,952326357	-0,162947983	0,131688163	-0,387132466	-0,121702403	-0,961686134	0,090647049	-0,956044793	0,890740931	-0,164473698
172921_Double_lange_change_80kph.mat	0,186381593	0,236796528	0,103473045	-0,095122933	-0,537088156	-0,619346917	-0,33979848	-0,750421643	0,629933357	-0,249822631
173614_Uphill_12perc_start_bottom_with_stop_start_middle.mat	-0,320490181	0,011730557	-0,018536504	0,090038471	0,095406331	-0,247787505	0,205005124	-0,294625312	0,110964365	0,109779902
174114_EuroComb_Hallered_2020_01_14.mat	-0,17068018	-0,281027615	0,067274913	0,140072569	-0,236363992	-0,573125303	-0,178826839	-0,209590986	-0,131074712	0,274912
174226_EuroComb_Hallered_2020_01_14.mat	-0,012041468	-0,694974065	-0,31755951	0,237512335	-0,106078856	-0,689632297	-0,367338836	-0,096412353	-0,062858425	0,711129427
174801_Gravel.mat	0,182664275	-0,179866299	-0,034503989	-0,305641174	0,313178748	-0,488375634	0,425046593	-0,233203679	0,64486742	0,221575305
175103_Landsvagsbanan_1lap_hitting.hinders.mat	0,14859648	0,117353596	-0,003579072	0,134241924	-0,02500738	0,029903254	0,062833816	-0,152001902	0,417155296	-0,139480844
180531_Roundabout_left_normal_driving.mat	-0,819139302	0,515666604	0,58792609	0,092340589	0,46283862	-0,391951263	0,157631636	-0,915720046	0,348097324	-0,27258417
180714_Acceleration_stand-still_turn_in_junction_left.mat	-0,81696701	0,193275005	0,391778499	0,233799279	0,327379078	-0,764829397	0,288301677	-0,884082317	0,604159176	-0,74954313
180834_Acceleration_stand-still_turn_in_junction_right.mat	-0,43878997	-0,154629335	-0,080637641	0,237891287	-0,351108253	-0,214357272	-0,201560989	-0,41623342	0,257031977	-0,092384219
181021_Full_throttle_from_stand-still.mat	0,299382567	0,527152061	0,396946281	-0,265652895	-0,278785199	-0,66961664	-0,001905209	-0,092574611	0,602574468	-0,519665062
181210_Hard_brake_evasive_50kph.mat	-0,766775548	0,001425769	0,178440869	-0,436538458	-0,104850642	-0,699061036	0,394728601	-0,70753485	0,410014272	0,028628873
181359_Smooth_double_lane_change_60kph.mat	0,160760328	0,767372847	0,108986385	0,352594167	0,605959356	-0,009474652	0,49529624	-0,656446457	0,593368173	0,353145391
181655_Handlingbana2_moderate_braking_end.mat	0,543237627	0,241396457	0,210365519	-0,138469085	0,020375894	-0,524341106	0,084904864	-0,222098678	0,63313216	-0,065181844
Total	-0,105495296	0,148072332	0,048724785	0,026823793	0,035110235	-0,116402499	0,041259028	0,003431818	0,222747386	-0,217404768

D

Correlation Between States and Diff Heading:Dynamics Based

File	mean_error_deg	art_heading	art_analog	time	x_speed_tract	x_lat_speed_tract	x_speed_trail	x_lat_speed_trail	x_yaw_tract	x_yaw_trail
162129_Standing_still_on_levelled_surface.mat	0	0	0	0	0	0	0	0	0	0
162346_EuroComb_Hallered_2020_01_14.mat	0,235498294	0,850120485	0,81249696	0,797938228	-0,809999764	0,749034584	-0,79835254	0,84919703	0,750526309	0,848300397
162842_Eight_with_small_radius_start_left.mat	1,485025644	-0,677530468	-0,648853779	-0,001516594	-0,067817897	-0,779034436	0,056297619	-0,662025392	-0,780983627	-0,651554883
163216_Driving_in_reverse_direction_slowly.mat	0,459304601	-0,433127075	-0,423087895	-0,074277267	-0,099130742	0,121502891	-0,365255445	0,389096946	0,120015532	0,39346233
163818_Radius_45m_increase_speed_stand-still_max_speed_left.mat	0,260079592	-0,701026499	0,157772407	-0,117804863	-0,53446877	-0,374163359	-0,531542063	-0,389821112	-0,506337464	-0,510655522
164228_Radius_45m_increase_speed_stand-still_max_speed_right.mat	0,625684738	-0,318888634	-0,050579984	-0,557081938	-0,549089372	0,455834448	-0,547656417	0,498104513	0,562749624	0,557661653
165218_Radius_45m_speed_30mps_counterclockwise.mat	0,793116987	-0,898335397	-0,149885193	0,725154519	-0,660961926	-0,622429252	-0,660103798	-0,645709634	-0,651709259	-0,654946864
165515_Radius_1250cm_outerwheel_low_speed.mat	1,200820088	-0,033425417	-0,05379932	0,202715203	-0,345441043	0,345198154	-0,530070841	0,002666282	0,377377182	0,011258909
170544_Acc_2mps2_stand-still_80kmh_decc_2mps2_stand-still.mat	0,564357817	-0,758637965	-0,62874043	0,746340275	0,736332536	-0,10594894	0,767327726	0,336457044	0,343645453	0,298828751
172134_ABS_braking_50kmh.mat	0,725533962	-0,25732666	-0,080668129	-0,147007585	-0,230836973	-0,495175242	-0,280937612	0,6203264	-0,367256135	0,261603564
172301_EuroComb_Hallered_2020_01_14.mat	0,137978703	0,374358922	0,499984562	0,049151298	0,348299176	0,294781446	0,321019232	0,608738959	0,512004077	0,619464397
172424_Drive_straight_50kmh_sine_steering_low_freq.mat	0,57960844	0,345970869	0,6194489	0,176363498	-0,565901518	0,3546149	-0,570937097	0,602177858	0,512043238	0,534423232
172642_Drive_straight_50kmh_sine_steering_high_freq.mat	0,298726588	-0,068063252	-0,116770178	0,562593102	-0,561562717	-0,766480565	-0,561143398	-0,056859039	-0,669782937	0,316196203
172921_Double_lange_change_80kph.mat	0,292924851	-0,406492084	-0,300957769	0,244249374	0,065412186	0,12080761	0,093050182	-0,049160041	-0,353295416	-0,212661475
173614_Uphill_12perc_start_bottom_with_stop_start_middle.mat	0,368428975	0,267805547	0,307601333	-0,124636248	-0,395027251	0,304980129	-0,386026859	0,495464027	0,318756819	0,522049129
174114_EuroComb_Hallered_2020_01_14.mat	0,193640381	0,321831435	-0,177643418	-0,806508303	0,429786831	0,098861068	0,437313825	0,168572992	0,375026107	0,646318734
174226_EuroComb_Hallered_2020_01_14.mat	0,141061142	-0,189581931	0,720308602	-0,76440686	-0,300904006	-0,389080703	-0,340796858	-0,227527454	-0,55820328	-0,161187574
174801_Gravel.mat	0,350959182	0,188739613	0,147978097	0,139836341	-0,002645084	0,265872061	-0,000346707	0,381924331	0,373816222	0,345016062
175103_Landsvagsbanan_1lap_hitting hinders.mat	0,314848393	-0,219824493	-0,145815313	0,321866572	0,044573568	-0,071271934	0,057160631	0,037111823	-0,081788227	-0,092510924
180531_Roundabout_left_normal_driving.mat	0,866141438	-0,773002028	-0,76407063	-0,195687771	-0,086370043	-0,546414971	0,102765501	-0,775432467	-0,547705472	-0,797388375
180714_Acceleration_stand-still_turn_in_junction_left.mat	0,467626005	-0,701638043	-0,6889202	-0,360306621	-0,567715049	-0,308859855	-0,486585051	-0,701214612	-0,328750581	-0,757926881
180834_Acceleration_stand-still_turn_in_junction_right.mat	0,600452483	-0,21739912	-0,121683657	-0,736180007	0,066782281	-0,51824069	0,022215642	-0,19002834	-0,521451235	-0,150341004
181021_Full_throttle_from_stand-still.mat	0,465508938	-0,310040712	-0,225287825	0,685532212	0,163481653	-0,049868412	0,183865905	0,029104281	-0,087018408	-0,136205018
181210_Hard_brake_evasive_50kph.mat	0,18762977	0,307520837	0,277383447	-0,486482829	-0,275355309	0,201743603	-0,296492785	0,450005859	0,167660162	0,264376998
181359_Smooth_double_lane_change_60kph.mat	0,198339775	-0,158600539	-0,082422696	-0,829420209	0,728881836	-0,248805299	0,699273229	-0,11377164	0,207695767	0,161511183
181655_Handlingbana2_moderate_braking_end.mat	0,351106107	-0,232121065	-0,118202776	0,389276981	0,175389275	0,148963615	0,183750108	0,186176449	-0,241483912	-0,25860545
Total	0,487271488	-0,107622884	-0,053336874	0,144138768	0,159478471	-0,182576999	0,169707522	-0,158065826	-0,185367465	-0,17852664

File	articulation	heading	steering	tractor_acc_x	tractor_acc_y	trailer_conti_acc_x	trailer_conti_acc_y	trailer_conti_acc_z	tractor_angrate_forward
162129_Standing_still_on_levelled_surface.mat	0	0	0	0	0	0	0	0	0
162346_EuroComb_Hallered_2020_01_14.mat	0,886312842	-0,860766768	0,798873365	-0,035217397	-0,32562387	-0,023903063	0,395614445	-0,093185425	0,199731484
162842_Eight_with_small_radius_start_left.mat	-0,649968743	0,093324088	-0,78258878	0,116336986	0,797431469	0,23179315	-0,707669318	0,03876463	-0,27150622
163216_Driving_in_reverse_direction_slowly.mat	-0,405852646	0,196669937	-0,142661437	-0,173467174	-0,324819773	-0,144512266	0,090661369	-0,055751931	0,136479795
163818_Radius_45m_increase_speed_stand-still_max_speed_left.mat	0,422205031	-0,012454828	-0,283366263	-0,047499146	0,559784949	0,148487821	-0,55620575	0,045952663	-0,009279561
164228_Radius_45m_increase_speed_stand-still_max_speed_right.mat	0,025817027	0,122160234	0,318515271	0,016518867	-0,592453599	0,152712449	0,595436037	0,081068754	0,004003073
165218_Radius_45m_speed_30mps_counterclockwise.mat	0,092898048	-0,350358635	-0,448772341	-0,114341125	0,648732185	0,079661287	-0,651264906	0,044628143	0,040624961
165515_Radius_1250cm_outerwheel_low_speed.mat	-0,011953671	-0,373261631	0,397584885	-0,052461449	-0,240547314	-0,073746726	0,234812945	-0,032655023	-0,051219013
170544_Acc_2mps2_stand-still_80kmh_decc_2mps2_stand-still.mat	0,265973926	0,869193912	0,232263833	-0,509068668	-0,054887757	-0,511670172	-0,056829244	-0,144468471	-0,00026397
172134_ABS_braking_50kmh.mat	0,563421369	-0,134826377	-0,298785567	0,147768915	0,081747554	0,271515638	-0,050335862	0,013790512	0,088859499
172301_EuroComb_Hallered_2020_01_14.mat	0,871357739	0,030388031	0,339448512	0,304120868	-0,003247562	0,308247477	0,108039744	0,108276844	0,02055829
172424_Drive_straight_50kmh_sine_steering_low_freq.mat	0,571357191	-0,225836709	0,43377921	0,280008048	-0,487518102	0,372027338	0,53620249	0,018869273	-0,099520415
172642_Drive_straight_50kmh_sine_steering_high_freq.mat	0,116823591	-0,327211738	-0,751549244	-0,010948143	0,743431211	-0,084110931	-0,374457031	0,012844418	-0,302618831
172921_Double_lange_change_80kph.mat	-0,258673102	0,367215723	-0,327870488	0,079226166	0,364569694	0,243642971	-0,313272119	0,031052412	-0,085049033
173614_Uphill_12perc_start_bottom_with_stop_start_middle.mat	0,328205466	0,41738686	0,234562546	0,155955344	-0,282146156	-0,022381376	0,464663684	0,010092194	-0,082293756
174114_EuroComb_Hallered_2020_01_14.mat	0,748079658	-0,242130816	0,379643857	-0,082680643	0,035180464	-0,751623929	0,109656587	0,24340117	0,100187041
174226_EuroComb_Hallered_2020_01_14.mat	0,218414888	-0,69413662	-0,780293643	0,669014812	-0,054895222	0,62734133	-0,239392936	0,263945818	0,433064908
174801_Gravel.mat	0,288698256	0,049204063	0,281509101	0,02662693	-0,382403165	-0,33207956	0,155981556	0,021807389	-0,144000188
175103_Landsvagsbanan_1lap_hitting hinders.mat	-0,070433892	0,603128195	-0,056230456	-0,172959089	0,105619311	-0,159779921	-0,064289711	0,005717727	-0,006324925
180531_Roundabout_left_normal_driving.mat	-0,745287716	0,128631398	-0,420006335	-0,060470756	0,437132567	0,171487004	-0,556317866	0,107655682	0,178993046
180714_Acceleration_stand-still_turn_in_junction_left.mat	-0,674645543	0,58552444	-0,182460502	-0,0398039	0,21273993	0,323642731	-0,42933321	0,091500312	0,204031274
180834_Acceleration_stand-still_turn_in_junction_right.mat	-0,151527196	-0,781117439	-0,540946305	0,22179985	0,580634892	0,189693615	-0,464432508	0,032431819	-0,18487151
181021_Full_throttle_from_stand-still.mat	-0,018037837	0,558314979	0,028010687	-0,496767044	0,146731436	-0,538497567	-0,148674533	-0,141850755	0,154012159
181210_Hard_brake_evasive_50kph.mat	0,420930922	0,27522707	0,299516946	0,310681611	0,079081848	0,321031213	0,154960275	0,065790728	0,099943362
181359_Smooth_double_lane_change_60kph.mat	0,055779248	0,449493319	0,18312563	0,695330739	-0,241196483	0,461890966	0,248481318	0,193302423	0,090809554
181655_Handlingbana2_moderate_braking_end.mat	-0,089953832	0,004669685	-0,165399417	-0,142354384	0,266166002	-0,123796567	-0,337341666	0,026622359	-0,056475013
Total	-0,047942296	0,082163043	-0,052488722	-0,015769269	0,153948113	-0,014286906	-0,154061854	0,006756728	-0,020764682

File	tractor_angrate_lateral	tractor_angrate_down	trailer_angrate_forward	trailer_angrate_lateral	trailer_angrate_down	tractor_vel_forward	tractor_vel_lateral
162129_Standing_still_on_levelled_surface.mat	0	0	0	0	0	0	0
162346_EuroComb_Hallered_2020_01_14.mat	-0,203772441	0,720463395	-0,033752412	-0,066803418	0,775705636	-0,798501432	0,643430531
162842_Eight_with_small_radius_start_left.mat	0,073652692	-0,778257072	-0,29364869	0,086938754	-0,644296885	0,059658434	-0,745892704
163216_Driving_in_reverse_direction_slowly.mat	0,098019131	0,075815283	-0,067514822	0,228440329	0,375330389	0,014485535	0,225927457
163818_Radius_45m_increase_speed_stand-still_max_speed_left.mat	-0,017911546	-0,51962477	-0,030200642	-0,00097231	-0,521958709	-0,531470597	-0,392602086
164228_Radius_45m_increase_speed_stand-still_max_speed_right.mat	0,043586474	0,561595917	0,039518297	0,00869272	0,552534044	-0,546998322	0,287238747
165218_Radius_45m_speed_30mps_counterclockwise.mat	0,025424818	-0,656591952	0,041705314	-0,030087363	-0,659417868	-0,653072774	-0,464405268
165515_Radius_1250cm_outerwheel_low_speed.mat	0,052578364	0,379309833	-0,105733432	0,047709391	-0,008687006	-0,313187242	0,219367817
170544_Acc_2mps2_stand-still_80kmh_decc_2mps2_stand-still.mat	0,056029592	0,178368941	-0,021128608	-0,009917882	0,159036115	0,770714045	0,886772871
172134_ABS_braking_50kmh.mat	-0,059733976	-0,218308702	-0,009438326	-0,029946011	-0,304197699	-0,303075254	0,247607812
172301_EuroComb_Hallered_2020_01_14.mat	-0,046744868	0,103780866	-0,049450886	-0,012710608	0,240129128	0,309325218	-0,246946126
172424_Drive_straight_50kmh_sine_steering_low_freq.mat	-0,086177208	0,552530289	0,148024857	-0,091451257	0,516520679	-0,573364377	0,126897663
172642_Drive_straight_50kmh_sine_steering_high_freq.mat	0,245559976	-0,634165108	-0,700631142	-3,00912E-05	0,313623534	-0,541324615	-0,616180837
172921_Double_lange_change_80kph.mat	0,065691814	-0,356392443	-0,211407542	0,041242074	-0,224615335	0,146859884	0,504564881
173614_Uphill_12perc_start_bottom_with_stop_start_middle.mat	-0,023806298	0,308903098	-0,272027791	0,057865404	0,587945342	-0,407870859	0,259868026
174114_EuroComb_Hallered_2020_01_14.mat	-0,250030458	0,367383689	-0,055456523	-0,364111573	0,556005836	0,437550098	0,464437515
174226_EuroComb_Hallered_2020_01_14.mat	-0,234778002	-0,156861991	-0,068100199	0,047949295	0,104894497	-0,316609681	-0,376331121
174801_Gravel.mat	-0,168638319	0,348214924	-0,457353771	-0,129271775	0,321657896	0,022907805	0,581810832
175103_Landsvagsbanan_1lap_hitting hinders.mat	-0,055734705	-0,109443277	-0,076125182	-0,035540514	-0,107470058	0,06142211	0,375335008
180531_Roundabout_left_normal_driving.mat	-0,061060838	-0,557019949	0,05133133	-0,322992176	-0,804885447	0,024395062	-0,621878207
180714_Acceleration_stand-still_turn_in_junction_left.mat	-0,049099881	-0,354463786	-0,261429787	-0,408494294	-0,779685259	-0,509681523	-0,429777145
180834_Acceleration_stand-still_turn_in_junction_right.mat	0,092757292	-0,516272545	-0,285341114	0,238099217	-0,128863692	0,001416408	-0,450078994
181021_Full_throttle_from_stand-still.mat	-0,055439468	-0,191836625	-0,092672713	0,057668708	-0,197225317	0,182960644	0,23691152
181210_Hard_brake_evasive_50kph.mat	-0,063749082	0,101916738	-0,070056215	-0,033398926	0,202648729	-0,292489082	0,120009333
181359_Smooth_double_lane_change_60kph.mat	-0,248253912	0,186445892	0,062488966	-0,22891821	0,163927823	0,701434612	0,255295783
181655_Handlingbana2_moderate_braking_end.mat	-0,039396074	-0,252659798	-0,159959778	-0,04280534	-0,268230259	0,193823144	0,759111702
Total	-0,018430138	-0,193002865	-0,075771086	-0,022478573	-0,182507202	0,165474802	0,007025593

File	trailer_vel_forward	trailer_vel_lateral	trailer_angroll	trailer_angpitch	tractor_angroll	tractor_angpitch	tractor_curvature
162129_Standing_still_on_levelled_surface.mat	0	0	0	0	0	0	0
162346_EuroComb_Hallered_2020_01_14.mat	-0,79808557	0,361064583	0,689336717	-0,601094842	0,352507353	-0,047611106	0,763933837
162842_Eight_with_small_radius_start_left.mat	0,053058028	-0,665463686	0,312593609	-0,162705436	-0,603422046	-0,049983013	-0,775619328
163216_Driving_in_reverse_direction_slowly.mat	-0,385330677	0,361007661	0,123388439	0,07880941	0,162960485	-0,195528805	-0,072039366
163818_Radius_45m_increase_speed_stand-still_max_speed_left.mat	-0,533642054	-0,411798328	-0,538627505	0,012048764	-0,544888854	0,412467182	0,212289512
164228_Radius_45m_increase_speed_stand-still_max_speed_right.mat	-0,545339108	0,087741323	0,573473573	-0,232490703	0,582604587	0,141506776	-0,01187369
165218_Radius_45m_speed_30mps_counterclockwise.mat	-0,662737787	-0,618311584	-0,631905615	-0,568152428	-0,669438899	0,22688736	-0,036865287
165515_Radius_1250cm_outerwheel_low_speed.mat	-0,509817839	-0,170847848	0,310299516	-0,159334049	0,363531351	0,06047656	0,380615741
170544_Acc_2mps2_stand-still_80kmh_decc_2mps2_stand-still.mat	0,772048354	-0,66559124	-0,469922125	0,190251261	-0,688531935	0,519440293	0,129519641
172134_ABS_braking_50kmh.mat	-0,2794469	-0,023094313	-0,264624536	0,253721863	-0,35790056	0,032915313	-0,296947628
172301_EuroComb_Hallered_2020_01_14.mat	0,308496505	-0,439195275	0,028125655	0,242930919	0,20568341	-0,269549608	0,089699239
172424_Drive_straight_50kmh_sine_steering_low_freq.mat	-0,567637146	-0,275942653	-0,025423063	0,275361985	0,502687931	-0,576033771	0,565054178
172642_Drive_straight_50kmh_sine_steering_high_freq.mat	-0,550922513	-0,132205278	0,083619252	-0,212583974	-0,688025892	-0,015326411	-0,583919406
172921_Double_lange_change_80kph.mat	0,060695723	-0,042897459	-0,266792446	-0,005168855	-0,38897863	0,056609716	-0,358491033
173614_Uphill_12perc_start_bottom_with_stop_start_middle.mat	-0,384248346	0,701934099	0,49752906	0,354970008	0,249151215	0,344665647	0,204282686
174114_EuroComb_Hallered_2020_01_14.mat	0,451424241	0,401904583	0,715156376	0,764194071	-0,729639769	0,685096562	0,299473435
174226_EuroComb_Hallered_2020_01_14.mat	-0,315390766	-0,35986203	-0,81360054	0,814871609	0,409659475	-0,575365067	-0,521159768
174801_Gravel.mat	0,020332307	0,453194857	-0,425578952	0,700397134	-0,541098475	0,699046671	0,217260063
175103_Landsvag3banan_1lap_hitting hinders.mat	0,056956716	-0,213041335	0,275247693	-0,155702174	0,173759431	-0,07315702	-0,097603679
180531_Roundabout_left_normal_driving.mat	0,104188673	-0,797299206	-0,118259475	0,074239813	-0,442051649	0,029919386	-0,445395201
180714_Acceleration_stand-still_turn_in_junction_left.mat	-0,486427128	-0,758415163	0,817105472	-0,547737837	-0,228977829	-0,541157365	-0,248337522
180834_Acceleration_stand-still_turn_in_junction_right.mat	0,027956715	-0,051243249	0,104287513	-0,313128471	-0,28445673	-0,138425276	-0,521409273
181021_Full_throttle_from_stand-still.mat	0,180723339	-0,042917136	-0,060467139	-0,198784605	-0,550924242	0,366703987	-0,213233978
181210_Hard_brake_evasive_50kph.mat	-0,295328796	0,32479912	0,502213776	-0,19302921	0,416102022	-0,341778964	0,253068745
181359_Smooth_double_lane_change_60kph.mat	0,702179909	-0,676214516	0,405413002	0,843231976	0,434753478	0,767860591	0,076701716
181655_Handlingbana2_moderate_braking_end.mat	0,18515572	0,08805348	-0,143369481	-0,029081807	-0,514617383	0,016973717	-0,14375113
Total	0,170502543	-0,198886082	0,018952623	0,070402354	-0,145502314	0,082969725	-0,043612406